Helsinki University of Technology

Faculty of Electronics, Communications and Automation

Department of Electrical Engineering

Monear Belkasim

IDENTIFICATION OF LOSS MODELS FROM MEASUREMENTS OF THE MAGNETIC PROPERTIES OF ELECTRICAL STEEL SHEETS

Master's thesis submitted for approval for the degree of Master of Science, Espoo, December, 2008

Supervisor _____

Professor Antero Arkkio, D.Sc. (Tech)

Instructor _____

Anouar Belahcen, D.Sc. (Tech)

Helsinki University of Technology | **Abstract of the Master's Thesis**

Author:	Monear Ali Belkasim
Name of the thesis:	Identification of Loss Models From Measurements of the Magnetic Properties of Electrical Steel Sheets
Date:	December 2008 **Number of pages:** 97
Department:	Electrical Engineering
Professorship:	S-17 Electrical Engineering (Electromechanics)
Supervisor:	Professor Antero Arkkio
Instructor:	Dr. Anouar Belahcen

Numerical simulations of electrical machines require good knowledge of the magnetic properties of the materials they are made of. The magnetic cores of these machines are made of electrical steel sheets, the magnetic properties of which are nonlinear and hysteretic. Moreover, the behavior of the magnetic flux density and the magnetic field strength of such materials depends on the form of the supply.

In the Laboratory of Electromechanics, there are several projects which aim to model correctly the behavior of the electrical steel sheet (hysteresis, stress-dependency, losses, etc.) when used in electrical machines. For this purpose, numerical models are developed and built in an in-house finite element program package. However, knowledge of the material properties and the parameters of loss models are necessary and needs to be measured. This work is proposed to measure the magnetization curves and specific losses of an electrical steel sheet. The measurements were carried out using a device specially designed for this purpose and adequate programs for field control. The measurements were conducted under rotating and alternating magnetic fields at different fundamental frequencies and amplitudes. The results of the measurements consisted of a large amount of data that has been analyzed, processed and presented in an appropriate manner. Moreover, the parameters of the loss models were estimated from the measurements through identification procedures that have been written and constructed in MATLAB software. The conclusions of this work provide the basis for a better understanding of the parameters needed to improve loss models.

Keywords: Magnetic Properties, Electrical Steel Sheets, Hysteresis Losses, Rotational Field, Loss Modeling, Loss-Models Identification.

Preface

This master's thesis has been carried out in the Department of Electrical Engineering, Faculty of Electronics, Communications and Automation, at the Helsinki University of Technology, Finland.

First of all I would like to thank my God for given me the health and blessing to complete this work.

I am thankful and indebted to my supervisor *Professor Antero Arkkio* for giving me the opportunity to work, develop, and improve myself in his Laboratory. I am sincerely grateful to my instructor, *Dr. Anouar Belahcen* for his invaluable guidance and patience during the work.

I am deeply grateful to *Dr. Emad Dlala* for giving me all his support, helps and encouragement, which I will never forget.

I wish to express my gratitude to *Mr. William Martin* for language revision work and to *Dr. Najy Elkalashy* for his strong moral support throughout my time in Finland

I would like to express my appreciation to *Mr. Ari Haavisto* and *Mrs. Marika Schröder* for all their help. I would also like to thank all the people in the Electromechanics Engineering Group for creating a welcoming atmosphere to work. Great thanks also go to all my friends here in Finland and in Libya for showing that you care!

To my sisters and brothers, thank you so much for all the love and support that you have given me during my life. Without that love and support, this thesis would never have been possible.

Finally, my dearest thanks go to my father *Ali*, to who's memory I dedicate this thesis, and to my mother *Hawwa*, for her years of sacrifice made for the family. I thank you from the bottom of my heart for being with me every step of the way.

Espoo, December, 2008

Monear Belkasim

List of Notations

Symbols

$\boldsymbol{B}$	Magnetic flux density
$\boldsymbol{H}$	Magnetic field strength
B_{x}	Magnetic flux density component in x direction
B_{y}	Magnetic flux density component in y direction
H_{x}	Magnetic field strength component in x direction
H_{y}	Magnetic field strength component in y direction
$\hat{B}$, $B_{\max}$	Maximum value of flux density
$\hat{H}$	Maximum value of magnetic field strength
B_n	Harmonic flux density
P_r	Rotational core losses
P_{total}	Total core losses
$P_{\mathrm{hys}}, P_{\mathrm{h}}$	Hysteresis power losses
$P_{\mathrm{exc}}, P_{\mathrm{e}}$	Excess power losses
$P_{\mathrm{hys}}^{\mathrm{circ}}$	Hysteresis loss under purely rotational flux
$P_{\mathrm{hys}}^{\mathrm{alt}}$	Hysteresis loss under alternating flux
$P_{\mathrm{hys}}^{\mathrm{ellipt}}$	Hysteresis loss under elliptical flux
$P_{\mathrm{total}}^{\mathrm{alt}}$	Total loss under alternating flux
$P_{\mathrm{total}}^{\mathrm{ellipt}}$	Total loss under elliptical flux
$P_{\mathrm{total}}^{\mathrm{circ}}$	Total loss under purely rotational flux
P_{c}	Classical eddy-current losses
K_H	Coil coefficient
V_H	Terminal voltage of the H sensing coil
μ_0	Magnetic permeability of the vacuum
N	Number of turns of the excitation winding
d	Thickness of the lamination
σ	Electrical conductivity of the material
f_{m}	Magnetizing frequency
K_{h}	Hysteresis loss correction factor
$\lvert B \rvert$	Absolute value of the flux density
i	Magnetization current
H_n	Harmonic field strength
$\hat{B}_n$	Amplitude of the actual harmonic flux density
α	Direction of the excitation

$\boldsymbol{M}$	Magnetization
$M_{\perp}$	The component of $\boldsymbol{M}$ perpendicular to $\boldsymbol{H}$
T	Time period of magnetization
T_{r}	Torque due to the rotational core losses in the sample
l_{m}	Mean length of the magnetic flux path
k_c	Classical eddy-current loss coefficient
k_{e}	Excess loss coefficient
k_{h}	Hysteresis loss coefficients
k_{r}	Rotational loss coefficients
B_{s}	Saturation flux density
ρ_{m}	Mass density of the sample

List of Abbreviations

1D	One Dimensional
2D	Two Dimensional
3D	Three Dimensional
AC	Alternating Current
DAQ	Data Acquisition
DC	Direct Current
FEM	Finite Element Method
FPGA	Field Programmable Gate Array
PWM	Pulse Width Modulation
SRM	Switched Reluctance Motor
SST	Single Sheet Tester

Contents

Chapter 1

Introduction

Electrical machines have been discovered in the 19th century and various magnetic materials have been used as the cores of these electromagnetic devices. The magnetic properties of the magnetic materials used have a strong impact on the performance of these devices, and should be carefully characterized. For evaluation and controlling the quality of magnetic materials, such as *B* (magnetic flux density)-*H* (magnetic field strength) curves and core losses, are measured under one-dimensional (1-D) alternating and/or two dimensional (2-D) rotating magnetic fluxes, according to the application requirement. It has been long known that the behavior of magnetic materials under a rotating flux (2-D) is quite different from that under an alternating flux (1-D). Therefore, the magnetic properties of the core materials under different rotational magnetizations should be investigated, understood, properly modeled, and employed in the design and performance analysis of electrical machines.

In typical rotating electrical machines, both alternating and rotating flux density vectors exist. The measurement techniques under alternating flux have become standardized and the alternating magnetic property data of magnetic materials is normally provided by the manufactures. However, the magnetic properties under the rotating flux are still lacking and have not been completely identified, and their measurement techniques and modeling approaches are still far from standardization.

1.1 Magnetization and Ferromagnetic Properties

A coil of wire, which has *n* turns around an iron rod of permeability μ, becomes a magnet when current *I* passes through that coil. This basic physical object will produce magnetic fields within the coil which are given the symbols (*B*, *H*). Magnetization as a result is a property of magnet materials that describes to what degree they are affected by magnetic fields, and also determines the magnetic field that the material itself creates (*materialization*).

Magnetization is defined as the amount of magnetic moment per unit volume, and in most materials, the moments are oriented almost at random which lead to weak magnetization and non-magnetic properties. In ferromagnetic materials such as iron, the moments readily align themselves along an applied field so inducing a large value of magnetization. Magnetization takes place not only in materials that have permanent magnetic moments but also occurs in any *magnetisable* material in a field which can induce a magnetic moment in its component atoms.

The relations between the magnetic fields (*B, H*), and magnetization *M* can be described by the equation

$$B = \mu_0 (H + M)$$

where *H* and *M* have the same units, amperes/meter.

And according to this equation we can say that, the *B-field* consists of two components, the first component which is presented by the externally imposed field $(\mu_0 H)$, and the second component called the materialization $(\mu_0 M)$, shows the creation of the results that occurred within the material due to the *HB-fields*.

If the material does not respond to the external magnetic field by producing any magnetization, this means that the relative permeability of this material is unity $(\mu_0 = 1)$.

The most important class of the magnetic materials that can be used to produce a large magnetization is the ferromagnetic material class, including iron, nickel, and cobalt, which are all strongly ferromagnetic, have Curie temperatures of about 1040, 630 and 1400 K respectively, and exhibit a strong magnetism to magnetic fields. Furthermore, they are able to retain their magnetic properties after the external field has been removed. The magnetization curve of the ferromagnetic materials and their behaviors within the field looks very different compared to other materials. The characteristics of these materials are all strongly dependent on the conditions of purity, heat treatment, hysteresis, *B*-field, and other factors.

1.2 Power Losses in Electrical Machines

The causes that might leads to the power losses in electrical machines are various, through several different mechanisms, for example, the resistance of the windings cause losses known as *copper loss* or *winding loss* which is increased with frequency and operates even when the current in the winding is not changing. Copper loss is the term

used to express the energy dissipated by resistance in the wire used to wind a coil (wrapped around an iron core). This wire is frequently made of copper whose resistivity is about 1.73×10^{-8} ohmmeters. As well, one of the greatest losses occurring in electrical machines result from the losses in the iron core, which can be separated into two different mechanisms. The mechanism due to the magnetic friction in the core and its effect within the ferromagnetic material (iron) will cause a loss known as the hysteresis loss, and the second mechanism caused by the electric currents induced in the core which generate the eddy current loss. The hysteresis and eddy current losses are collectively known as iron loss or core loss, even if a ferrite core is used. Iron loss is a form of energy loss occurring in electrical machines due to a variety of mechanisms related to the fluctuation of the magnetic field, such as eddy currents and hysteresis. Most of the energy is released as heat, although some may appear as sound. Core losses do not include the losses due to resistance in the conductors of the windings, which is often termed copper loss.

1.3 Understanding and Modeling of Rotational Core Losses

In the past hundred years, a lot of work has been carried out by various researchers on the rotational core losses. Earlier effort focused on rotational hysteresis loss with a purely circular rotational magnetic field. Since the 1960s, total core losses of magnetic materials under both circularly and elliptically rotating magnetic field excitations of different frequencies have been studied.

1.3.1 Rotational Hysteresis Loss

The first quantitative investigation on the rotational hysteresis loss of hard steel and soft iron was conducted in 1896 by Baily. Figure 1.1 shows the results obtained under rotating and alternating magnetic fields. For a range of flux density up to about 70% of the saturation, the rotational hysteresis losses in both hard steel and soft iron are larger than the alternating hysteresis losses. However, when the flux density further increases, the rotational hysteresis loss drops quickly and vanishes when the flux density reaches the saturation value, while the alternating hysteresis loss continues to increase. This indicates that the mechanism of the rotational hysteresis loss is different from that of its alternating counterpart.

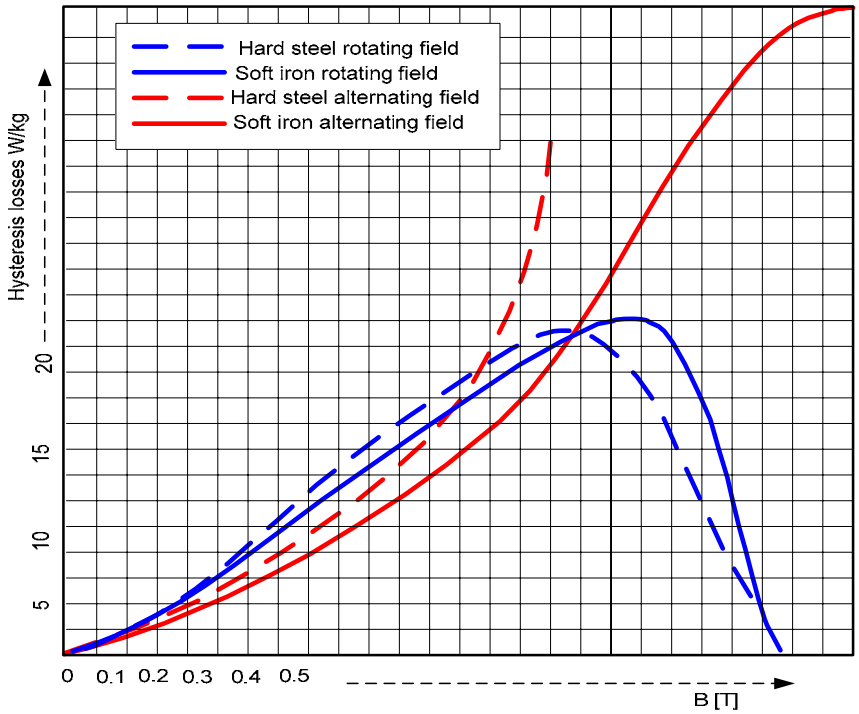

Figure 1.1: Hysteresis losses of soft iron and hard steel under rotating and alternating magnetic fields obtained by Baily (1896).

A qualitative explanation of the rotational core loss phenomenon was made based on the domain theory of ferromagnetism. According to this theory, magnetization below the knee of the *B*-*H* curve proceeds in steps, corresponding to the Barkhausen discontinuities, each step representing a reversal or sudden change in direction through 90^{o} of the spontaneous saturation in a domain. In addition, there may be a parallel reversible process, involving no hysteresis loss. For any particular domain, a sudden change in direction may be expected when a certain value of the field acting on it in the final direction of its magnetization has been reached. The total change in energy involved in this discontinuous change is then dissipated as hysteresis loss, a function of the volume of the domain, the saturation magnetization, and the effective field strength.

At the knee of the *B*-*H* curve, the field required to produce the discontinuous rotating has already been reached or exceeded for most of the domains contribute further to the total magnetization on a further large increase of magnetic field strength *H*, by a rotating of the spontaneous magnetization in the domains from the easy direction towards the direction of the applied field. There are some domains remaining, however, which are not acted upon until *H* has increased beyond its value at the knee. The contribution to the magnetization due to these domains is only that corresponding to their volume, but the

contribution to loss is high on account of the high value of H at that point at which the sudden change in direction of the magnetization occurs. The loss will, therefore, rise steeply with the increase of magnetization.

Similar ideas may be applied to the portion of the loss curve near saturation. For a very high field, the spontaneous magnetization is always in the direction of the field, and as the field is rotated, it rotates smoothly and without the discontinuities which results in hysteresis loss. Hence, the hysteresis loss may then be zero.

1.3.2 Methods for Measuring Rotational Core Loss

Considerable progress has been achieved in terms of measuring techniques and systems for rotational core loss evaluation. There are four major methods for measuring the rotational core loss which can be described in the following sections (see Guo et al. 2008 for more details).

A. Torque-Metric Method

The torque-metric method is usually used in apparatus which use a disk or ring sample. The torque due to rotational core loss occurring in the sample is measured by using mechanical torque meters, or calculated from the variation of the sample angular speed. The advantages of this method are the direct reading of the torque corresponding to the rotational core loss from the torque meter, and the ability to measure the rotational core loss even with the highest levels of flux densities. The disadvantage is the difficulty of torque meter construction owing to the complicated mechanics.

B. Thermo-Metric Method

In the thermometric method, the temperature of the sample is obtained by thermocouple, thermistors, or thermoviewers. The rotational core loss is proportional to the initial rate of the sample temperature rise if no cooling process is involved. The following formula shows the relation between the rotational loss and temperature of the sample

$$P_{\mathrm{r}} = C\frac{d\theta}{dt}$$

where P_{r} is the specific rotational core loss in W/kg, C the specific heat of the sample material, θ the temperature of the sample, and t the time instant. The method is very

adaptable and widely used in apparatus using various types of sample, such as square, disc, ring, and cross, with various types of rotating magnetic field. Moreover, the method is able to measure localized core losses at the T joints of a three-phase transformer core. The major disadvantages of this method are the difficulties of installation and the calibration of thermosensors, and isolation against the surrounding. It is, therefore, being more and more replaced by the field-metric technique.

C. Field-Metric Method

In the field-metric method, the rotational core loss is calculated from the measured magnetic field strength ***H*** at the sample surface and flux density ***B*** inside the sample. The method features high accuracy and great versatility. Moreover, the set of measured instantaneous ***H*** and ***B*** values can yield more desirable information, such as various loss contributions, the loci of the ***H*** and ***B*** vectors, and harmonics among others. the main disadvantages of this method are the difficulties of manufacture, calibration, and installation of the ***B*** and ***H*** sensors, and the sensitivity to preamplifier phase angle errors. For the evaluation of rotational core loss, two formulas which are referred as the field metric-method type I and type II, respectively. Type I calculates the total specific core loss P_{total} from the measured magnetic field strength ***H*** and magnetic flux density ***B*** components, by using the Poynting theorem as

$$P_{\text{total}} = \frac{1}{T\rho_{\text{m}}}\int_0^T \left(H \cdot \frac{\mathrm{d}B}{\mathrm{d}t} \right) \mathrm{d}t = \frac{1}{T\rho_{\text{m}}}\int_0^T \left(H_{\text{x}} \frac{\mathrm{d}B_{\text{x}}}{\mathrm{d}t} + H_{\text{y}} \frac{\mathrm{d}B_{\text{y}}}{\mathrm{d}t} \right) \mathrm{d}t$$

where T is the time period of magnetization, ρ_{m} is the mass density of the sample, and H_{x}, H_{y}, B_{x}, and B_{y}, are the X and Y components of ***H*** and ***B***, respectively.

In the field-metric method type II, the torque per unit volume due to the rotational core loss in the sample is calculate by

$$T_{\text{r}} = \mu_0 \left| \boldsymbol{H} \times \boldsymbol{M} \right| = \mu_0 H M \sin\alpha = \mu_0 H M_{\perp}$$

where μ_0 is the magnetic permeability of the vacuum, ***M*** is the magnetization, α is the angle between the ***H*** and ***M*** vectors, and $M_{\perp}$ is the component of ***M*** perpendicular to ***H***.

D. Watt-Metric Method

The Watt-metric method differs from the field-metric method in that ***H*** is determined by the magnetization current, and this method is widely used in the Epstein frames or single sheet testers for alternating core loss measurements. Initially, ***H***, ***B***, and the core loss were measured by ammeters, voltmeters, and wattmeters, respectively. That is why this method is known as the watt-metric method. An outstanding advantage of this method is the simplicity of determining ***H***. However, in apparatuses for rotational core loss measurement, this method can only be applied to the vertical yoke single sheet tester, because of the absence of air gaps between the sample and the yokes. The magnetic flux paths in the sample and the yoke system of the rotational core loss testers are not well defined compared to the alternating core loss testers. This causes an extreme systematic error in the magnetic field strength measurement by applying Ampere's law. Since the flux density is not uniformly distributed in the sample, the magnetic flux density is measured in the center of the sample by coils wound through holes in the sample, or *B* tips. The accuracy of measurement strongly depends on the structure of the yoke and the shape of the sample, which define the path of the magnetic flux.

1.3.3 Techniques for Measuring the Components of H and B

Precise evaluation of the core loss measurement in electrical steel sheets depends on the measuring accuracy of the magnetic field strength on the surface of the sample and magnetic flux density inside the sample. Therefore, developing and improving the techniques for measuring such components, becomes a necessity. There are many methods and techniques that have been used for measuring the ***H*** and ***B*** components. The only methods with a close connection to the method which has been used in this thesis will be discussed.

A. Magnetization Current Method

In this technique, the magnetic field strength *H* can be determined from the magnetization current *i* by applying Ampere's law

$$H = N\,i / l_{\mathrm{m}}$$

where *N* is the number of turns of the excitation winding, and l_m is the mean length of the magnetic flux path. This method is widely used in apparatus for the alternating core loss

measurement, such as annular rings, Epstein frames, and single sheet testers, where the magnetic flux paths inside the sample can be well defined. However, the method is not accurate when used in rotational core loss testers, since the magnetic flux paths inside the sample are vague.

B. Sensing Coil Method

The sensing coil is one of the methods that can be used for measuring the magnetic field strength component on the surface of the sample by a thin search coil placed on the surface, as shown in Figure 1.2.

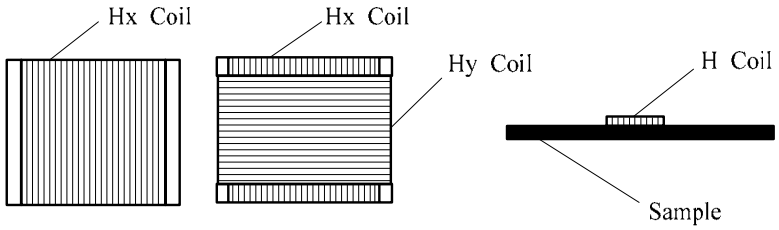

Figure 1.2: (a) 1-D H coil, (b) 2-D H coil, and (c) position of H coil.

When the magnetic field is parallel to the surface, the magnetic field strength can be calculated by

$$H = \frac{1}{\mu_0 K_H} \int V_H \, dt$$

where K_H is the coil coefficient determined by calibration, and V_H is the terminal voltage of the H sensing coil. The method is commonly used in both alternating and rotational core loss testers, and can yield accurate results if the magnetic field on the sample surface is uniform. However, in square rotational core loss testers with horizontal yokes, the magnetic field varies significantly with the distance between the sample surface and the ***H*** coils, and in order to reduce the error, the sensing coils must be made extremely thin and installed as close to the sample surface as possible, which is often very difficult. Moreover, to reduce the error caused by the variation of the magnetic field with the distance above the sample surface, a two ***H*** coil arrangement, as shown in Figure 1.3, can be used

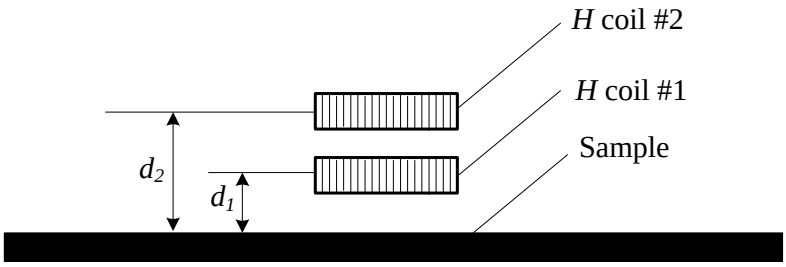

Figure1.3: Two *H* coil arrangement.

and the magnetic field strength at the sample surface can be calculated as

$$H = \frac{d_2 H_1 - d_1 H_2}{d_2 - d_1}$$

where H_1 and H_2 are the magnetic field strength measured by ***H*** coil #1 and ***H*** coil #2 which are placed not far away from the sample, and d_1, d_2 are the distances of two ***H*** coils away from the sample surface.

Concerning the magnetic flux density ***B*** in core loss testers, this also can be measured by using a sensing coil as shown in Figure 1.4.

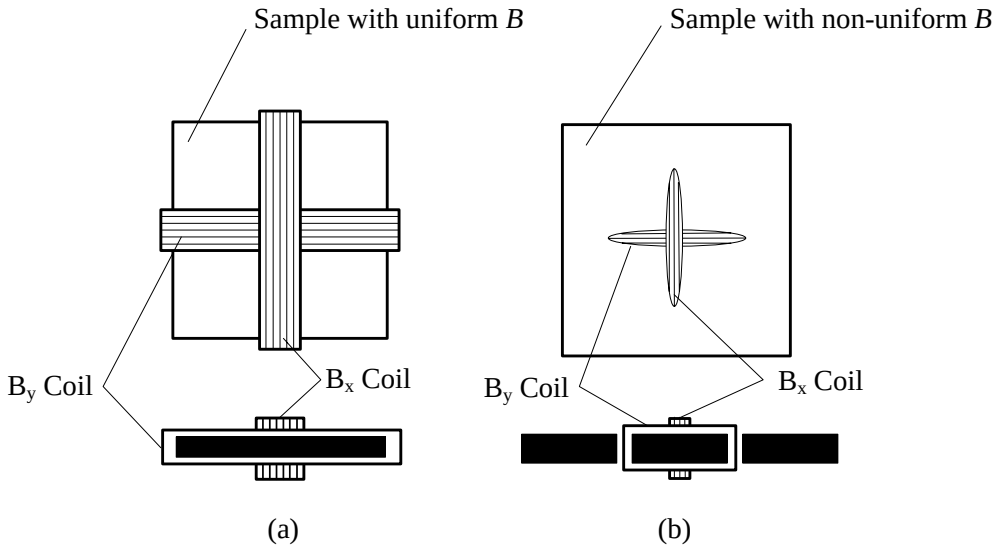

Figure 1.4: *B* coil settings for sample with (a) uniform *B*, and (b) nonuniform *B*.

When the magnetic flux density is uniformly distributed over the cross section of a sample, the sensing coil can be wound around the whole sample, as illustrated in Figure 1.4 (a). If the flux density is nonuniform over the cross section of a sample, the sensing

coil can be threaded through small holes at the position of interest, as shown in Figure 1.4 (b).

Besides the methods described above, the Hall Elements method can also be used for measuring the magnetic field strength at the surface sample, but because of the difficulty of installation, this method is not commonly used in rotational core loss testers, except the one using a rotating disk sample developed by Flanders in 1985.

In addition, there is a method equivalent to a one-turn search coil called ***B*** tips, which is more suitable than ***B*** sensing coils for batch measurements. In practical measurement, high-quality preamplifiers are required, since the voltage signal obtained from the tip is very weak. The method is also very difficult to exclude stray fluxes through the air, which may become significant when the sample size is small. Therefore, the sensitivity of this method is lower than that of the ***B*** search coil.

1.4 Motivation and Aim of the Work

Data obtained from the test apparatus which has been used in this thesis for making alternating and rotational loss measurements could aid machine designers and provide useful information for the modelling of magnetic properties, such as core losses. Such data may also help electrical sheet producers to improvement and develop low loss materials for use in rotating machine cores. Many researchers have studied rotational losses in electrical steel sheets over the years and a number of techniques for making measurements have been described in Chapter 3. However, at the present time, no international standard has been agreed for measuring the power losses under rotational field excitations.

The aim of this work is to measure the magnetic properties of an electrical steel sheet under alternating and rotating flux with different fundamental frequencies and different values of flux density. Power losses under one and two-dimensions are then calculated in the electrical steel sheet by using these measurements. In addition, a loss model has been proposed with different parameters. The data obtained from the experimental work is being used to identify these parameters.

1.5 Outline of the Thesis

An introduction to the work is presented in the first chapter, the methods and techniques used for measuring the magnetic properties of magnetic materials are briefly detailed. In Chapter Two, a literature study about loss calculations in electrical steel sheets is introduced, while the measurements of magnetic properties of these electrical steel sheets are shortly mentioned in Chapter Three. In Chapter Four, the measurement apparatus used in the experimental work for measuring the magnetic properties of an electrical steel sheet is presented and the results obtained from the experimental work are reported and discussed in the same chapter. The data obtained from the measurement device is used in Chapter Five to optimize the parameters of the dynamic loss-model by using the nonlinear least-squares method. A general discussion and conclusion of the work is stated in Chapter Six.

Chapter 2

Literature Review on Iron-Loss Calculations

This part of the thesis, attempts to places emphasis on the iron loss calculation methods used nowadays and reviews the published literature that has been made by many authors dealing with iron loss calculation methods in electrical machines and electrical steel sheets, associated with the distribution and computation of the magnetic field.
The published literature has shown that there are two types of methods that can be used to calculate and evaluate the iron loss (core loss) in electrical machines and electrical steel sheets (Saitz 1997).

The first method (experimental approach) that has to be used is connected to a simplified model of the core which deals with exclusion and omits the iron loss effects from the field calculation. After solving the magnetic field by means of the simplified model, the calculation of the iron loss can be evaluated by using the empirical or semi empirical formula, which concerns the rotating and alternating flux conditions in terms of magnetic flux density and magnetic field strength.

The experimental method (simple models) gives only quantitative information and it does not allow separation of the iron loss into hysteresis, classical and excess losses. Therefore, in order to fully understand the sources of the core loss and the physical substance behind this loss, mathematical modeling and computation of the iron loss are required.
The computational approach which includes all methods dealing with the magnetic field calculation considering the iron loss, is the second method that can be followed to calculate the iron loss precisely. This method can be combined with the magnetic field analysis and the inclusion of the iron loss effects through the computational process of the magnetic field is taken into account.

2.1 Iron Loss Calculations under Alternating Flux

Typically, the variation of the flux density can be either alternating or rotating. Moreover, the alternating flux density can be purely sinusoidal or non-purely sinusoidal, and the non-sinusoidal flux density may (or may not) cause minor loops from the point of view of the hysteresis phenomenon.

Rotational variation of the flux density in a similar way can be divided into purely rotational (circular) or non-purely rotational (elliptical), which can yet take any particular shape. In typical situations, it has been generally accepted for a long time that the average power loss in unit volume per cycle of any material consists of the sum of a hysteresis, P_{hys}, and eddy-current (dynamic), P_{dyn}, contributions.

$$P_{\text{total}} = P_{\text{hys}} + P_{\text{dyn}}$$

The eddy-current loss, P_{dyn}, can be separated into classical loss, P_{class}, and excess loss, P_{exc}, and by using these two contributions of the eddy-current loss and relating them to any predictive approach is the phenomenological concept of loss separation where the total power loss, P_{total}, at a given magnetizing frequency is expressed as

$$P_{\text{total}} = P_{\text{hys}} + P_{\text{class}} + P_{\text{exc}}$$

Pry and Bean (1958) used a simple domain wall model to calculate the energy loss resulting from eddy currents in magnetic sheet materials. The eddy current losses have been calculated explicitly for the sinusoidal induction excitation.

According to the statistical loss theory based on the work of Bertotti (1988) and Fiorillo and Novikov (1990), in the case of a lamination of thickness *d* and in the range of magnetizing frequencies where the skin effect is negligible, the dynamic loss is equal to the classical loss, and the next expression holds only for low frequencies or low conductivities.

$$P_{\text{dyn}} \equiv P_{\text{class}} = (\pi^2 \sigma d^2 B_{\text{max}}^2 f_{\text{m}}^2)/6$$

where B_{max} is the peak value of the flux density, *d* is the thickness of the lamination, σ is the electrical conductivity of the material, and f_{m} is the magnetizing frequency. It is important to note that the expression for the classical eddy-current loss neglects the reaction of eddy-currents on the distribution of magnetic field, i.e. the magnetic flux density is assumed to be uniform over the cross-sectional area of the lamination, and this

will be approximately correct only when the lamination is effectively thin. When the frequency increases or laminations are thick, errors in this situation may occur. This may explain the difference between the predicted and measured results investigated by Zhu et al. (1993), who found that the difference was higher under square wave than under sine wave voltage excitation.

According to the statistical theory of eddy-current losses developed by many authors, the basic physical mechanism governing excess losses in soft materials is identified with the competition between the external magnetic field, applied uniformly in the sample, and highly inhomogeneous local counter fields due to eddy-currents and micro structural interactions (Bertotti 1988), and the expression of the excess losses can be written as

$$P_{\text{exc}} = C_0 (B_{\max} f_{\text{m}})^{1.5}$$

where C_0 is the fitting parameter identified from the sinusoidal alternating single sheet loss measurements. One has to keep in mind that the discussion presented above is restricted (except the hysteresis loss) to the sinusoidal shape of the flux density waveform. The quasi-static hysteresis loss P_{hys} can either be obtained experimentally or estimated and among the hysteresis models available, the Preisach model appears to be the most practical model due to its easy parameter identification and considerable accuracy.

Based on the previous discussion, it is obvious that the behavior of the total loss in unit volume per cycle, P_{total} , under sinusoidal magnetization at the frequency f_{m} , can be written as

$$\begin{aligned} P_{\text{total}} &= P_{\text{hys}} + P_{\text{class}} + P_{\text{exc}} \\ &= P_{\text{hys}} + (\pi^2 \sigma d^2 B_{\max}^2 f_{\text{m}}^2)/6 + C_0 (B_{\max} f_{\text{m}})^{1.5} \end{aligned}$$

and it is clear from the expression of the total power losses that the eddy-current losses will dominate the total loss at high frequencies.

As mentioned previously, one of the field excitations can be an alternating waveform, which can be either sinusoidal or nonsinusoidal.

Methods proposed so far in the literature to predict magnetic losses under nonsinusoidal induction appear unable to give accurate results.

These models always assume that the dynamic loss under a generic flux induction can be directly expressed in terms of the effective value of the waveform derivative $(\mathrm{d}B/\mathrm{d}t)$.

Practically, magnetic flux in electrical machines such as transformers and rotating machine cores is often a non-sinusoidal flux waveform, and leads to an overall iron loss figure different from the one expected under a sinusoidal situation. Correct predictions of power losses under nonsinusoidal (distorted) flux waveforms is , therefore, an important condition to machine design, especially when dealing with large apparatus where rigorous efficiency standards are required. From the hysteresis phenomenon point of view, this nonsinusoidal flux density variation can be such that it either causes minor loops or it does not. In cases where minor loops do not occur, the hysteresis loss, P_{hys}, does not depend on the magnetic waveform, and it will be only related to the maximum value of the flux density, $B_{\max}$. In such a case, the hysteresis loss, P_{hys}, can be approximately calculated by using an empirical Steinmetz formula

$$P_{\mathrm{hys}} = C_{\mathrm{h}}\, f_{\mathrm{m}} B_{\max}^{n}$$

where C_{h} and n are constants depending upon the material used. The Empirical Steinmetz formula is not valid in cases where the induction waveform causes minor loops, and alternative methods have to be used.

Lavers et al. (1978) proposed a simple and practical method of correcting the hysteresis loss in a thin lamination for the effects of minor loops, and they suggest an empirical correction to the Steinmetz formula as follows

$$P_{\mathrm{hys}} = K_{\mathrm{h}} C_{\mathrm{h}}\, f_{\mathrm{m}} B_{\max}^{n}$$

where K_{h} is the hysteresis loss correction factor, which can be written as

$$K_{\mathrm{h}} = 1 + \frac{k}{B_{\max}} \sum_{i=1}^{N} \Delta B_i$$

the exact correlation gives values of k in the range 0.6 to 0.7, depending on the material being considered, and ΔB_i, $i = 1,2,...,N$, is the magnitude of the i'th flux reversal, and in any given half cycle, reversals of magnitude ΔB_i occur either singly or in pairs. These flux reversals result in the so-called *minor* hysteresis loops.

Another method presented by Arkkio and Niemenmaa (1992) tackled the problem of the minor loop by introducing a weighting function $f(|B|)$, where $|B|$ is the absolute value of the flux density. The value of the weighting function was taken as half of the horizontal distance between the walls of the major hysteresis loop. Through their measurements, they found that the weighting function first increases with the flux density and then rapidly decreases to zero when the flux density reaches saturation. They used two simple weighting functions, the first weighting function is constant and the second grows linearly with the flux density up to 2.16 T. At higher flux densities both functions were equal to zero and when the flux density is zero, both functions were equal to the coercivity. The energy density $\mathrm{d}w$ dissipated by the flux density change $|\mathrm{d}B|$ was expressed by

$$\mathrm{d}w = f(|B|)|\mathrm{d}B|$$

Arkkio and Niemenmaa obtained excellent results for no-load iron losses for both sinusoidally-excited and inverter-excited induction machines. Their iron loss model had two components, corresponding to eddy-current and hysteresis loss. Eddy-current losses were obtained by decomposing the flux in each element into its time-harmonic components, and then summing on a harmonic-by-harmonic and element-by-element basis. The flux density was calculated as the root of the square sum of orthogonally directed flux densities. The hysteresis loss was determined using either the same harmonic decomposition, or by a method based on an idealization of the shape of minor loops.

Fiorillo and Novikov (1990) showed that it is possible to predict the power losses precisely in ferromagnetic laminations under nonsinusoidal magnetic flux by specifically considering the dependence of the hysteresis loss, P_{hys}, the classical loss, P_{class}, and the excess loss, P_{exc}, components on the derivative of the magnetic waveform, $(\mathrm{d}B/\mathrm{d}t)$.

Through the generalization of experimental and theoretical results under sinusoidal excitation, they assumed that

$$P_{\mathrm{hys}} \propto \left\langle \left| \frac{\mathrm{d}B}{\mathrm{d}t} \right| \right\rangle, \quad P_{\mathrm{class}} \propto \left\langle \left(\frac{\mathrm{d}B}{\mathrm{d}t} \right)^2 \right\rangle, \quad P_{\mathrm{exc}} \propto \left\langle \left| \frac{\mathrm{d}B}{\mathrm{d}t} \right|^{1.5} \right\rangle$$

The component, P_{hys}, the hysteresis loss, is the area of the quasi-static hysteresis loop multiplied by the magnetizing frequency, and the component, P_{dyn}, the dynamic loss, is in turn assumed to be the sum of a classical contribution, P_{class}, and an excess one, P_{exc}. In the limit of a perfectly homogeneous material there are no excess losses, and P_{dyn} reduces to the rigorously computable classical loss P_{class}.

Fiorillo and Novikov (1990) worked on the case where no local minima appear in the induction waveform (absence of minor hysteresis loops). They assumed that the hysteresis loss, P_{hys}, is independent of the particular wave shape and it is only related to the maximum value of the flux density, $B_{\max}$, which is a condition that is met in the practical devices, and because of this their application was only concentrated on the role of dynamic loss, P_{dyn}. The expression of the induction as a Fourier expansion:

$$B(t) = \sum\nolimits_n B_n \sin(2n\pi f_{\text{m}} t + \varphi_n) \qquad (n = \text{odd};\ \varphi_1 = 0)$$

with B_1 the peak amplitude of the fundamental component, and the values for B_n and φ_n are the amplitude and phase of the *n*th harmonic component, respectively. Standard calculations give the classical power loss per unit volume

$$P_{\text{class}} \propto \left\langle \left(\frac{\mathrm{d}B}{\mathrm{d}t} \right)^2 \right\rangle \Rightarrow P_{\text{class}} = \frac{1}{T} \cdot \int_0^T P_{\text{class}}(t)\,\mathrm{d}t = \frac{\sigma d^2}{12T} \cdot \int_0^T \left(\frac{\mathrm{d}B(t)}{\mathrm{d}t} \right)^2 \mathrm{d}t = \frac{\sigma \pi^2 f_{\text{m}}^2 d^2}{6} \cdot \sum_{n=0}^{\infty} n^2 B_n^2$$

where the instantaneous value $P_{\text{class}}(t)$, proportional to $(\mathrm{d}B/\mathrm{d}t)^2$, and this equation has generally been assumed in the literature to describe *all* of the dynamic losses

$$P_{\text{dyn}} = k \cdot f_{\text{m}}^2 \cdot \sum_{n=0}^{\infty} n^2 B_n^2$$

where *k* is a constant which has to be determined by the measurement of P_{dyn} under sinusoidal flux density conditions. The excess power loss expressed by Fiorillo and Novikov (1990) can be written as

$$P_{\text{exc}} \propto \left\langle \left| \frac{\mathrm{d}B}{\mathrm{d}t} \right|^{1.5} \right\rangle \Rightarrow P_{\text{exc}} = \frac{1}{T} \cdot \int_0^T P_{\text{exc}}(t)\,\mathrm{d}t = \frac{C_0}{T} \int_0^T \left| \frac{\mathrm{d}B(t)}{\mathrm{d}t} \right|^{1.5} \mathrm{d}t$$

where the instantaneous value $P_{\text{exc}}(t)$, proportional to $|\mathrm{d}B/\mathrm{d}t|^{1.5}$, the parameter C_0 is a fitting parameter identified from sinusoidal alternating single sheet loss measurements,

and T is the time period of the fundamental frequency component. Existing techniques for calculating iron losses based on a non-sinusoidal waveform typically resolve the flux density into a series of time-harmonic sinusoidal components. The total iron loss is then determined by simply adding the sinusoidal losses for each harmonic. This principle, however, is only valid for linear circuits and can lead to serious errors.

Moses and Shirkoohi. (1985) showed that the total iron losses can be determined from the harmonic field components as follows

$$P_{\text{total}} = \pi f_{\text{m}}^2 \cdot \sum_{n=1}^{\infty} n \cdot B_n H_n \sin\varphi_n$$

where B_n and H_n are the harmonic flux density and field strength respectively, and φ_n is the phase angle between B_n and H_n.

Nakata et al. (1970) identified the importance of the phase angle of the flux density harmonic components in the occurrence of minor loops in the hysteresis loop and the influence of these loops on the iron losses. The authors also introduced waveform distortion factors to account for the harmonic phase angles and described their application to the prediction of non-sinusoidal iron losses. The objective of the nonsinusoidal iron loss measurements was, therefore, to assess the influence of the harmonic phase angle on the total iron losses and to develop an empirical method based upon the form factor for modeling the losses.

Smith and Phipson (1991) used the variation of the form factor with the phase angle from the experimental measurements to define a distortion factor as follows

$$D = (1 + \Delta F)^2$$

where $\Delta F = 1.11 - F$. The factor 1.11 represents the form factor for a pure sinewave and F is the form factor of the distorted flux density waveform. This can be expressed simply in terms of the harmonic flux density components. The distortion factor is then used to modify the amplitude of each flux density component as in the following expression

$$\hat{B}_n^* = D\hat{B}_n$$

where $\hat{B}_n$ is the amplitude of the actual harmonic flux density and $\hat{B}_n^*$ is the modified value. The prediction of the iron loss can be calculated by summing the sinusoidal iron

loss appropriate to each modified flux density component. The authors showed that the modified method can predict the measured losses to an accuracy of approximately $\pm 5\%$ and represents a significant improvement on the conventional approach. Subsequently, the method described above is used to predict the iron losses for a distorted flux density waveform containing many harmonic components at differing phase angles.

Pry and Bean (1958) calculated the energy loss resulting from the eddy-currents in magnetic sheet materials by using a domain model. The domain model used was considered to be applicable for any induction up to saturation and for the frequency range up to that used in most electrical power applications. The eddy-current losses that have been calculated were for the case of sinusoidal induction excitation, and expressed in terms of the ratio of domain wall spacing to sheet thickness. There was good correlation between the results obtained and the measured values.

Walker et al. (2007) investigated the variation of the iron losses due to the effects of the nonsinusoidal alternating flux in electrical machines. The authors demonstrated how the flux waveform in the core of an electrical machine can vary nonsinusoidally which complicates the calculation of the iron loss in the machine. They conducted a set of measurements using an Epstein square arrangement where different degrees of harmonic are injected into the flux waveform which varies in both magnitude and phase. This was set up and calibrated against a single sheet tester and it included full compensation. The measurements were put forward to illustrate the additional iron losses and by using a set of linear approximations, the iron loss was calculated from the solution of the finite element analysis of the machine.

Mueller et al. (1995) have advanced a technique for calculating the iron losses in a cage induction motor using time-stepping finite-element analysis, which has given good correlation with measured iron losses under both no-load and full-load conditions. The model has been used to investigate the variation of iron loss with the load. It has been shown, both experimentally and theoretically, that the iron losses increase significantly from no-load to full-load. Theoretically, it has also been shown that this increase is due entirely to the increase in the harmonic fields caused by slotting.

2.2 Iron Loss Calculations under Rotating Flux

It has been estimated that motor core losses in the United States accounted for approximately 45 billion kWh of the energy generated in 1985 (Werner and Jaffee 1991). These losses cost motor users approximately 3 billion dollars in that year alone. Iron losses in motors occur due to alternating, high frequency, and rotational fluxes. Alternating losses occur predominately along the outer periphery of machine stators and in machine teeth. High frequency losses occur in machine teeth and rotor surfaces. Rotational losses occur at the roots of stator teeth and all along the inner portions of the stator yoke. At a given induction level, rotational losses may be several times larger than alternating losses. To a lesser extent, rotational losses also occur in the rotors of induction motors due to the difference in rotational velocity between the rotor and the main magnetic flux. As a consequence, it has been estimated that over 50 % of the iron losses in an induction motor are caused by rotating magnetic flux conditions.

Even though it has long been realized that a considerable amount of the total core loss in the stator core of a rotating electrical machine is caused by the rotating magnetic field, alternating core loss models were generally employed due to the lack of data and correct models for rotational core losses.

The iron loss associated with the torque caused by the angle of lag between $\boldsymbol{H}$ and $\boldsymbol{B}$ is called the rotational power loss which is as important as the alternating loss.

The total magnetic power losses are computed by using the Poynting vector theorem which can be written as

$$P_{\text{total}} = \frac{1}{T}\int_T H \cdot \frac{\mathrm{d}B}{\mathrm{d}t}\mathrm{d}t = \frac{1}{T}\int_T \left(H_{\text{x}} \frac{\mathrm{d}B_{\text{x}}}{\mathrm{d}t} + H_{\text{y}} \frac{\mathrm{d}B_{\text{y}}}{\mathrm{d}t} \right) \mathrm{d}t$$

and similar to the case of the alternating core loss, the rotational core loss in an electrical steel sheet can also be separated into rotational hysteresis, eddy current, and excess losses. The rotational power loss occurs in the regions of electromagnetic devices such as rotating machines and transformers, where the direction of the flux density varies in the plane of the laminations. These regions in rotating machines are at the roots of stator teeth and all along the yoke of the stator.

There are a number of different methods that have been proposed to improve the accuracy of the core loss estimation, but most of these methods require measurements on the motors and they cannot be applied if a prototype is not available. In other cases a great amount of data about the behavior of the magnetic material is needed.

Fiorillo (1991) discussed the quantitative connection between rotational and alternating hysteresis losses in isotropic polycrystalline magnetic laminations, with special emphasis placed on the magnetization process in the weak field domain. Such a model, however, is unable to correctly predict the experiments at medium and high flux densities. With circular *B*, the rotational eddy current loss is twice as much as the alternating eddy current loss. The rotational excess loss can be modeled using the same formula as for the alternating excess loss, but the coefficient of the rotational excess loss is generally a function of flux density, and eventually reduces to zero when the material is saturated and all domain walls disappear.

An improved approach to iron losses prediction in rotating electrical machines was proposed by Bertotti et al (1991). The core losses in rotating electrical machines (induction motor) are estimated through direct use of the standard Epstein loss data of the employed magnetic laminations, without introducing empirical correction factors. The prediction was based on a numerical finite element approach to magnetic flux distribution, coupled with a physical model of losses in ferromagnetic laminations under generic flux excitation, which takes into account the specific role of the hysteresis, classical and excess loss components. In a more realistic approach, the role of harmonics and rotational fluxes must be accounted for, in association with the basic concept of loss separation.

Based on the loss measurements under 50 Hz sinusoidal alternating flux and purely rotating flux, in non-oriented FeSi laminations which have been done by Fiorillo and Rietto (1990), Bertotti et al (1991) suggested a general relationship between alternating (P_{hys}^{alt}) and circular (purely rotational P_{hys}^{circ}) hysteresis loss components as a function of peak flux density (B_{max}). Under purely rotational flux, the relation was performed by the expression

$$P_{hys}^{circ} = r_{hys}\, P_{hys}^{alt} \Rightarrow r_{hys} = P_{hys}^{circ} / P_{hys}^{alt}$$

which found that r_{hys} is a monotonous decreasing function of induction. Their experiments showed that r_{hys} is fairly independent of the type of lamination and it is always lower than 1 when above approximately 1.5T. In the case of elliptic flux density, the authors computed the hysteresis core loss under elliptical flux (purely elliptical or

distorted) $P_{\text{hys}}^{\text{ellipt}}$ using a linear interpolation between the alternating and purely rotational loss, giving

$$P_{\text{hys}}^{\text{ellipt}} = \left[1 + \text{c}(\text{r}_{\text{hys}} - 1)\right] P_{\text{hys}}^{\text{alt}}$$

where c is the ratio of the minor to major axis of the ellipse $(\text{c} = B_{\text{min}} / B_{\text{maj}})$. According to this ratio, hysteresis loss under the elliptical flux will be equal to the hysteresis loss under the purely rotating flux density $(P_{\text{hys}}^{\text{ellipt}} = P_{\text{hys}}^{\text{circ}})$ if c = 1, and it will be equal to the hysteresis loss under the purely alternating flux $(P_{\text{hys}}^{\text{ellipt}} = P_{\text{hys}}^{\text{alt}})$ if c = 0. The flux waveform distortion does not affect the hysteresis loss (provided there are no minor loops) which means that the equation above can be used for the calculation of $P_{\text{hys}}^{\text{ellipt}}$ even if the orthogonal components of the flux density $\boldsymbol{B}$ are non-sinusoidal.

Zhu and Ramsden (1993) used the same linear interpolation to calculate the hysteresis core loss under elliptical flux density using another expression

$$P_{\text{hys}}^{\text{ellipt}} = \text{c} P_{\text{hys}}^{\text{circ}} + (1 - \text{c}) P_{\text{hys}}^{\text{alt}}$$

where the alternating hysteresis loss $P_{\text{hys}}^{\text{alt}}$ can be calculated by using the law of Steinmetz

$$P_{\text{hys}}^{\text{alt}} = C_{\text{h}} f_{\text{m}} B_{\text{maj}}^{n}$$

and the hysteresis loss component under the circular flux $P_{\text{hys}}^{\text{circ}}$ is obtained from the measurements, which has been modeled as well by Zhu et al. (1995).

The work of Zhu et al. (1995) presented the measurement and modeling of core losses with various rotating flux density vectors in electrical steel sheets. The models were applied to the calculation of the core losses in the stator core of a permanent magnet motor at no load. The model presented by the authors was based on the similarity between the curve of the rotational hysteresis loss against the flux density $\boldsymbol{B}$ or magnetization $\boldsymbol{M}$ and the torque/slip curve of a single-phase induction machine, it is postulated that the specific rotational hysteresis loss per cycle in an electrical steel sheet can be expressed in terms of four parameters a_1 (in J/Kg), a_2, a_3 (non-dimensional), and M_{s} (saturation magnetization in T). The model was verified by fitting the curves of the rotational hysteresis loss for both grain oriented and non-oriented electrical steel sheets reported by the researchers Cecchitti et al. (1978) and measured by the authors, where an error

estimator assessed the accuracy of the model. With a circular flux, the authors also calculated the rotational eddy current loss in thin laminations, and similarly, the rotational excess loss was given.

Zhu et al. (1994) have shown by the measurements that the linear interpolation between alternating and circular (purely rotational) hysteresis loss is a rough estimation. For better estimation they proposed a quadratic function in terms of the total rotational loss as a more accurate formula

$$P_{\text{total}}^{\text{ellipt}} = \text{c} \cdot P_{\text{total}}^{\text{circ}} + (1\text{-c})^2 \cdot P_{\text{total}}^{\text{alt}}$$

where $P_{\text{total}}^{\text{ellipt}}$ is the total loss under elliptical flux, $P_{\text{total}}^{\text{circ}}$ the total loss under purely rotational flux and $P_{\text{total}}^{\text{alt}}$ the total loss under alternating flux (sinusoidal or distorted).

Zhu and Ramsden (1995) used the same equation above to calculate the total hysteresis loss under elliptical flux density. In essence, an arbitrary flux density waveform contains higher harmonics, which are neither circular nor strictly elliptical. For orthogonal components of the magnetic flux density, a series of elliptical harmonic flux density vectors will be obtained by using a Fourier series

$$B_x(t) = \sum_{n=0}^{\infty} B_{xn} \sin(2\pi n f_{\text{m}} t + \varphi_{xn}),\ B_y(t) = \sum_{n=0}^{\infty} B_{yn} \sin(2\pi n f_{\text{m}} t + \varphi_{yn})$$

with which the total hysteresis loss is then evaluated as a sum of the contributions from these harmonics.

Atallah et al. (1992) predicted the core loss of two permanent magnet brushless dc motors of different types of laminations under different operating modes with the three-term model for alternating core losses proposed by Bertotti (1988) and Fiorillo and Novikov (1990), but the rotational effects were not included. Instead, the core loss was calculated from the loss deduced for each of the two equivalent orthogonal alternating flux density components. Unfortunately, the theoretical results were not compared with the measurements.

Zhu et al. (1992) calculated the core loss of a permanent magnet motor using the finite element method and the three-term model. The loss terms for classical eddy current and excess losses were modified to include the rotational effects, but owing to the lack of

rotational hysteresis loss data of the material, the alternating hysteresis loss was calculated. The calculated results were about 20% lower than those measured at 1200 rev/min. Zhu and Ramsden (1993) improved the model by including the rotational hysteresis loss, and the difference was reduced to 10% instead of 20% at 1200 rev/min.
In this calculation, however, the hysteresis loss with an elliptical $\boldsymbol{B}$ was obtained by a linear interpolation between the rotational and alternating core losses. As was mentioned previously, this is a rough estimation.

Findlay et al. (1994) discussed the measurement of the rotational core loss in electrical steel sheets, and calculated the loci of $\boldsymbol{B}$ in the stator core of a three phase induction motor using a 2D finite element package *MagNet2D*, but the total core loss in the motor was not calculated due to the lack of data for the rotational core loss in the steel sheet.

In the switched reluctance motor (SRM), the flux waveforms are nonsinusoidal, and different parts of the magnetic circuit have different waveforms. Hayashi and Miller (1994) presented a new approach to taking into account these flux waveforms in the calculation of core losses. The relations between the fluxes of different parts of the magnetic circuits were given in the form of matrix equations, and eddy current losses for the complicated flux waveforms of the stator and rotor yokes were calculated. The matrices have shown the easiness of counting how many times the major and minor hysteresis loops occur at each pole and yoke segment. The approach proposed by the authors gives a systematic procedure for the core loss calculation. Although the approach is basically identical to a graphical approach, it has led to efficient mathematical calculations. The derived equations were simple and useful for the design of a switched reluctance motor. The need for accurate performance predictions for a switched reluctance (SR) motor has lead to the dynamic simulation, which is of interest to the investigation of the current waveforms, the voltage waveforms, the torque and the different losses of the motor.

A dynamic simulation of the switched reluctance motors (SRMs) including iron losses was reported by Li and Jufer (1994). The dynamic simulation model described by the authors was dedicated solely to a high speed analysis of a massive rotor switched reluctance motor. In this case, the motor saturation was relatively low, but the iron losses

in the rotor were so important that the rotor eddy current effect must be considered. The model proposed by the authors takes into account not only the main parameters of the motor and the driver device, but also the iron losses effect in the rotor was considered. The simulation results have proved that the model with the consideration of the eddy currents effect is significantly better than the one which the eddy currents effect was neglected.

Pasquale and Bertotti (1996) applied the dynamic Preisach model of hysteresis to the simulation of circuits coupled by soft magnetic cores. Hysteresis loops and secondary waveforms were measured and simulated in various conditions and frequencies. The dynamic Preisach model capabilities were extended to allow for the calculation of loaded secondary waveforms. Controlled primary current conditions were used to simulate the voltage and current response of the secondary circuit under different resistive loads with no free parameters.

Materu and Krishnan (1988) studied core losses using the harmonic analysis of the flux density at different parts of the magnetic circuit. This method has the advantage that the losses contributed by each harmonic can be obtained by a look-up process from the core loss data in the form of the curves of core loss at different frequencies and flux densities. The method makes no attempt to separate the eddy current and hysteresis losses based on physical theory, and it presupposes that the core loss data is valid in the presence of arbitrary combinations of harmonics.

The conventional approach to core loss prediction using the Fourier series of the space wave of the air gap flux density is not applicable for surface mounted permanent magnetic motors. Gordon and Liu (1990) proposed an alternate approach based on the concept that the eddy current losses are proportional to the square of the time rate of the change of flux density. Since the permanent magnet motors with surface-mounted magnets have no rotor windings and thus no rotor resistance loss, the authors focused only on the remaining loss component and prediction of the hysteresis and eddy current losses in the stator teeth and yoke. The results of the core losses prediction were compared to the losses measured on a 4-pole permanent magnet motor to confirm the applicability of their approach.

Amar and Kaczmarek (1995) proposed a simple, efficient, and general method for the estimation of the iron loss under any nonsinusoidal voltage without multiple zero crossings (without minor hysteresis loops). The method was based on the principle of the loss separation model, where the iron loss is decomposed into hysteresis, classical and excess loss components. The voltage waveform was identified by the form factor coefficient, making it easily accessible. The method proposed by the authors does not require any knowledge of the voltage harmonic spectrum. The case of three regimes, the rectangular pulse, the pulse width modulation (PWM), and the fundamental, plus the controlled third harmonic voltages, were treated and a satisfactory prediction of the iron loss was obtained.

A method predicting the iron losses in magnetic laminations for various excitations, using a reduced number of parameters was done by Darwaz et al. (1994). A dynamical presentation model of the instantaneous magnetic flux has been presented under the assumption of losses separation. In order to enlarge the validity area of this behavioral technique, the authors have presented an improved model which takes into account at the same time, the eddy current and hysteresis effects. The experimental device was used to perform the validity tests, and comparison between the computed and experimental losses. The method applied to the prediction of the iron losses gives results showing good correlation with the experiment.

Saari and Arkkio (1994) dealt with the calculation of losses in a high-speed asynchronous motor. The authors used a time-stepping, finite element method to calculate the electrical losses and semi-empirical equations to evaluate the friction losses (losses in air). The calculated losses were compared with the measured ones for a 60 kW, 100,000 rpm induction motor. The calculated electrical losses were compatible with the measured ones. The difference between the measured and calculated air friction losses increased with the rotational speed, and the error was about 20% at a speed of 100,000 rpm.

An improved method for predicting iron losses in brushless permanent magnet dc drives was reported by Atallah et al. (1992). The procedure has been developed to predict the stator iron loss in a brushless dc motor operating under any specified load condition. Finite element analysis was employed to obtain a series of instantaneous magnetostatic field distributions within a motor. The iron loss was computed from the temporal and

spatial variation of the flux density distribution. The method showed that the operating condition can have a significant effect on the level and distribution of iron losses. The method can also be applied to other types of machine and drive formats.

From the flux density waveforms, the associated harmonics and flux density reversals were analyzed, and the corresponding impact on the hysteresis and eddy current losses was computed using a well known method first introduced by Lavers et al. (1979), in conjunction with the Epstein core losses curves of the laminations. The authors stated that, even under the present sinusoidal excitation conditions, the harmonic contents in the radial and tangential flux density waveforms in the motor core have a direct effect on the magnitude of the core loss. The losses computed from the distorted flux density waveforms were compared with conventionally computed core losses obtained using only the fundamental components of the flux density waveforms. It was reported that the hysteresis core loss for the distorted flux density waveforms increased by about 25% from the loss obtained using the conventional method, while the eddy current loss for the distorted waveforms was 125% higher than the eddy current loss calculated by the conventional method. Therefore, harmonic effects should be taken into consideration in computing core losses of such machines, even for sinusoidal voltage excitation.

Akbaba and Fakhro (1992) calculated the iron loss from the field distribution in reluctance augmented shaded-pole motors using the finite element method. No-load and loaded cases were considered separately. The effect of the shading coil on the spatial distribution of the air-gap flux density was examined and it was found that the demagnetizing effect of the shading rings helps towards more uniform distribution of the air-gap flux. The correct paths of various flux linkages and saturating locations were identified. The authors solved a non-linear Poisson's equation using the finite element method in order to obtain the magnetic field distribution in the machine. The iron losses were calculated using the flux density distribution obtained over the cross section of the machine. The comparisons between the calculated and measured results were in good agreement.

Zuh et al. (1992) used the finite element method to calculate the core losses in complex geometries of a permanent magnet motor with nonsinusoidal, rotational fields. Techniques were developed for determining flux density waveforms from finite element

calculations, and their use in predicting core losses using a combination of frequency and time domain methods. The improved model for alternating core losses in electrical steel sheets under both sinusoidal and nonsinusoidal flux density waveforms was studied. The core loss model was applied to a permanent magnet motor, taking into account only the rotational effects on the eddy current and excess losses. The comparison of the calculated and measured core losses was very close. Under sinusoidal and nonsinusoidal excitation, the authors found that the calculated and the measured core losses were closely correlated. Regarding the losses under the rotating field, the authors stated that the calculated loss was approximately 20% less than the measured loss and the difference between the calculated and measured loss was attributed to rotational hysteresis.

In rotational electrical machines, core losses are caused not only by alternating magnetic fields but also by rotational magnetic fields and it is important to be modelled correctly in an optimum design. Based on this fact, Zhu and Ramsden (1993) investigated the iron loss in electrical machines considering the rotational hysteresis loss. The authors constructed a single sheet core loss tester to measure the core losses of electrical steel sheets with an arbitrary flux density $\boldsymbol{B}$ and a novel sandwich arrangement of the magnetic field intensity $\boldsymbol{H}$ sensing coils was proposed to improve the accuracy of the rotational magnetic field measurement in a single sheet square specimen core loss measuring system. The losses were calculated from the measured magnetic field intensity and flux density.

A new approach was presented to resolving the total loss into four portions depending on the rotational and the alternating components of the magnetic field and flux density. Using this combined data and calculated flux density vector trajectories (FEM), the authors estimated the iron loss in a motor and only a rough estimation of the elliptical rotational hysteresis loss was used. When compared with the measurements, the differences between the measured and calculated core losses were now less than 10% at 1200 rpm, since the rotational hysteresis was taken into account. The authors concluded that the remaining discrepancy might be attributed to the possible rotor surface loss caused by the tooth ripples and the eddy current loss in the stator case.

Findlay et al. (1994) discussed rotational losses and how they are produced in the core materials of induction motors. The authors described a test procedure for determining the rotational losses in electrical steel sheets and a methodology for establishing the regions

where rotational losses occur, and the anticipated effects, and afterwards, they compared the results with standardized tests from an Epstein test procedure. They found that there was a significant difference in the loss results obtained for the rotational test versus the alternating current test and they stated that the rotational losses in electrical steel sheets were substantially larger than the alternating losses for the flux density investigated. In some regions, the alternating flux loss curves can be used with reasonable accuracy, in large areas of the machine, however, these values give losses that contain considerable errors. The authors also used the finite element method to investigate the magnetic flux density in the vicinity of a stator slot and the results of their preliminary investigation suggest the existence of regions of differing polarization. Particularly at the back of both the slot and tooth, an elliptical to nearly-circular polarization was found as was expected.

Nee and Nipp (1994) described a method to calculate the harmonic iron losses and eddy-current losses of inverter-fed induction motors. Particularly, a general method for the determination of hysteresis losses was presented. The authors described the principles of the iron loss evaluation in electrical machines and stated that the only rigorous way of determining this loss is the time-stepping of the system with the inverter and the motor. Moreover, the modeling of the iron should be taking the hysteresis and eddy-currents into account. However, this way of computing the iron loss takes much time and for this reason the authors calculated the magnetic field using FEM, where the magnetization curve was without hysteresis. The iron loss was then evaluated using a combination of the Jiles-Atherton hysteresis model, the Rayleigh theory and empirical expression. The calculated results were compared with the measurements carried out on the toroidal cores of laminated non-oriented standard silicon sheet steel. The major loop losses, minor loop losses and hysteresis losses of a flux with two superimposed frequencies were investigated. Then, the harmonic iron loss was also computed and measured on the PWM inverter-fed induction motor. The values calculated were found larger than the measured ones, which was attributed to the fact that the iron was not modeled correctly in the finite element analysis.

Cecchetti et al. (1978) used a technique proposed first by Kelly (1957) to measure the rotational power losses as a function of frequency and magnetization in grain oriented and isotropic 3% SiFe. All loss measurements were performed on disks of 19 mm diameter and thickness 0.33 mm, under different magnetization conditions, up to almost complete

saturation. The comparison between the predicted and measured losses gave excellent correlation.

Sanada et al. (2003) proposed a simple model to predict the iron loss in rotating machines considering the rotational variations of the flux vectors as well as the flux harmonic using the 2-D finite element method. The short-axis-to-long-axis rate of the flux vector trajectory ellipse at each harmonic frequency was utilized to calculate the additional iron loss due to the rotational field in the core of the rotating machine. By comparing the calculated results obtained by the conventional method and the proposed method with the experimental results, it has been verified that the precision of iron loss prediction on a rotating machine can be improved significantly.

Since the iron loss accounts for a large percentage of the total energy loss, there is an increasing need to predict this loss with satisfactory precision in the stage of design or during analysis to realize higher efficiency and performance. The iron loss calculations carried out by numerous researchers is an important issue in both design and analysis of electrical machines, and because of their complicated structure, flux distribution, and rotational variation of this flux, the iron loss calculations of electrical machines still present substantial difficulties and the accuracy form of such losses is still not available.

Chapter 3

Literature Review on Iron-Loss Measurements

The basic aim of this chapter is to give a general idea and survey of methods and techniques which have been recently used for core loss measurements of electrical steel sheets as a part of electrical machines, considering the measurement under alternating and rotating field excitations. Although quite a few rotational core loss measurements and domain structure observations have been carried out on different ferromagnetic materials by various researchers, the *mechanisms* of rotational core loss are still far from being fully understood.

3.1 Power Loss Measurements under alternating Field Condition

For the measurement of iron losses in electrical steel sheets, and because of the obvious considerable simplifications, the iron loss is mostly measured in electrical steel sheets using special configurations. As with the measurement of the alternating iron loss, the iron loss is usually measured in electrical steel sheets using the Epstein test (IEC 1978) method. The Epstein test (IEC 1978) is the standard test for detecting the alternating magnetic properties of materials at power frequencies using the wattmeter-ammeter-voltmeter method and Epstein test frame. This frame basically consists of a square iron core fabricated from strips of the lamination materials to be tested. The Epstein test can be approximately used for transformer design, but in rotating electrical machines, where a substantial portion of the iron core is magnetized under rotating flux condition, the Epstein test (IEC 1978) is, therefore, not enough to give reasonable results. Besides the Epstein tester, the single sheet tester (IEC 1992) and the ring method (IEC 1995) are widely used nowadays for the determination of the magnetic characteristics of materials under alternating field conditions.

3.2 Power Loss Measurements under Rotational Field Condition

The concept of rotational power loss and the general shape of the power characteristics were first discovered in the nineteenth century. Since then, a number of various approaches have been taken to study this phenomenon. Rotational power loss is important as it contributes up to 50% of the total core loss in rotating electrical machines. The rotational power loss also occurs in the T joints of three-phase transformers. Although the area subjected to rotational field is rather small, the increased losses may cause local overheating and consequently even destruction of such transformers. As for the measurement of the power loss under the condition of rotating flux and as was mentioned previously, a single sheet square specimen tester (single sheet tester) initiated by Brix et al (1982) appears to be the most favorable method, because of its flexibility to control the rotating magnetic flux pattern and the uniformity of the magnetic field in the sample, which results in high accuracy. The method is widely used by various researchers with many different modifications in order to determine the magnetic characteristics under rotating field conditions. The method is based on the measurement of the orthogonal components of the magnetic flux density and magnetic field strength B_x, B_y, H_x, and H_y. Using this method the rotational power loss is measured as the torque loss caused by the angle of lag between $\boldsymbol{H}$ and $\boldsymbol{B}$.

3.3 The Influence of PWM Inverter Supply on the Iron Loss

Many papers have been published recently on the issue of power loss measuring in electrical machines which have dealt with the measurements concerning the influence of the PWM inverter supply on the iron loss in electrical machines.

Based on the measurements, Boglietti et al. (1993) presented a complete analysis of the motor losses due to the inverter supply. The authors started from the analysis of the results obtained through the standard tests (no-load, short-circuit and load). The standard tests have been performed on 7.5 kW standard induction motors using a sinusoidal supply, square wave and PWM inverter supplies. The energetic comparison with different supply sources has been made using as a reference the same voltage and current fundamental values. To obtain the iron loss, the authors used the results of the no-load test. The no-

load loss minus the stator and copper losses gives the sum of the iron loss and mechanical loss. Since the mechanical loss could be approximately considered as constant, the sum expressed the behavior of the iron loss. The authors stated that the worst supply condition was represented by the PWM source from the energetic point of view. Three years after the publication of this work, the same authors continued their previous studies of the effects of the inverter characteristics on the iron loss increment in induction motors fed by pulse width modulation controlled converters. Laboratory tests based on no-load input power measurement were carried out and in order to avoid the influence of mechanical losses and rotor copper losses, difficult to be measured or computed, a special test bench with an unconventional test device was constructed. The test bench consisted of a standard industrial induction motor with a slotless rotor instead of the standard one. Practically, the rotor has been constructed as a laminated cylinder with the same diameter of the standard one. Under these conditions the rotor was not able to start and to rotate by itself, but it had to be put into rotation at the synchronous speed by connecting the rotor to a DC motor, as shown in Figure 3.1.

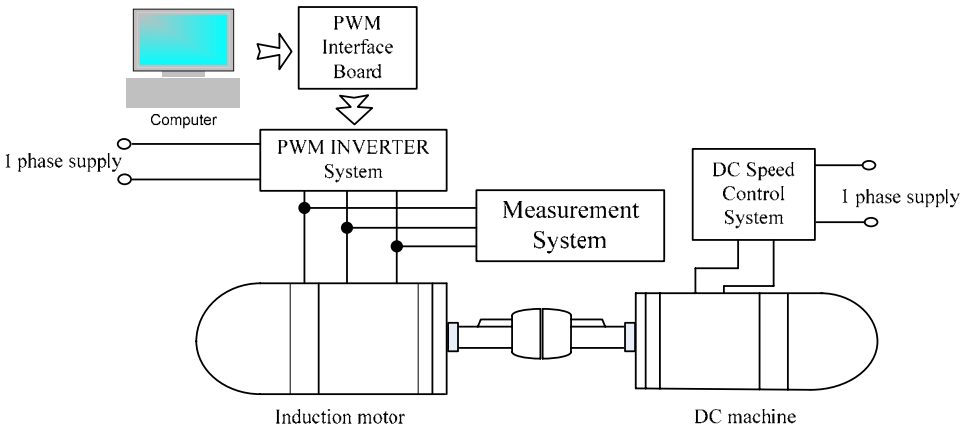

Figure 3.1: Proposed test rig.

With the two machines connected together a no-load test was performed and the influence of the modulation index, modulation waveform, and switching frequency of the inverter on the iron loss was under investigation. From the obtained results the authors suggested the operation of the inverter with the highest allowed modulation index. In this way the iron loss was reduced. They did not find the switching frequency as important as the modulation index from the core loss point of view. With the switching frequency increase,

a small diminishing of the iron loss was observed. However, the loss increase inside the power switches should also be taken into account. The modulation function waveform was not found to be an important factor on the iron loss increase. As mentioned above, the tests were carried out at no-load and the authors concluded that the result regarding the influence of the inverter characteristic on the iron loss could also be considered valid for a motor running under load condition. The reason for this generalization was that the only difference between no-load and load working conditions in an industrial induction motor, from the magnetic flux point of view, is the voltage drop on the stator impedance.

In (1990) a setup was developed by Fiorillo and Novikov to measure the alternating magnetic power loss in laminations (single strips, toroids, Epstein frames) under controlled induction waveform in the frequency interval 1 Hz - 100 kHz by means of a relatively complicated experimental setup with many electronic devices controlled by a personal computer as shown in Figure 3.2.

The basic elements of this setup were:

(1) A personal computer, which coordinates all the relevant measuring operations.
(2) A programmable 12 bit arbitrary function generator (Wavetek mod. 275).
(3) A circuit for the supply of power to the primary winding and for induction waveform control.
(4) A programmable transient recorder/data analyzer DATA 6000 (two channels, 9 bit, 18 MHz sampling rate).

In order to accomplish the waveform over a wide frequency range, the system was able to switch between two different circuits. Circuit b), which exploits negative feedback, was employed at a relatively low frequency (up to about 2 kHz). The programmed waveform $\dot{B}$ provided by the generator was compared, by means of the differential low noise amplifier A_2 (PAR mod. 113), to the signal induced on the secondary winding W_B, which was suitably amplified, if necessary, through A_4. The power amplifier A_3 (KEPCO mod. 72/5) provided in cascade the magnetizing current to the primary winding W_H. To ensure a symmetrical applied field, the integrating chain A_1, R_b, C_b was employed. It can be easily realized that, if the time constant R_bC_b is sufficiently large, any voltage offset arising on the resistor R_H would be automatically compensated by the integrator. Circuit c) was preferentially used at high frequencies, where the pervious feedback system became prone to spurious.

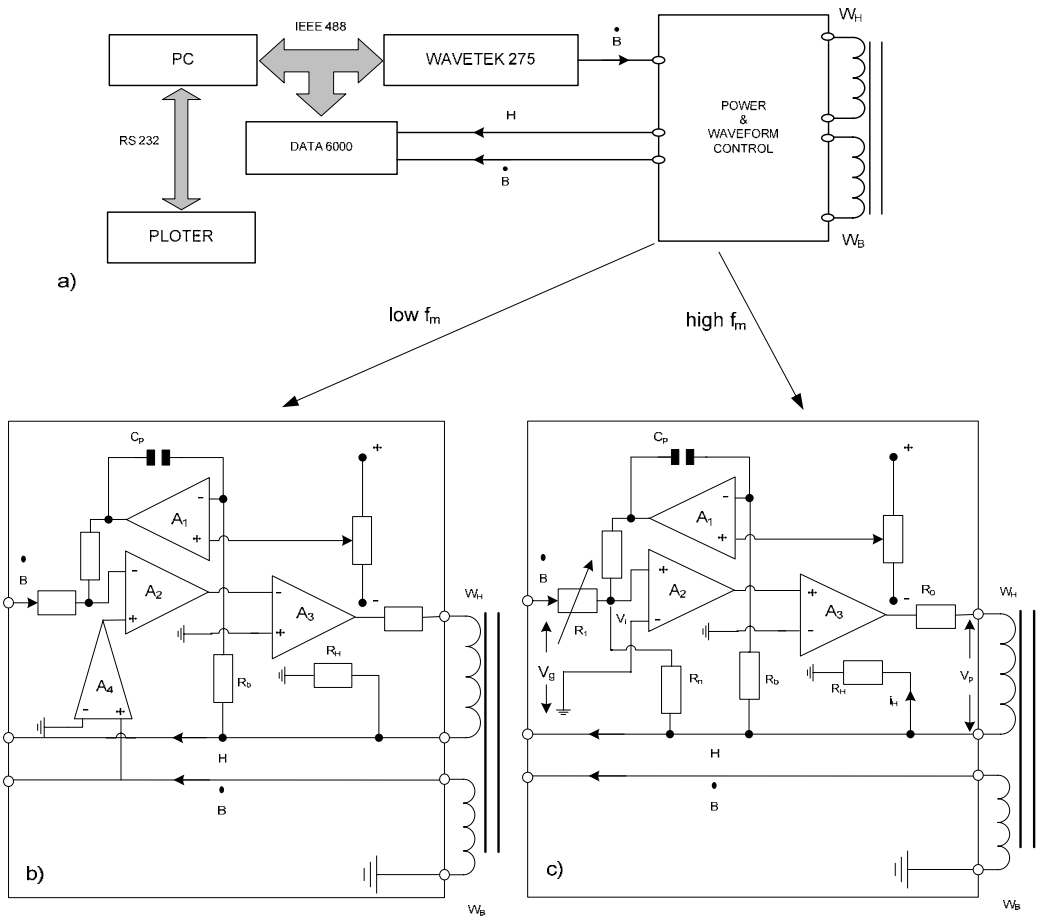

Figure 3.2: (a) Block scheme of the loss and *B-H* loop measuring set up. The system switches between two different waveform control circuits, shown in detail in (b) (low frequencies) and (c) (high frequencies).

In order to understand the principle work of the setup, an input voltage V_i is considered which can be expressed, if $R_H \ll R_n$, as

$$V_i = V_g \cdot R_n/(R_1+R_n) + i_H \cdot R_H R_1/(R_1+R_n)$$

where V_g is the voltage provided by the function generator. If K is the combined gain of the amplifiers A_2 (PAR mod. 113) and A_3 (0-500 KHz power amplifier Khron-Hite mod. DCA-50), the authors obtained the voltage on the primary winding as

$$V_p = KV_i - (R_o+R_H)\cdot i_H$$

$$V_p = KV_g R_n/(R_1+R_n) + Ki_H R_H R_1/(R_1+R_n) - (R_o+R_H)\cdot i_H$$

Therefore, if the condition

$$KR_1/(R_1+R_n) = (R_o+R_H)/R_H$$

is satisfied, the voltage on the primary winding V_p will be proportional to the programmed voltage V_g, independent of the actual value of the magnetizing current. To achieve this condition one regulates the amplifier gain K and the value of the resistor R_1. The primary current drop on the calibrated resistor R_H and the signal on the secondary winding W_B are sampled and processed by the DATA 6000 analyzer. A single 512 point period is stored, on both channels, up to about 30 kHz. It reduces to 180 point period at 100 kHz. At very low frequencies the H and B signals have to be amplified before sampling. The authors used a couple of PAR mod. 113 amplifiers for such a purpose. Care was taken in this case to avoid spurious phase shifts between the two channels. Since the DATA 6000 can be internally programmed, peak induction and loss values can be displayed, upon arming of the input amplifiers, in a continuous way, thereby providing an effective averaging of the results. Finally, the hysteresis loop can be recorded, if desired, through data transfer to the PC, scaling and digital plotting. The results were discussed in association with a general theoretical approach, where the hysteresis, classical and excess losses were separately considered. A formulation of the total power loss was presented and showed an excellent agreement with the experiment.
As mentioned previously, numerous papers have been published dealing with the influence of the inverter supply on the iron loss in electrical machines. This subject is largely investigated even in the magnetic materials using the Epstein frame.

Experimentally, Boglietti et al. (1991) studied the energetic behavior of two samples of soft magnetic materials (wound cores) fed by inverters. The authors dealt with the increase of iron losses by explaining them due to non-conventional voltage supply. Six-step and PWM inverter output voltages were selected as the excitation waveforms for the samples under test. This experimental setup has been used to measure the cores characteristic loops and the magnetic losses as shown in Figure 3.3.

The voltage distortion in the secondary winding of the transformer T_1 must not exceed the value limit accepted by the international standards. In order to check time by time the voltage quality, the following method has been proposed. Two voltmeters V_1 and V_2 have been installed in the secondary side of the step down transformer T_1. In particular, V_1 is a voltmeter to measure the rms voltage and V_2 is a voltmeter to measure the average voltage. The ‘voltage from factor’ (V_{FF}) can be defined by dividing the rms voltage by the

average one. The system shown in Figure 3.3 consists of a programmable function generator (F.G.) in order to supply a low power pure sinusoidal supply, power linear amplifier (A.M.), step down transformer (T_1) in order to increase current of the core under test and improve the current measurements, RC filter in order to cut down the dc current components and to avoid unwanted T_1 transformer saturations, digital scope (D.O.) in order to check the voltage waveform and the current peaks, digital multifunctionmeter (M.F.) which is a very flexible instrument and suitable for measurements in nonsinusoidal environment, and finally, a small adjustable resistance (RX) to limit the maximum core current during the hard saturation conditions.

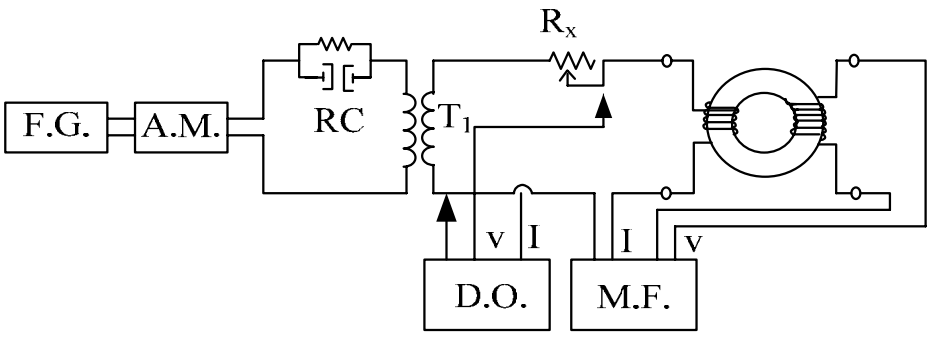

Figure 3.3: Measurement system setup.

The wound cores structured as samples had two windings, the primary with N_1 turns and the secondary with N_2 turns, which were wound together in order to achieve the best coupling. The results were quite informative and quantify the iron loss increase with a non-sinusoidal supply when compared to the results obtained by the standard tests (sinusoidal supply and Epstein method). However, with PWM supply the iron loss increased considerably. The authors attributed this increment to the heavy eddy current increase inside the iron core linked to the very particular waveform of the PWM supply. Furthermore, the authors stated that the comparison with the results obtained by a sinusoidal supply gives useful indications to electromagnetic-device designers, in order to develop the derating factors that have to be used for different magnetic materials used in devices fed by static power sources.

Kinnares et al. (1996) presented a novel measurement method for determining the extra harmonic loss in an induction machine fed from a PWM inverter. A significant improvement of this method over others is that the measurement is made whilst the machine is running normally or under any other defined operating condition.

The experimental setup for loss measurement is shown in Figure 3.4. The motor under test (7.5 kW induction motor of standard design) is fed from a commercial IGBT inverter that has been modified to accept PWM signals from a specially developed PWM generator. This PWM generator can produce all of the well-known PWM strategies with a user defined switching frequency as well as special PWM strategies that have been developed for loss measurement. For comparative tests, the system allows switching between the PWM strategies while the motor is running. The mechanical load on the test machine is provided by a DC dynamometer, which is controlled by using the classical Ward-Leonard Drive System. A field chopper on the Ward-Leonard machine allows the dynamometer armature current to be controlled in response to a torque demand input. A further slow integrating control loop operating on the actual shaft torque is used to trim the current demand. The harmonic power input to the machine is determined by measuring two line-to-line voltages and two line currents, which are fed into a 4 channel 12-bit transient digitizer. The voltages are measured using potential dividers, LEM hall effect transducers are used for current measurement, and then the voltage and current data are fed into a PC for postprocessing.

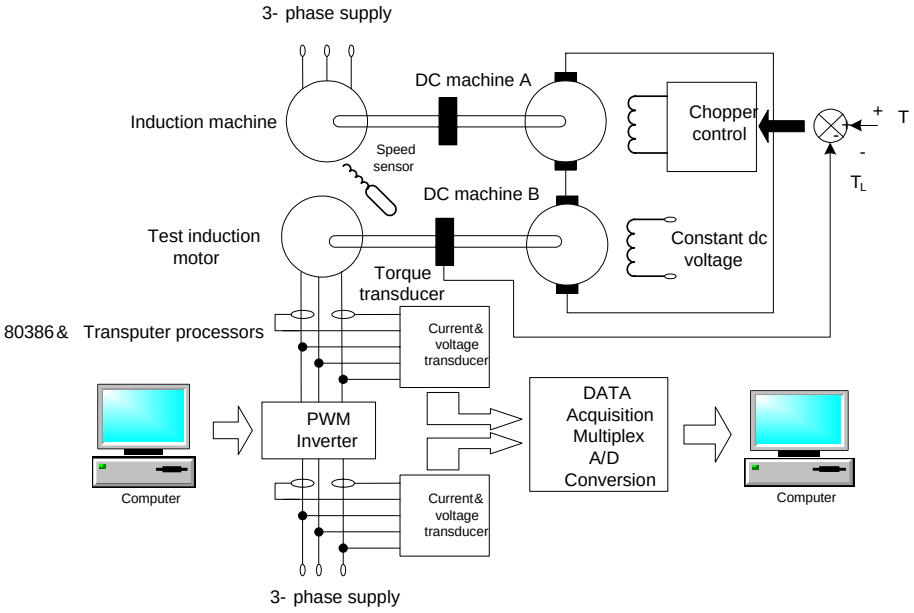

Figure 3.4: Experimental system for harmonic loss measurement.

To calculate the harmonic power input, a data record spanning an integer number of fundamental cycles is taken, and by taking the mean of the instantaneous voltage-current product, the total power input is calculated. The fundamental power for the same record

can be determined by using an FFT analysis to give the fundamental amplitude and phase information. The difference gives the total harmonic power input for a particular fundamental cycle. Alternatively, the power due to each harmonic can be calculated by using an FFT analysis to give the amplitude and phase information provided that the frequency components present have an integer number of cycles in the record length. From the loss measurement results, a loss factor can be defined which allows the loss on any PWM scheme to be predicted with a good degree of accuracy. Experimental results have been presented to confirm this.

Since more and more electromagnetic devices are supplied by static converters, the classification and evaluation of the energetic performance of soft magnetic materials with a static supply are really becoming mandatory. However, the papers that have been published on this issue are difficult to cover in a single report.

3.4 Methods for Measuring the Core Loss and Magnetic Properties of Magnetic Materials

A review of methods and techniques which have been investigated and used by numerous researchers in order to measure the power loss in electrical steel sheets from the obtained magnetic properties B_x, B_y, H_x, and H_y, will be discussed and explained through the following paragraphs.

Archenhold et al. (1960) measured the rotational hysteresis loss in grain-oriented silicon iron for various orientations and thicknesses with a rotating disk sample. The experimental results were discussed in terms of the multidomains concepts and of the Stoner-Wohlfarth single particle, of which the rotational hysteresis behavior has been evaluated.

Kaplan (1961) measured the core losses of grain-oriented and non- oriented silicon iron using cross samples under various flux conditions ranging from a pure alternating flux to a pure rotating flux. It was found that the grain-oriented iron was a lower loss material under all flux conditions, but this is not always true. Since a grain-oriented steel sheet has stronger anisotropy due to a texture which causes higher hysteresis loss, the rotational core loss in grain-oriented steel sheets can be higher than that in non-oriented steel sheets.

Strattant and Young (1962) studied the power frequency losses in a silicon iron alloy due to an elliptically rotating magnetic field with disk samples placed in the center of two perpendicular pairs of rectangular Helmholtz-type air-core coils, and predicted the losses approximately using a simple model without any physical basis. However, the model used only simulated core loss with elliptically rotating magnetic fields, while the basic physical phenomena were not described.

Boon and Thompson (1965) measured the alternating and rotational core losses at 50 Hz under various flux densities for both a hot rolled and cold rolled 3% silicon iron in a square sample of 0.33 mm laminations, using an improved thermometric method, and found that the ratio of rotational loss to alternating loss at 50 Hz in four squares SiFe samples was about 2:1 over a wide range of flux densities except at high flux densities.

Flanders (1967) developed a rotating sample magnetometer, which could be used for multiple purposes such as the measurements of magnetic moment and rotational hysteresis. The measurements were performed on a single-piece rotating sample. Sensing coils were used to detect the magnetization perpendicular to the applied magnetic field. The field metric method was used to evaluate the torque due to rotational hysteresis. To minimize the pickup error due to the variations in magnetic field or to coil motion relative to the magnetic field strength $\boldsymbol{H}$, a setup of two coils connected in series was employed. The method gives better results than the torque magnetometer, since the effect of mechanical friction has been removed.

Moses and Thomas (1973) measured the rotating magnetic flux and rotational core loss in silicon iron laminations with cross samples. The 2-D magnetic field was generated by the excitation windings wound on the cross sample. The rotational core loss was measured by the sensing coils ($\boldsymbol{B}$-coils) wound through very small holes in the center of the cross, while the magnetic field strength was determined from the magnetization current. In their setup, there was no flux density feedback control. Therefore, in grain-oriented samples, the magnitude of flux density was not kept constant.

Brix et al. (1982) built a fully computerized control and measurement system with cross samples of non-oriented steel sheets. In this system, both magnetic field strength $\boldsymbol{H}$ and

magnetic flux density ***B*** were obtained by the sensing coils, and the power loss was determined by the field-metric method (Poynting vector). However, the magnetic field in the center of the sample was not homogenous due to the shape of the sample, and the high values of the magnetic field in the center of the sample were difficult to reach.

Sasaki et al. (1985) built a measuring system using a single Epstein strip. Sensing coils were used to measure the magnetic field strength and magnetic flux density, and the core loss was calculated by the field-metric method. This system is quite similar to those using cross samples. A large amount of research on rotational core loss with cross samples, has been conducted by many other researchers, for example, Basak and Moses (1978), who studied the sensitivity to mechanical stress of the rotational power loss in silicon iron with cross samples and flux density feedback.

Brix et al. (1984) found that, the magnetic field was more uniform in a square sample than in a cross sample, and high values of magnetic field density can be reached in the center of the square sample. The authors developed a tester using square samples. This kind of tester system is known briefly as the square sample tester. In this system, ***B*** tips were exploited for detecting the magnetic flux density.

Enokizono and Sievert (1989) developed a very flexible system consisting of a horizontal magnetic circuit with a square single sheet sample and adjustable air gaps, an analog electronic circuit for flux density feedback control, and a computer which performed function generation and data acquisition in rotational core loss measurement. The magnetic field strength was picked up by conventional surface ***H*** sensing coils. For the flux density measurement, ***B*** sensing coils threaded through small holes in the center of square sample were adopted by Enokizono (1991), while ***B*** tips were used by Sievert (1991), which is more convenient for batch measurements. This system can be used to examine the behavior of ferromagnetic materials under either rotational or alternating magnetic field. Measurements of the rotational core losses of various electrical steels under rotational field have been performed with this system.

Zhu (1992) developed a system comprising a horizontal magnetic circuit with a square single sheet sample, feedback control system, and digital signal processing for the specification of flux density waveforms and data acquisition. Figure 3.5 illustrates the

schematic diagram of the whole testing system and the square sample tester. Guo et al. (2006) have used this tester and investigated the alternating and rotational magnetic properties of several magnetic materials, including the measurement, modeling, and application in analysis of rotating motors.

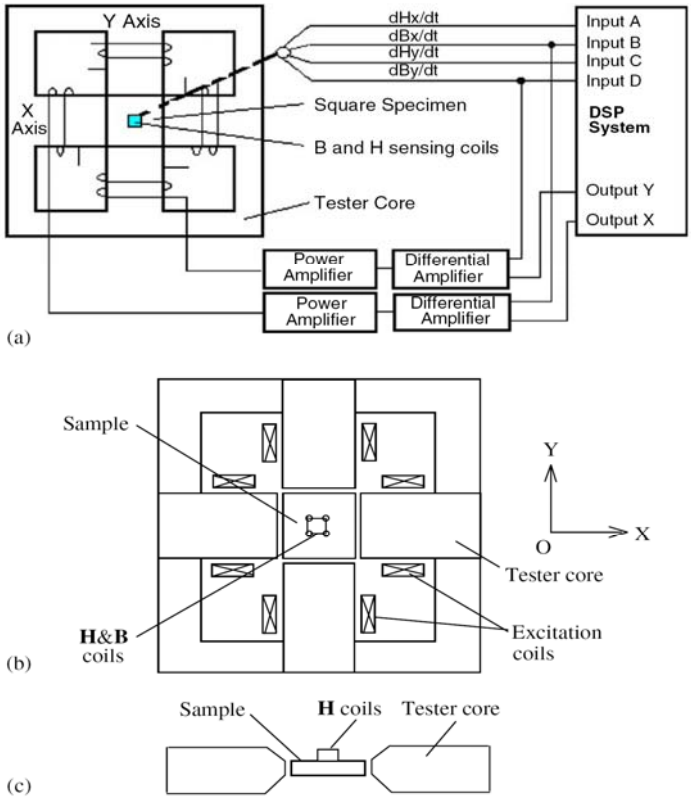

Figure 3.5: Schematic illustration of (a) block diagram of the 2D magnetic testing system, (b) the square specimen SST, and (c) position of the sample between magnetizing poles.

In conclusion, the computer-controlled square sample testing system is more advantageous than other types in the following aspects.

- Since the magnetic fluxes in the two perpendicular directions are controlled by feedback, the generated magnetic field excitations of various complex magnetic flux patterns can be used to simulate the actual situation happening in electrical machines where the magnetic field is rotating with either constant or varying magnitude.
- The measurement is carried out in the center of the sample where the field appears to be most uniform, which leads to more accurate results.

- More information can be obtained from the measured *B* and *H* waveforms which help in understanding the mechanisms of rotational core losses.
- Preparation of the sample is much simpler.
- The system can be conveniently incorporated into a system for domain structure observation, which is very important for understanding the mechanisms of rotational core losses.

The major drawback of the system is that it is difficult to control the flux density waveforms on the X and Y axes to be sinusoidal when the sample is close to saturation.

The Epstein frame has been used by Reyne et al. (1988) in order to obtain the experimental data from different samples of ferromagnetic materials. The principle of the Epstein frame used as shown in Figure 3.6 comprises

- A sample with dimensions of (0.24 × 0.03 × 0.0005 m) placed between two horizontal parallel windings.
- Two horizontal parallel windings, one used to provide the sample with a uniform excitation field as possible, and the other used to measure the field in the sample.
- A pickup head with a piezzo-electric transducer used to measure the deformation at one end of the sample, which depends on the value of the flux density, while the other end is fixed.
- A yoke made from ferromagnetic material.

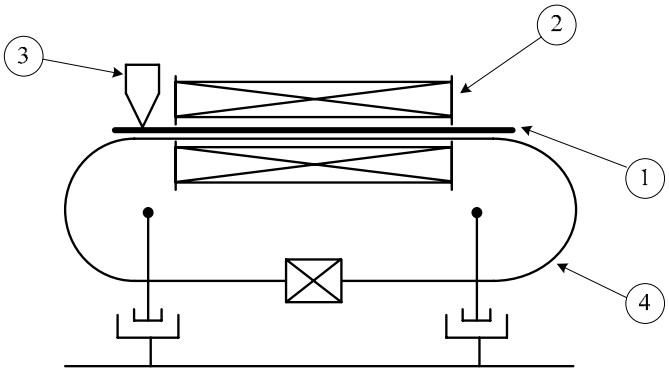

Figure 3.6: Principle of the Epstein frame used.

However, one of the reasons why the Epstein device cannot be easily replaced by sheet testers is that, systematic errors arise due to the overlapping of the sheet pieces in the corner of the Epstein core.

Zhu and Ramsden (1993) introduced a novel sandwich arrangement of magnetic field sensing coils to improve the precision of two-dimensional magnetic filed measurement in a single sheet tester. The authors calculated the total losses from the measured magnetic field intensity and flux density. Furthermore, the total loss was divided into four portions by resolving the magnetic field strength and flux density into rotational and alternating components.

A single sheet tester for rotational loss was used by Morino et al. (1993) to measure the iron loss in grain-oriented silicon steel under the alternating flux in any particular direction. Moreover, the measurement and approximation of the magnetization characteristic in any particular direction were performed and discussed. One of the observed results of the iron loss measurement at 50 Hz showed that below 1 T, the iron loss curves in all other directions were located between the iron loss curves in the rolling and perpendicular directions. However, at values above 1 T, there were iron loss curves in some directions having values greater than those of the iron loss curve in the perpendicular direction.

A new simplified rotational loss tester was presented by Enokizono and Tanabe (1997). The advantage of this tester is that, it can be applied to any sized sample sheet in the manufacturing process, since the properties can be measured by putting the sample between the sensors of the tester. The construction of the tester and the size and arrangement of the sensors are shown in Figure 3.7, (a) and (b) respectively. The part (a) shows two U-shaped yokes positioned in the x-and y-directions under the specimen. The sensors for measuring the magnetic properties of the electrical steel sheet were placed on and under the surface of the specimen at the inner part of the crossed yokes (Sensor-A) and at the upper surface (Sensor-B). Part (b) shows the exciting coils wound at each foot of the yokes (Coil-A) and at the straight-backed parts of the yokes (Coil-B). The specimen used for testing was a non-oriented silicon steel sheet (H50, 0.5 mm in thickness).

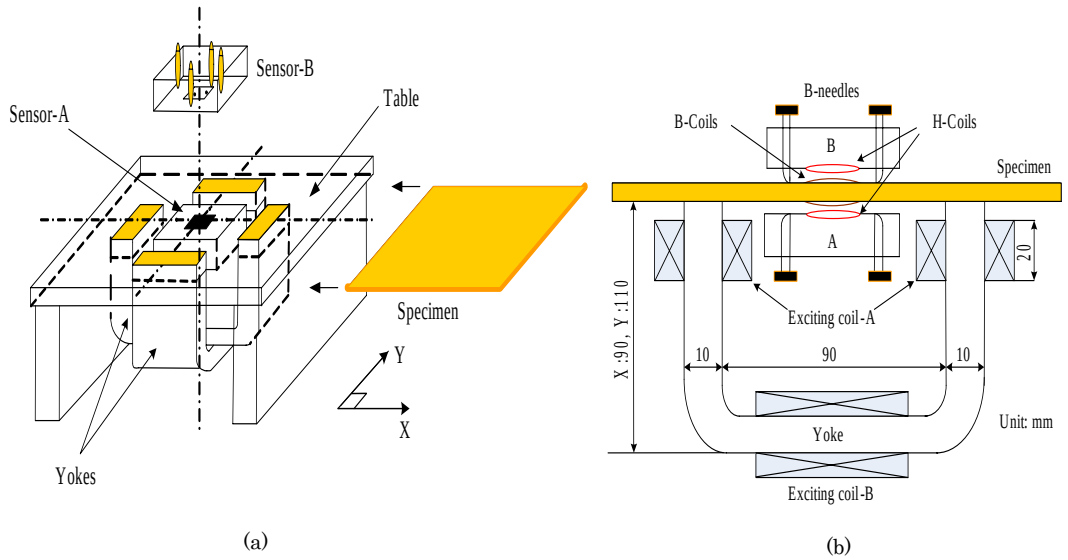

Figure 3.7: Schematic illustration of (a) the structure of the simplified loss tester, and (b) the size and arrangement of the sensors.

The sensors are based on the field-metric method to measure x- and y-directional components of the magnetic field strength and flux density. The two H-coils are for measuring the field strength vector, and the two sets of the double-stylus probes are for the flux density vector. A spring was fixed inside of each needle in order to absorb the variations of the specimen. The H_x-coil was wound over a Bakelite plate, and the H_y-coil was wound around the H_x-coil. The B-coils were wound on the sheet through four 0.6 mm holes in x- and y- directions and the width between the holes in each direction was 24 mm. The flux density measured with each sensor was compared to that of the B-coil. The basic characteristics of the loss measurements were investigated and compared with those of the conventional accurate apparatus. The results obtained from the measurements, however, have shown some problems in accuracy. The authors attributed these problems to the yoke construction.

Since the rotational power loss can be measured as the torque loss generated from the angle of lag between the ***H***-vector and the ***B***-vector caused by the rotating field. Findlay et al. (1994) used a method similar to one used by Enokizono et al. (1990). The basic features of this method are shown in Figure 3.8, (a) and (b). A Keithley arbitrary waveform generator was used to create two quadrature sinusoidal voltages. These are fed to a power amplifier, which energizes two pairs of coils on a yoke. A rotating magnetic field is induced in an 8 cm square sample, which has search coils wound through two sets

of holes. Two tangential field strength-sensing coils are orthogonally wound on a 2 cm square form. The sample sits centered on these double H coils. Signals proportional to B_x, B_y, dH_x/dt, and dH_y/dt are fed into a Keithley DAS16F analog to digital conversion board for processing. A personal computer is used for data storage, signal processing, and the calculation of the rotational losses.

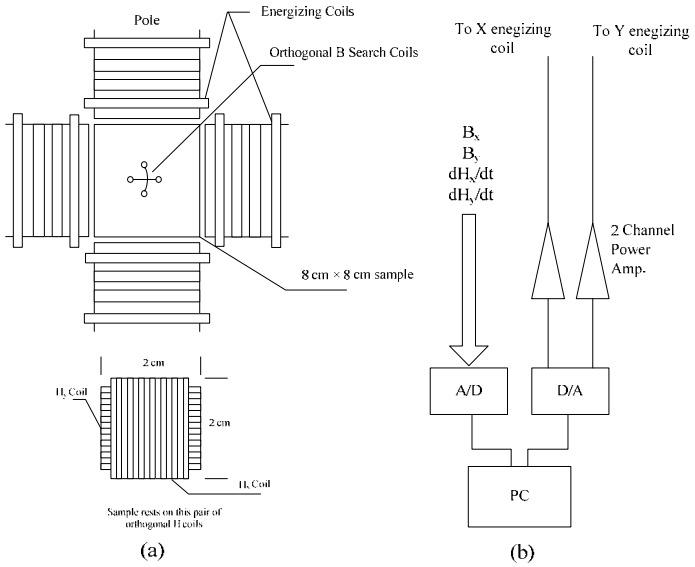

Figure 3.8: Schematic illustration of (a) test apparatus, sample and sensing coils, and (b) the Data Acquisition and quadrature voltage generation.

The loss curves obtained by the authors have shown that, the rotational losses are much larger than the alternating losses in the rolling and transverse directions of the steel. The results were compared to standardized tests from an Epstein test procedure. The comparison shows a significant difference in the loss results obtained for the rotational test versus the alternating current test.

The field metric technique was employed by Zurek and Meydan (2006) for measuring the rotational power loss, whose value was calculated from the orthogonal components of ***B*** and ***H*** by using the conventional equation. The samples were cut as discs 80 mm in diameter and were placed in a round magnetizing yoke, whose internal diameter was 84 mm, thus leaving a 2-mm air gap between the sample and the yoke for better homogeneity of the magnetization. The form factors of the orthogonal components of *dB/dt* and *dH/dt* and the radii of *B* and *H* loci were controlled to be within 2.0% of the desired values. The *B* components were measured by means of 20-mm-wide search coils

threaded through 0.3-mm holes drilled in the center of the sample. The *H* components were measured by means of 20-mm-wide *H* coils positioned immediately at the surface of the sample. The voltages from all the sensors were detected through a 16-bit data acquisition card. A digital feedback algorithm was used in the measuring program written in LabVIEW. The rotational power loss and loci of the *B* and *H* vectors have been measured for three types of electrical steels (fully processed nonoriented-No, conventional grain oriented-CGO, and high permeability grain oriented-HPGO) over a *B* range from 0.5 to 2.0 T or over a range of *H* from 50 to 20 kA/m, at 10, 50, and 250 Hz. However, the results that have been reported were only that measured at 50 Hz. The authors concluded that, for anisotropic materials, the losses under controlled *H* can be higher by nearly six times when compared to the standardized method of measured losses, by which the soft magnetic materials are categorized. The *B* and *H* values have very similar properties in the frequency range from 10 to 250 Hz.

Mori et al. (2005) developed a new method of two-dimensional magnetic measurement to measure the rotational losses in an electrical steel sheet. In this method, square samples were used for measuring the rotational power losses at a high magnetic flux density. The magnetic properties of the ***B-H*** loops and the losses were measured at 50 Hz. The magnetic field was subjected in both directions; clockwise and anticlockwise. When the magnetic flux density increased up to 1.7 T, the losses in the clockwise direction were increased, while reduced in the anticlockwise direction. However, the relationship between ***B*** and ***H*** vectors was not accurate.

Concerning the 3-D magnetic property, in some electromagnetic devices such as a claw pole/transverse flux motor, the local flux density locus may follow an irregular loop in 3-D space when the rotor rotates (Guo 2003 and Guo et al. 2005). In fact, even under 1-D alternating or 2-D rotating magnetic excitation, a magnetic material shows a 3-D magnetic property due to the rotation of the magnetic domains (Zhu et al. 2003).
Zhong and Zhu (2001) developed 3-D magnetic testing system to investigate the 3-D magnetic properties of magnetic materials. By controlling the magnetic excitation in three axes, this tester is able to generate different magnetic flux patterns, such as alternating in any given orientation and rotating in two and three dimensions.

Chapter 4

Experimental Work

To determine the *B*-*H* relationships and total power loss in two dimensions in an electrical steel sheet, the flux density inside the sample and the surface field strength should be measured accurately.

In this part of the work, the method that has been used in this thesis for measuring the magnetic properties and power losses in an electrical steel sheet will be described. The method consists of a measuring device, a Labview FPGA module and data acquisition card (PCI-7831R) to collect the magnetic flux density and magnetic field strength components and display them through a personal computer for analyzing and processing.

4.1 Measurement Apparatus of Dynamic Hysteresis Loops

Several methods have been proposed for the measurement of the dynamic hysteresis loops in an electrical steel sheet. Among these, the method based on the measurement of the field quantities B_x, $B_{y,}$ H_x and H_y appears to be the most convenient, as far as the preparation of the test specimen is concerned (Enokizono et al. 1989).

The measurement of the *B*-*H* loops under alternating and rotational flux excitations was carried out using a vertical yoke setup. The setup consisted of two pairs of double U-shaped yokes as shown in Figure 4.1. Each yoke was built of 520 thin electrical steel sheets with a thickness of 0.2 mm and wound with 400 turns of exciting coils. The arrangement of the exciting coils made it possible to apply a high flux density through the yokes to the sample sheet (see Katarzyna et al. 2008 for more details).

A programmable Elgar (SW5250A) power amplifier was used to create arbitrary waveforms. These were fed to the yoke device in order to energize the exciting coils wound on the yokes. The field sensing measurement system is depicted in Figure 4.4.

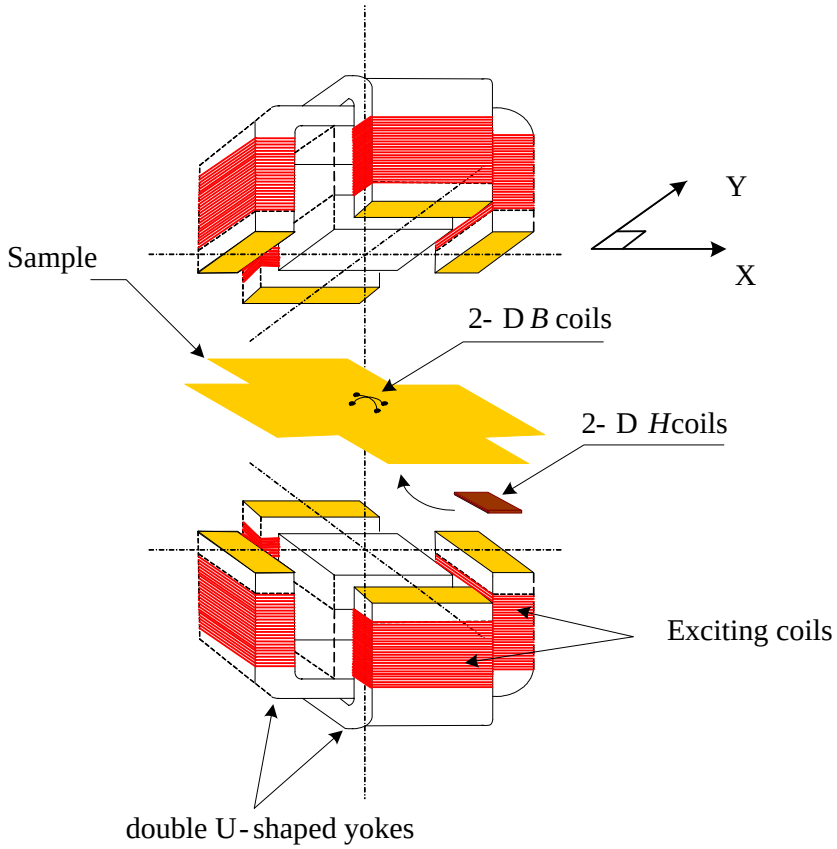

Figure 4.1: Apparatus for 2-D measurements with vertical yokes.

Alternating and rotating magnetic fields were induced in an area of over 400 mm^2, a cross-shaped sample which is illustrated in Figure 4.2 with its dimensions included. The sample investigated consisted of

1. Flux density search coils (*B*-coils) wound through two sets of very small holes drilled in the center area of the sample. Each axis has two holes, and each hole is located at a distance of 10 mm from the sample center.
2. Two tangential field-strength sensing coils (*H*-coils) wound orthogonally on a 2 cm square form as shown in Figure 4.3, and this form is affixed on the under surface of the sample.

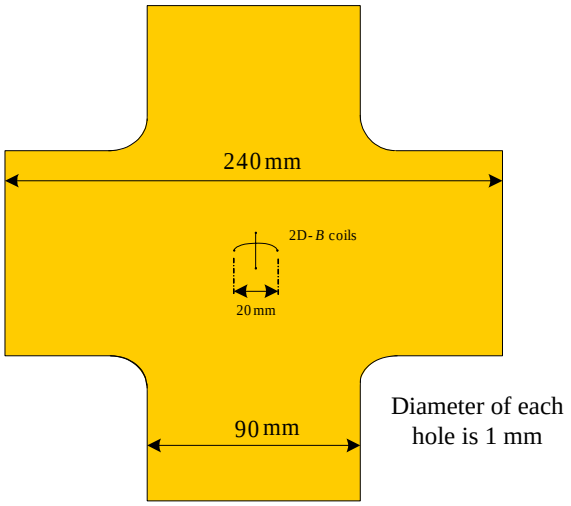

Figure 4.2: Dimensions of the cross-shaped sample and position of *B*-coils.

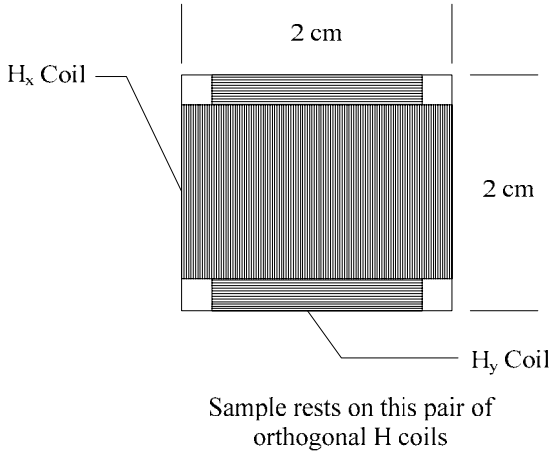

Figure 4.3: 2-D *H* sensing coils.

The sample was inserted between the two pairs of double U-shaped yokes in a centralized position. The *B*-coils were used for measuring the flux density components, B_x and B_y inside the sample, and the *H*-coils were used for measuring the magnetic field strength components, H_x and H_y on the surface of the sample.

The signals of $\boldsymbol{B}$ and $\boldsymbol{H}$ were acquired using a data acquisition card (PCI-7831R) and a Labview FPGA module (see Alkar 2007 for more details). A personal computer was used for data storage, signal processing, and calculation of the losses through subroutines written in MATLAB software.

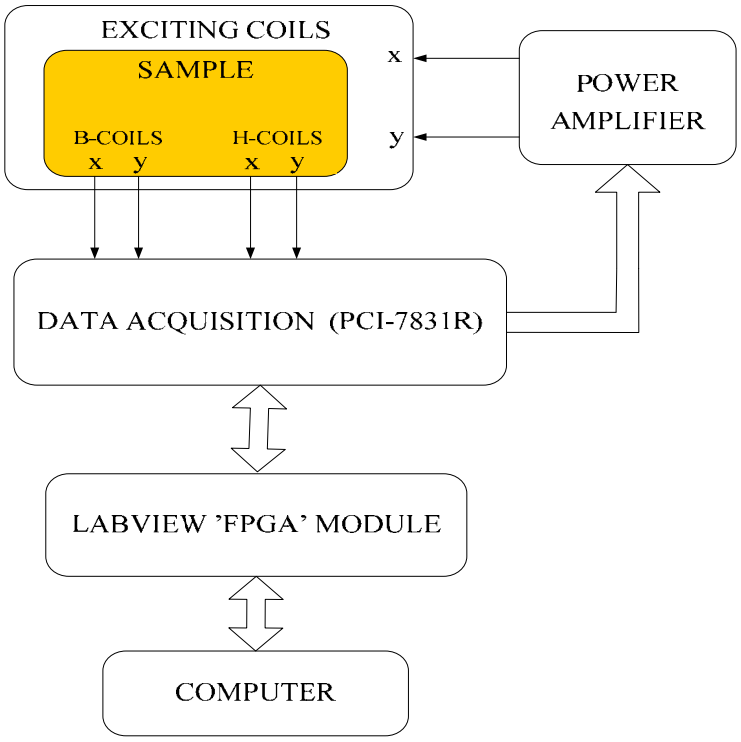

Figure 4.4: Data acquisition and field sensing system.

The power losses were investigated under a range of fundamental frequencies (10 Hz to1 kHz) applied for alternating and rotating field excitations and various peaks of flux density. The total power losses measured, P_{m}, in an electrical steel sheet were determined by using the Poynting vector theorem as

$$P_{\mathrm{m}} = \frac{1}{\rho T}\int_0^T \boldsymbol{H}\cdot\frac{\mathrm{d}\boldsymbol{B}}{\mathrm{d}t}\mathrm{d}t = \frac{1}{\rho T}\int_0^T \left(H_x\cdot\frac{\mathrm{d}B_x}{\mathrm{d}t} + H_y\cdot\frac{\mathrm{d}B_y}{\mathrm{d}t}\right)\mathrm{d}t. \qquad \mathrm{W/kg} \tag{4.1}$$

where

ρ is the mass density of the material (kg/m^3),

T is the period of magnetization (s),

H_{x} is the magnetic field strength in the x direction (A/m),

H_{y} is the magnetic field strength in the y direction (A/m),

B_{x} is the sample flux density in the x direction (T), and

B_{y} is the sample flux density in the y direction (T).

4.2 Measurement Results

The magnetic properties of the *B*-*H* loops and the corresponding losses were measured under several values of fundamental frequencies and peak flux densities. The field of 10 Hz to 1 kHz was applied with three types of field conditions by using the voltage model power amplifier, Elgar SW5250A as a power source. Each frequency was changed in the range from 0.2 T to the saturation value 1.8 T, when wherever this was possible. The data acquisition card (PCI-7831R) was used for acquisition of the signals B_x, B_y, H_x, and H_y. The data received was analyzed and used to plot the magnetic flux density vector vs. the magnetic field strength vector which are known as *B*-*H* loops or hysteresis loops. In addition, some of the other properties that were measured will be illustrated such as the waveforms corresponding to the *B*-*H* loops under the alternating field and loci of both, the flux density and magnetic field strength vectors in the case of rotational field excitation.

4.2.1 Alternating Field

Figure 4.5 shows the hysteresis loops under an alternating field condition in the transverse direction (H_y, B_y) that were saturated approximately with the same magnetic flux density (1.6 T). The frequencies of these loops were 10 Hz, 50 Hz, 200 Hz and 500 Hz respectively as detailed in the figure, while Figure 4.6 illustrates the waveforms corresponding to these $\boldsymbol{B}$ and $\boldsymbol{H}$ vectors for each frequency which are also known as the instantaneous values of the magnetic flux density and magnetic field strength. It has been shown that, for high frequencies such as 800 Hz and 1 kHz, the possibility of reaching a maximum peak of flux density becomes difficult and the shapes of the *B*-*H* loops became wider with the increase of the exciting frequency, while the value of the flux density was saturated.

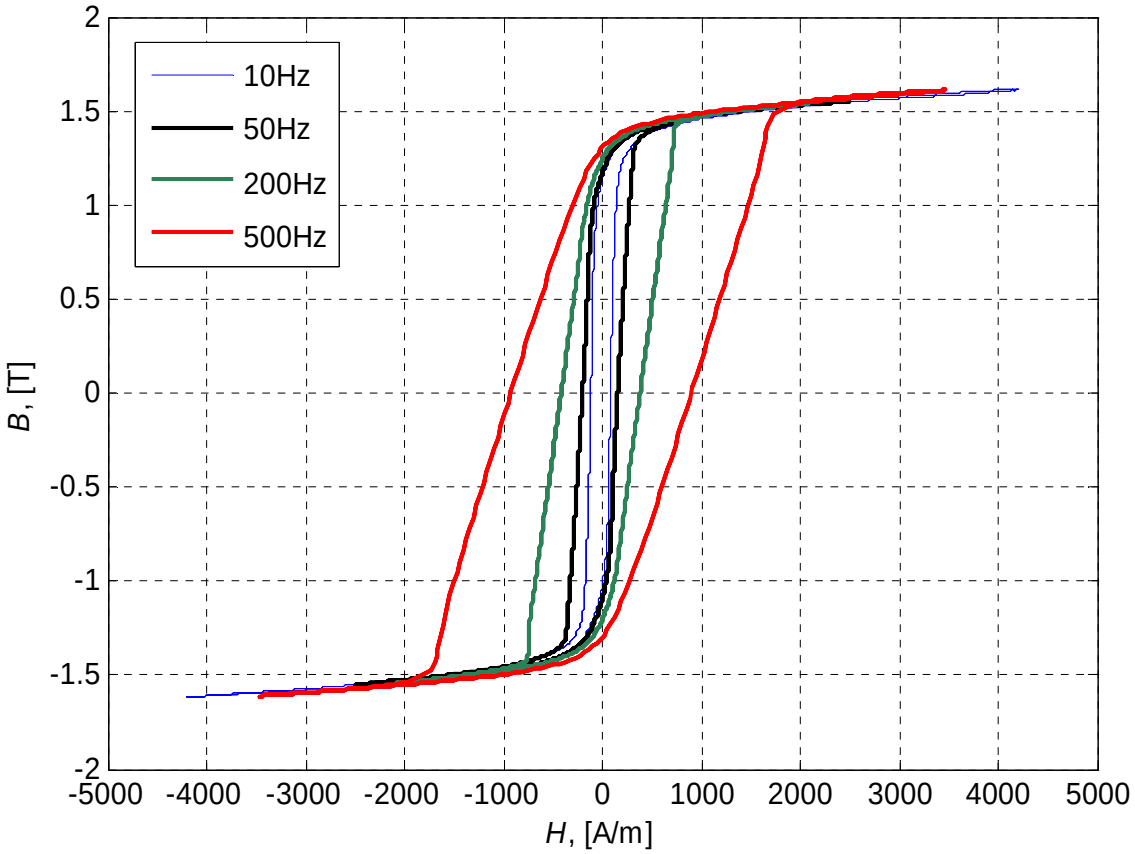

Figure 4.5: The dynamic hysteresis loops at saturated flux density (1.6 T) which have been measured in the transverse direction of the electrical steel sheet under different fundamental frequencies as shown in the figure.

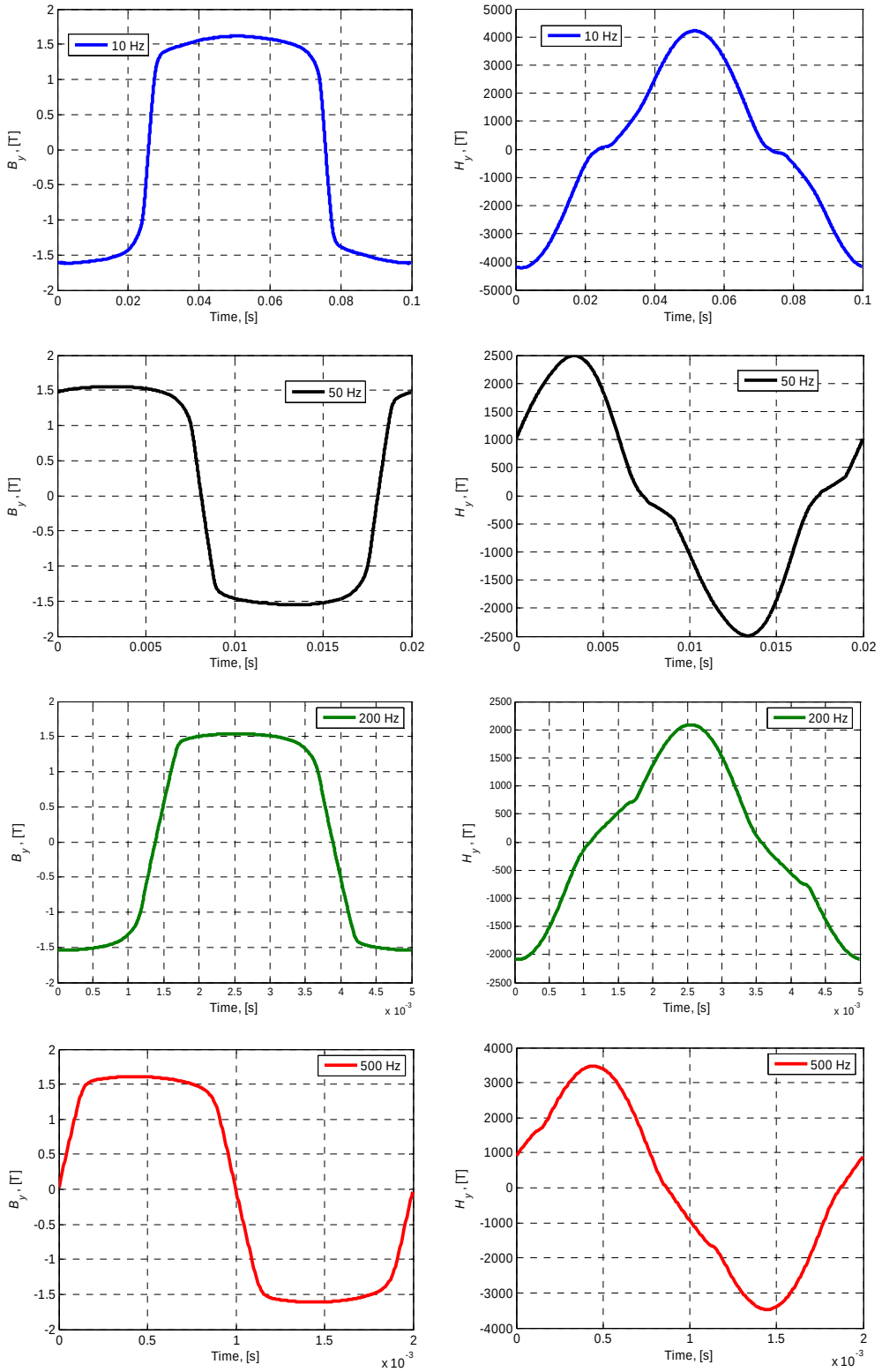

Figure 4.6: The instantaneous values of magnetic flux density and magnetic field strength for each loop illustrated in Figure 4.5.

On the other hand, Figure 4.7 shows the behavior of the dynamic loops under 100 Hz, an alternating field in the transverse direction and the effect of increasing the flux density on these loops when the frequency remained constant. Figure 4.8 illustrates the instantaneous values of the *B* and *H* vectors for the loops of 0.2 T, 0.6 T, 1.0 T and 1.4 T respectively.

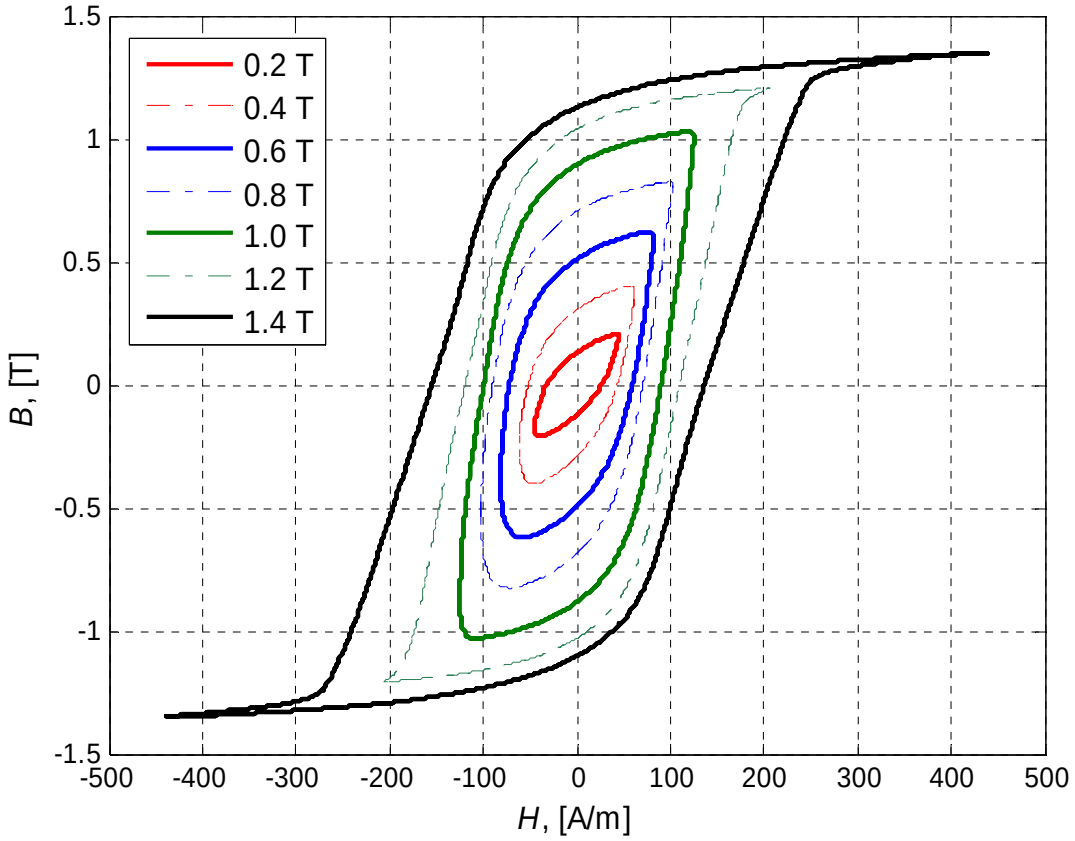

Figure 4.7: Hysteresis loops in electrical steel sheet during the increasing of the flux density in the transverse direction of the sample, under 100 Hz.

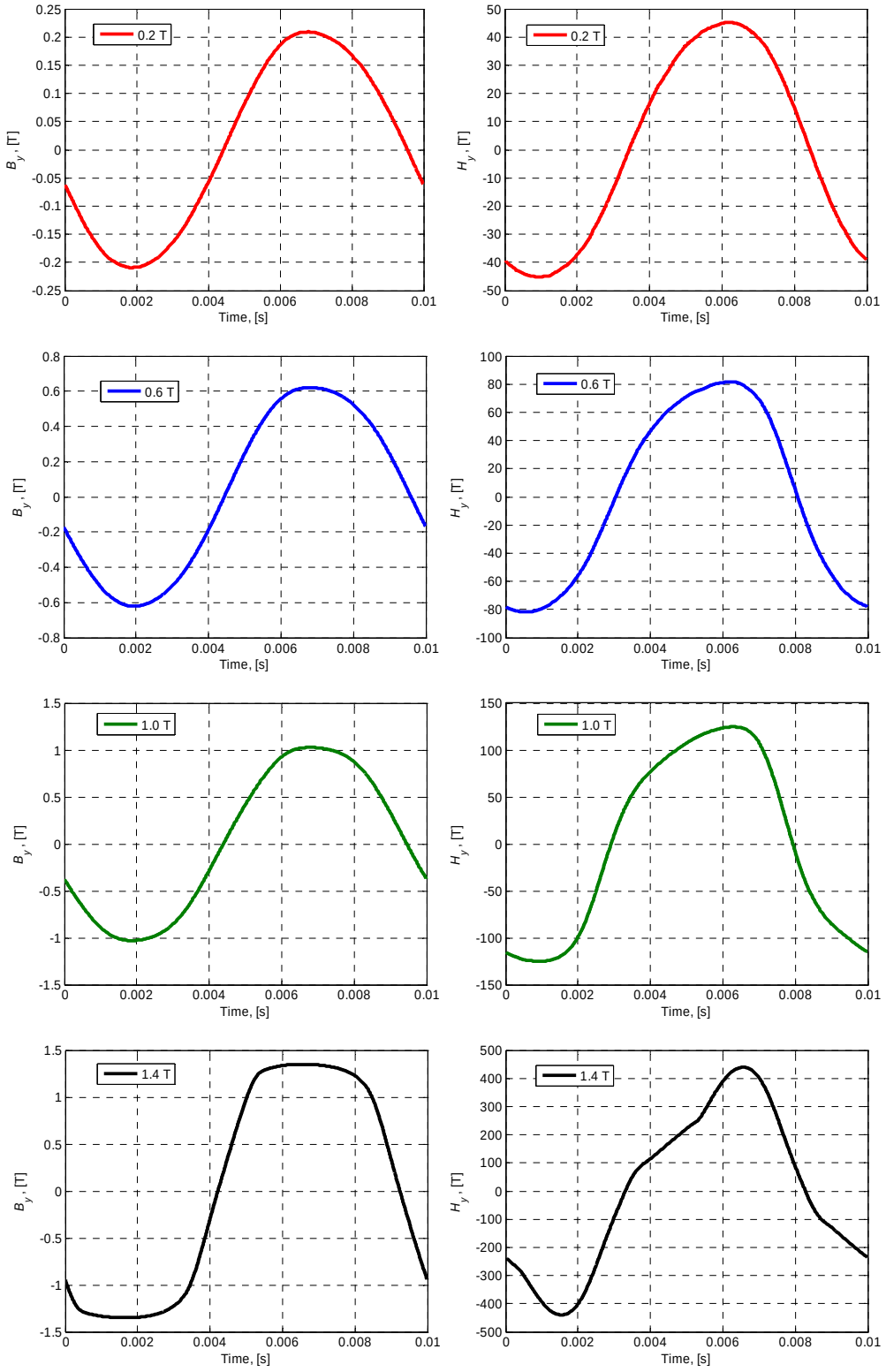

Figure 4.8: The instantaneous values of the vectors B and H under fundamental frequency 100 Hz and different peaks of flux density as shown in the figure.

4.2.2 Rotating Field

Concerning the behavior of the dynamic hysteresis loops when the field applied on the electrical steel sheet is rotational, the curves illustrated in Figure 4.9 show these hysteresis loops under rotational field conditions in the rolling and transverse directions that were saturated with the magnetic flux density which was obtained under different excitations of the fundamental frequencies. The frequencies of these saturated fluxes were 10 Hz, 50 Hz 500 Hz and 1 kHz respectively, as shown and detailed in the figure.

The data illustrated in Figure 4.10 shows the loci of the magnetic flux density (B_x, B_y) and the magnetic field strength (H_x, H_y) of the loops presented in Figure 4.9. The loci of the B and H vectors were presented in the x and y-direction.

Figures 4.11 and 4.12 show the instantaneous values of the magnetic flux density and magnetic field strength respectively in rolling and transverse directions which corresponds to the dynamic hysteresis loops shown in Figure 4.9.

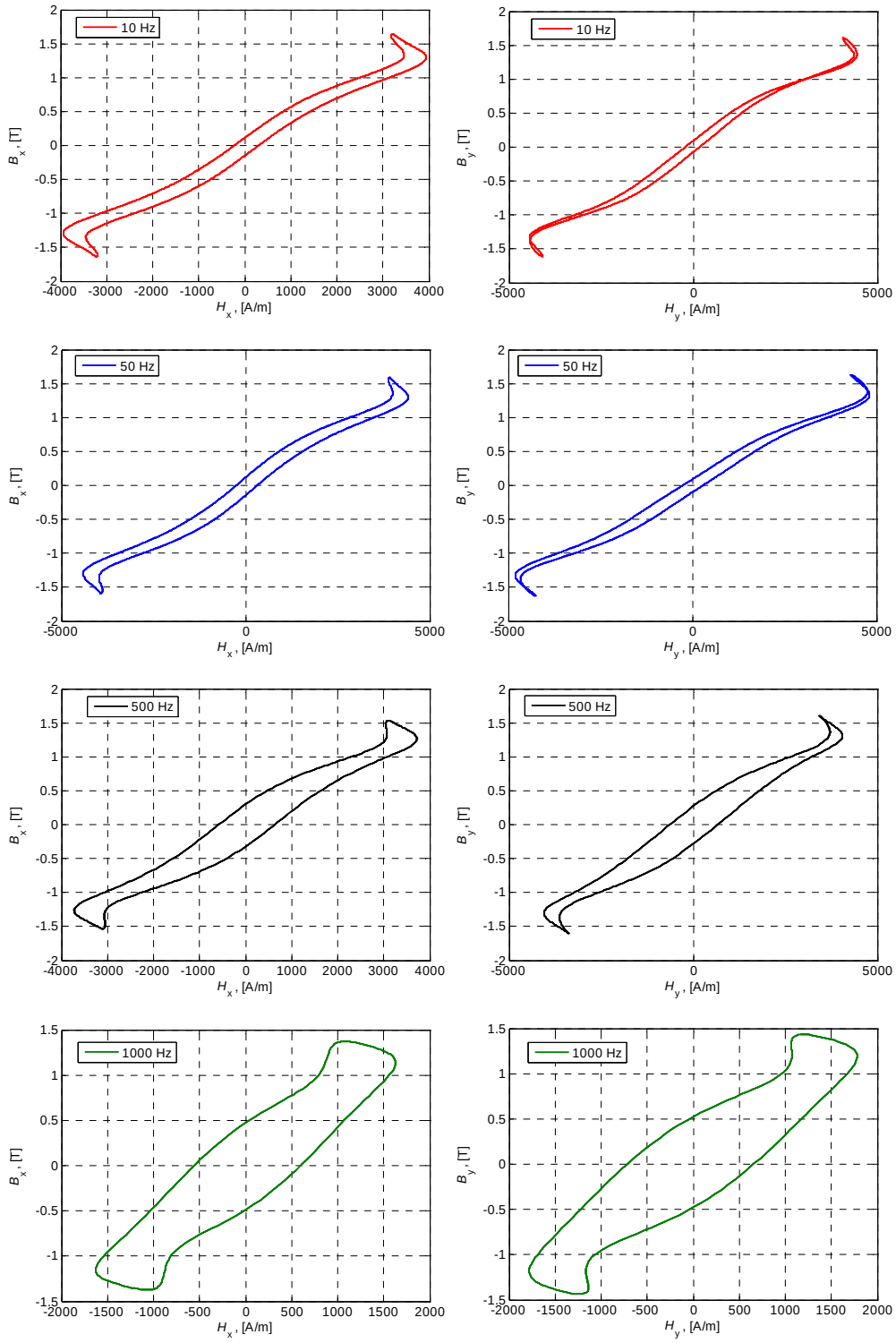

Figure 4.9: The saturated hysteresis loops in the rolling and transverse directions of a sample under a rotational field and different fundamentals of exciting frequencies.

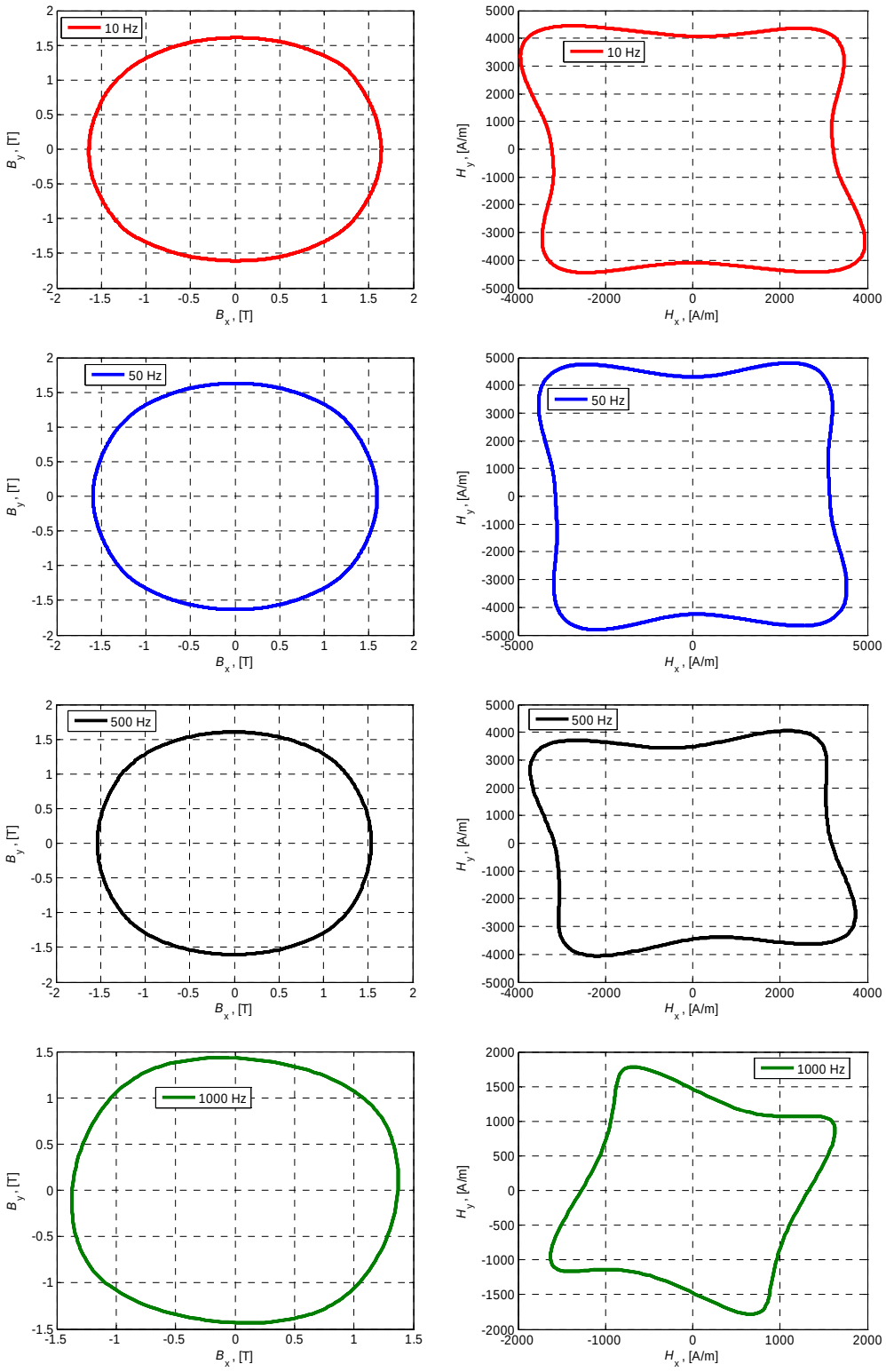

Figure 4.10: Loci of magnetic flux density and magnetic field strength in x and y-direction of the loops illustrated in Figure 4.9.

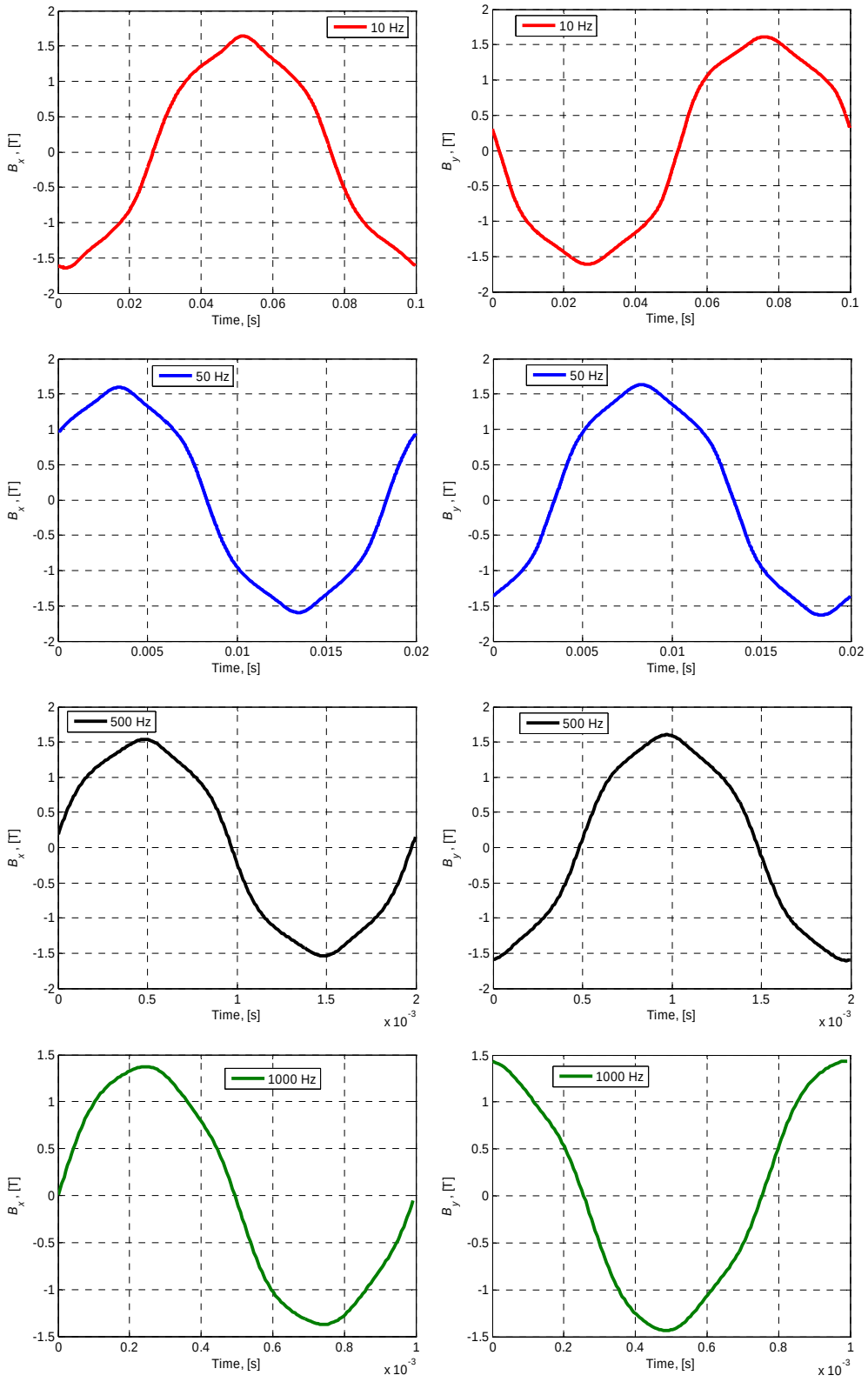

Figures 4.11: The instantaneous values of the magnetic flux density in rolling and transverse directions of the hysteresis loops illustrated in Figure 4.9.

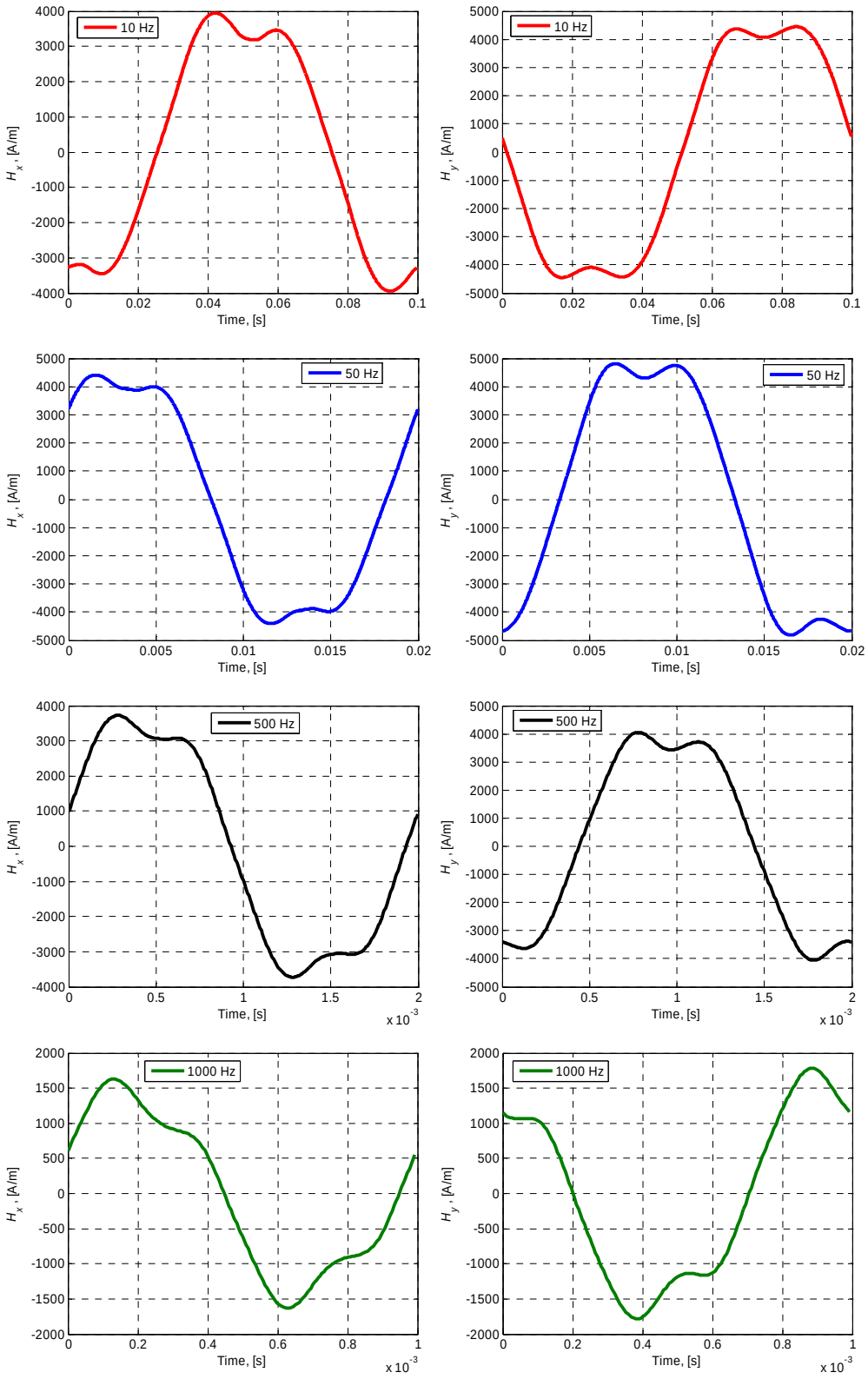

Figures 4.12: The instantaneous values of the magnetic field strength in rolling and transverse directions of the hysteresis loops illustrated in Figure 4.9.

The behavior of the dynamic loops due to the rotational field applied on an electrical steel sheet under 50 Hz is shown in Figure 4.13. The *B-H* loops in the x and y-direction illustrated in this figure are dissimilar. The difference could be attributed to the anisotropy of the material used and the magnetic properties of this material were measured without using a control system. In addition, it is likely that the *B-H* coils and search coil holes could have a larger effect on this issue. The figure shows the effect of increasing the flux density on the *B-H* loops in the case of a rotational field and when the frequency remained constant.

The loops depicted in Figure 4.13 were chosen for four different peaks of flux density in the x and y-direction as shown and detailed in each curve illustrated in the figure. Furthermore, Figure 4.14 presents the loci of the magnetic flux density and magnetic field strength of these loops in two-dimensions, while Figures 4.15 and 4.16 show the instantaneous values of the magnetic flux density and magnetic field strength respectively in two-dimensional form for each loop illustrated in Figure 4.13.

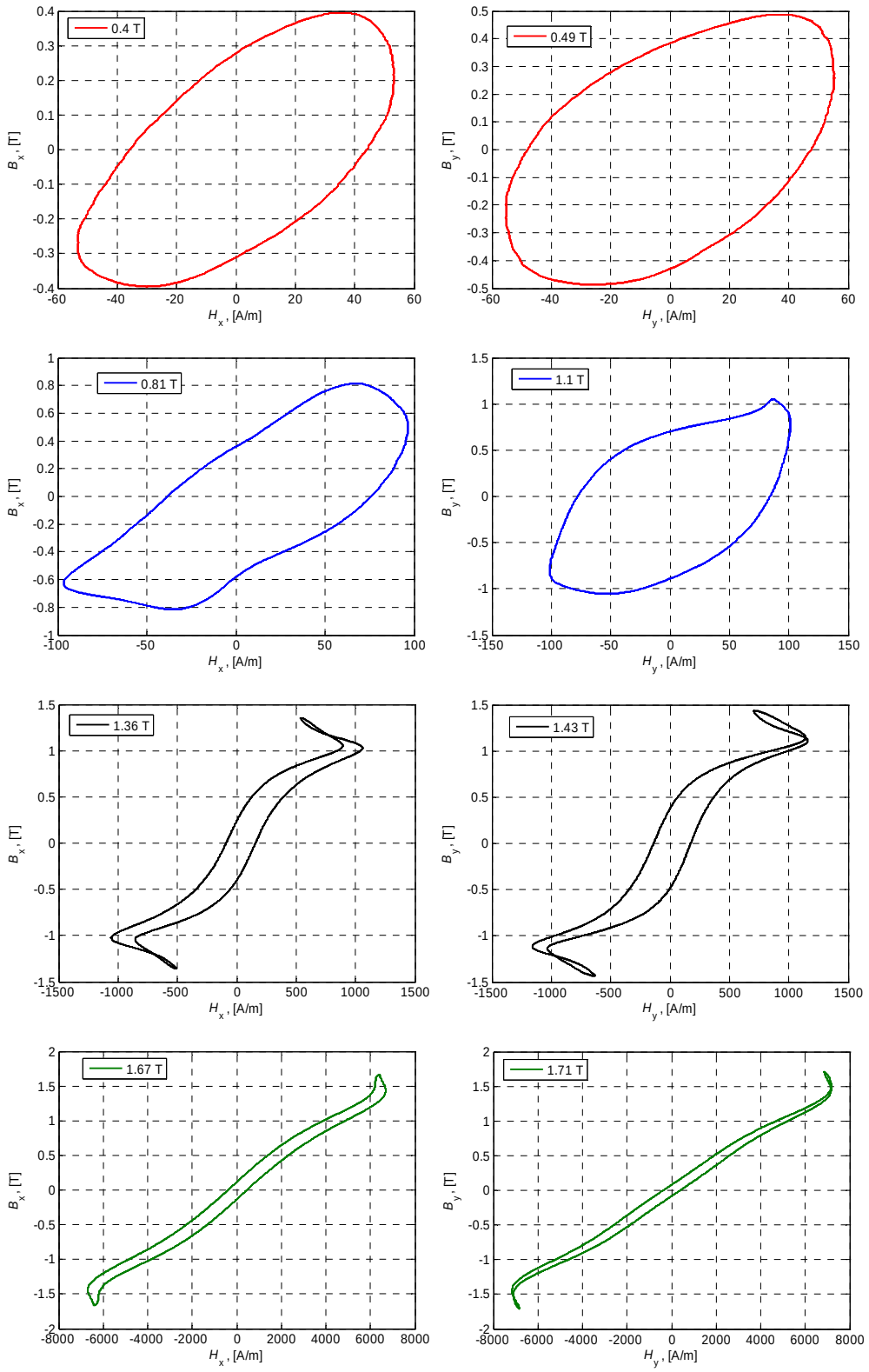

Figure 4.13: The hysteresis loops of electrical steel sheet under rotational field condition, 50 Hz, and different peaks of flux densities.

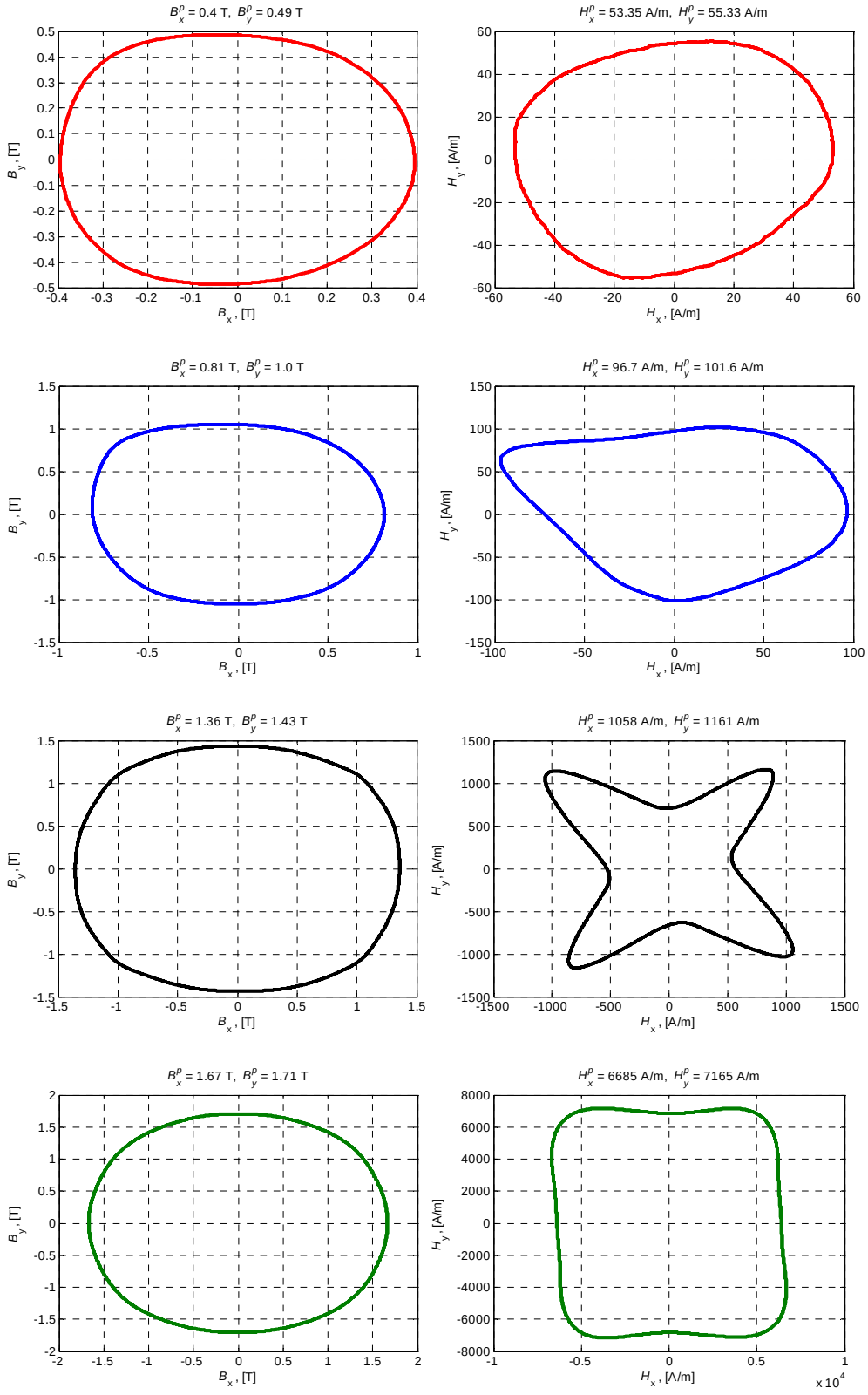

Figure 4.14: The loci of magnetic flux density and magnetic field strength in x and y-direction of the loops illustrated in Figure 4.13.

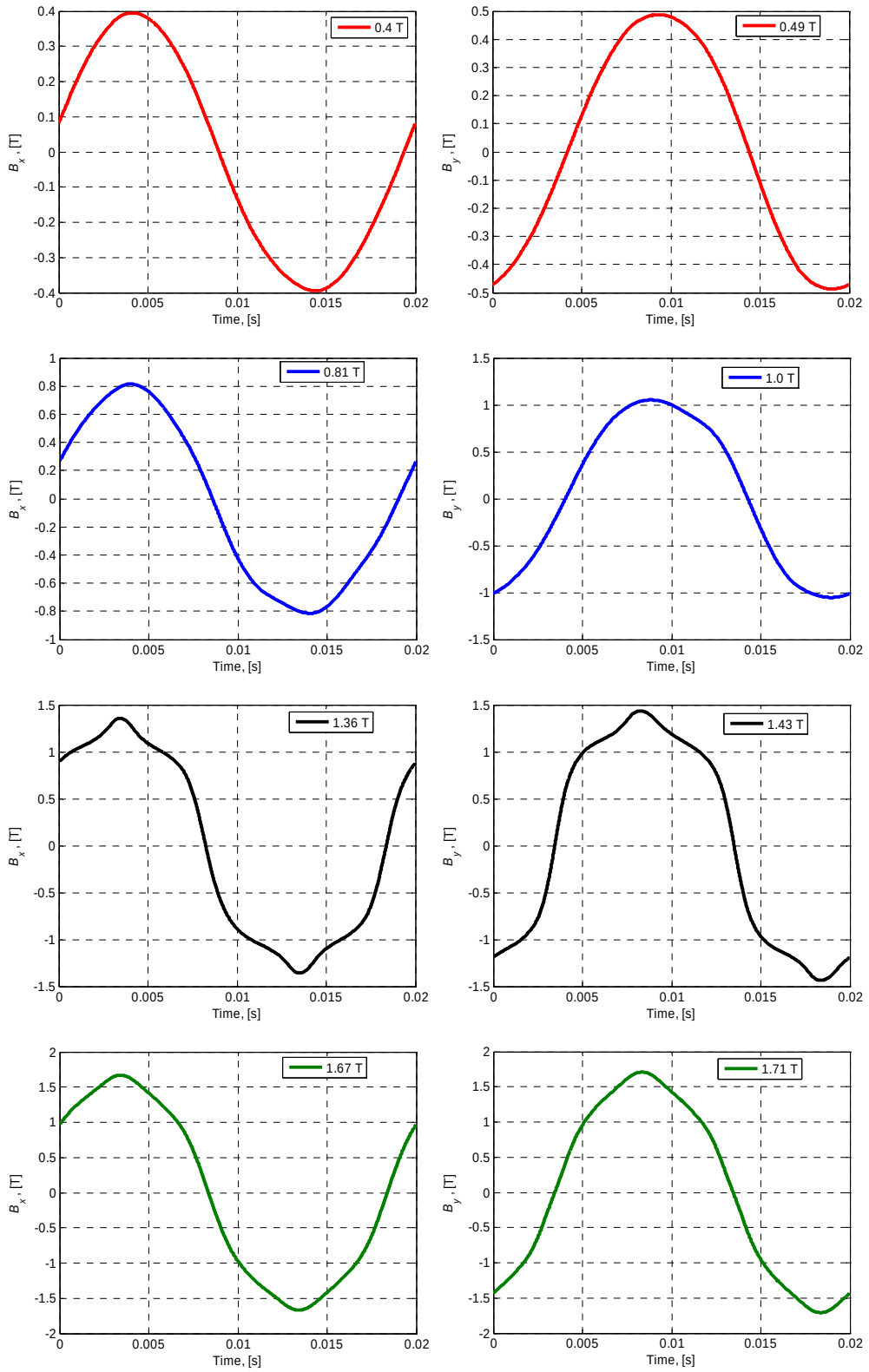

Figures 4.15: The instantaneous values of the magnetic flux density in two-dimensional form for each loop illustrated in Figure 4.13.

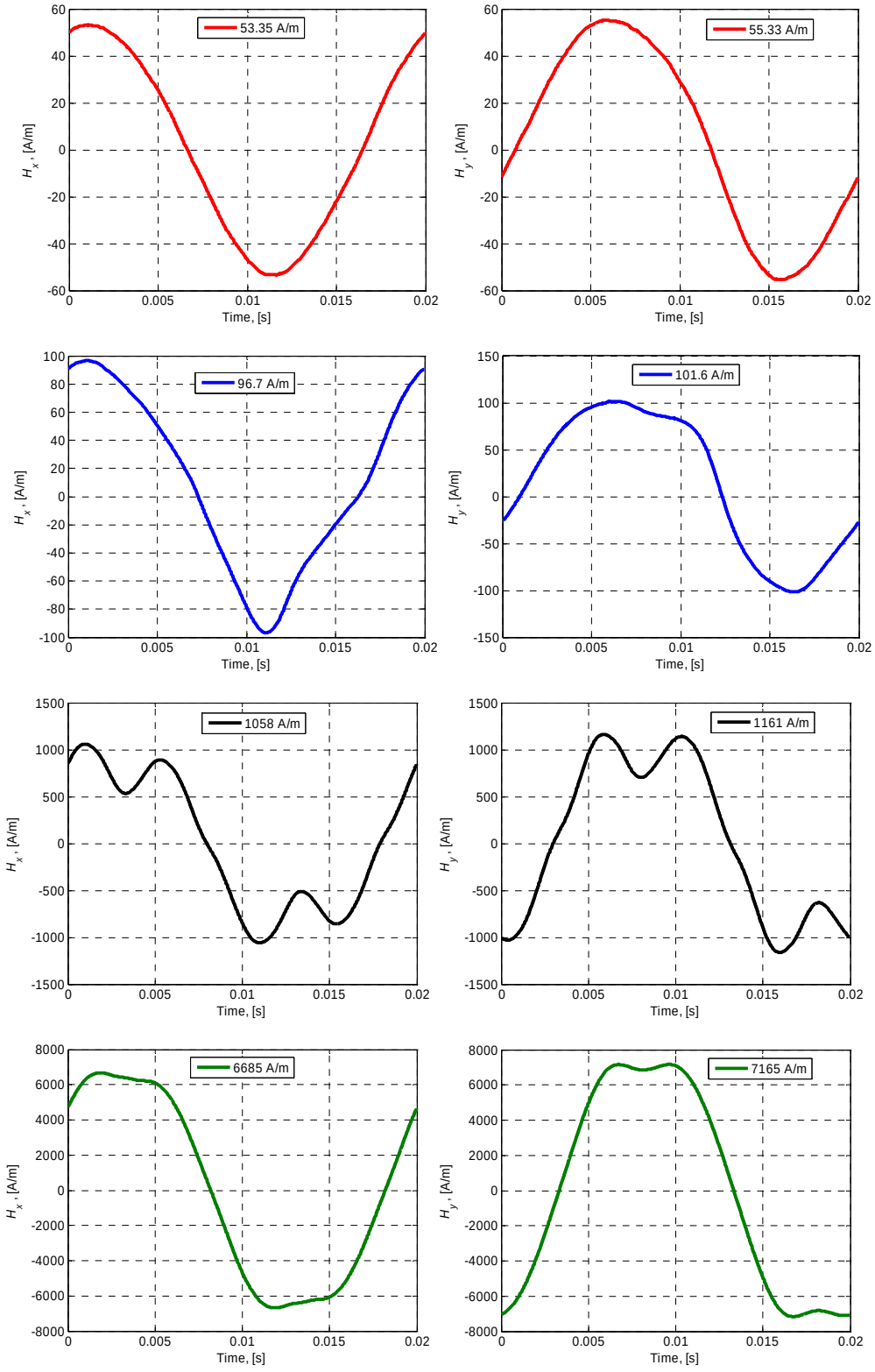

Figures 4.16: The instantaneous values of the magnetic field strength in two-dimensional form for each loop illustrated in Figure 4.13.

4.3 Power Losses Measured in Electrical Steel Sheet

Data obtained from the measurement of the magnetic properties under alternating and rotating field excitations were used to calculate the power losses in an electrical steel sheet by using the formula illustrated in Equation (4.1).

A huge amount of data has been received from the measurement device through the data acquisition card and stored in a personal computer as text files, each file consisting of five columns containing the time of the magnetization (t), the magnetic flux density components (B_x, B_y), and the magnetic field strength components (H_x, H_y).
Loss calculations were estimated under two types of field conditions, different types of fundamental frequencies, and different peaks of flux density. The frequencies used for such calculations were between 10 Hz as a minimum fundamental frequency and 1 kHz which was the maximum frequency. The maximum peak of flux density (saturated value) was recorded from the measurements that fluctuated between 1.2 T and 1.8 T under an alternating and rotating fields. However, at high frequencies (1 kHz) in our measurements, the maximum peak of flux density reached was about 1.2 T under an alternating field and 1.6 T under a rotating field.

The loss due to the rotational flux is called the rotational power loss. It is higher than that caused by the alternating flux and it increases with an increase of the magnetic flux density. The figures illustrated below show that the power losses measured in an electrical steel sheet under a rotational field were substantially larger than those obtained under an alternating field for the flux densities and fundamental frequencies investigated.

Figure 4.17, (a) and (b), shows the performance of the losses measured in an electrical steel sheet under an alternating field, applied in the transverse direction of the sample. The losses were measured under different peaks of flux density and different excitations of fundamental frequencies. The curves illustrated in part (a) show the losses obtained under frequencies of 10 Hz to 50 Hz, while the curves presented in part (b) show the losses behavior when the frequency is 100 Hz and above. The two parts of the figure show the power losses in the sample up to the peak flux density of 1.6 T.

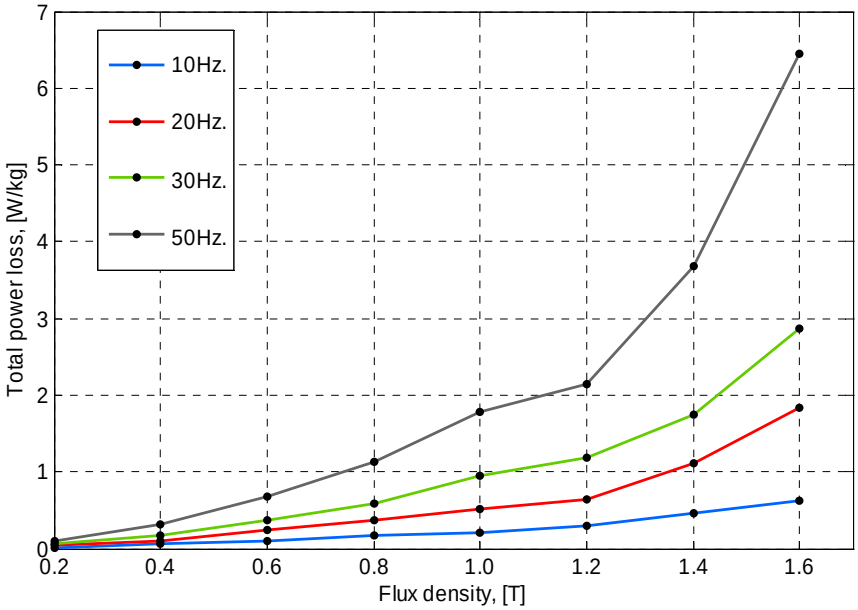

(a)

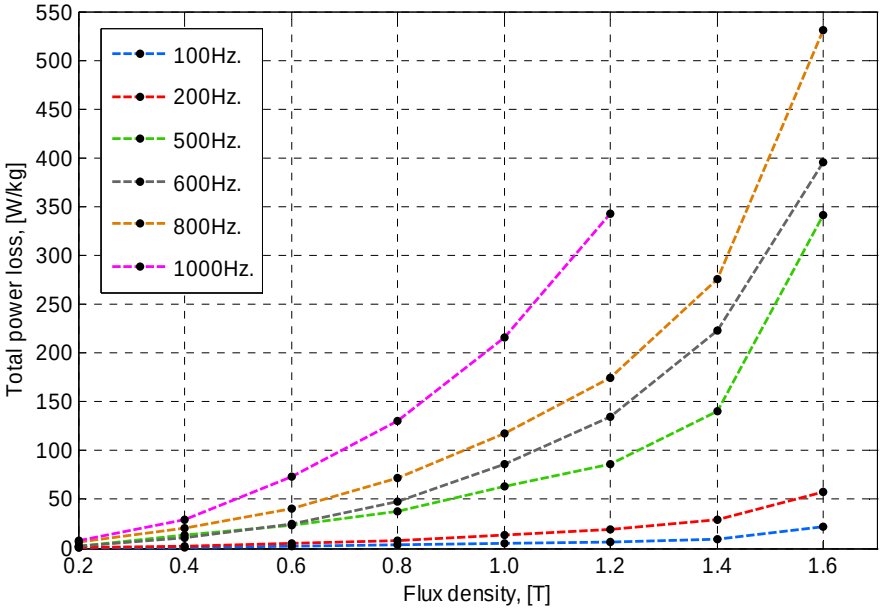

(b)

Figure 4.17: Alternating power losses in (W/kg) vs. increasing flux density (0.2 T - 1.6T) for different fundamental frequencies on cross-sample, (a) frequencies 10 Hz-50 Hz, and (b) frequencies 100 Hz - 1000 Hz.

If an electrical steel sheet is placed in a magnetic field rotating in the plane of the sheet one finds different magnetic behavior than the case of a field changing its magnitude with time, but keeping its direction constant. Losses due to rotational field excitation vs. an increasing flux density under different rotational frequencies are illustrated in Figure 4.18, (a) and (b). The curves illustrated in part (a) show the rotational losses obtained under frequencies of 10 Hz to 100 Hz, and the curves presented in part (b) show the rotational losses measured for other different rotational fundamental frequencies. Every loss value increases with increasing magnetic flux density. The loss curves show the maximum peak for the sample.

Under a rotating flux condition, the magnetic material will exhibit rotational hysteresis losses and eddy current losses. The hysteresis losses under a rotational flux condition are very different from those obtained due to an alternating flux. The data illustrated in Figures 4.17 and 4.18 showed that the rotational power losses were much larger than the losses resulting under an alternating field condition in the transverse direction of the sample and both losses increase when both the flux density and frequency increases.

As the sample becomes saturated under only a purely circular field, a peak loss is reached, and the loss value quickly drops to zero. However, this case was excluded from our work because the magnetic properties of the sample were measured without using a control system and the field applied to the sample in the case of rotational excitation was not purely circular.

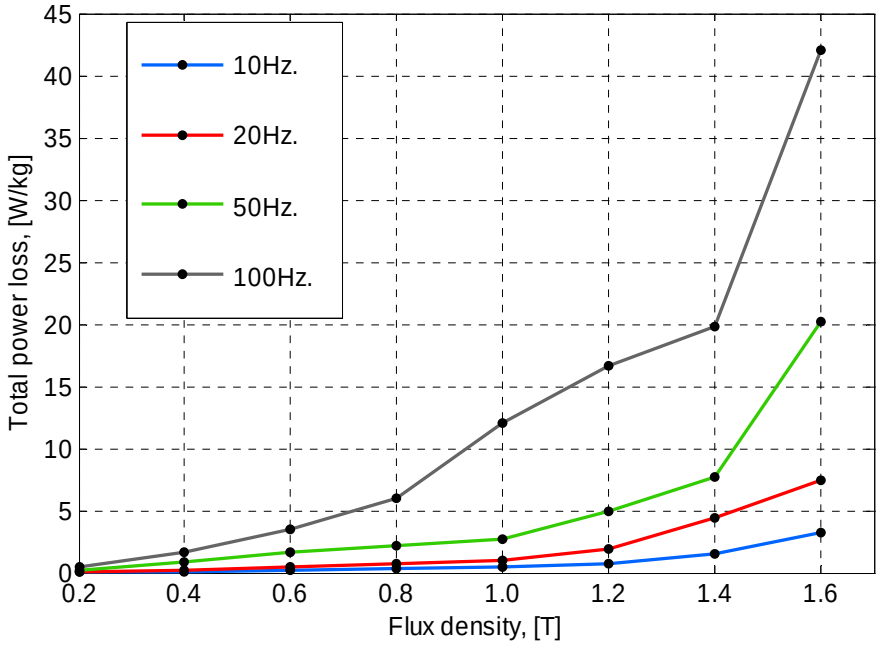

(a)

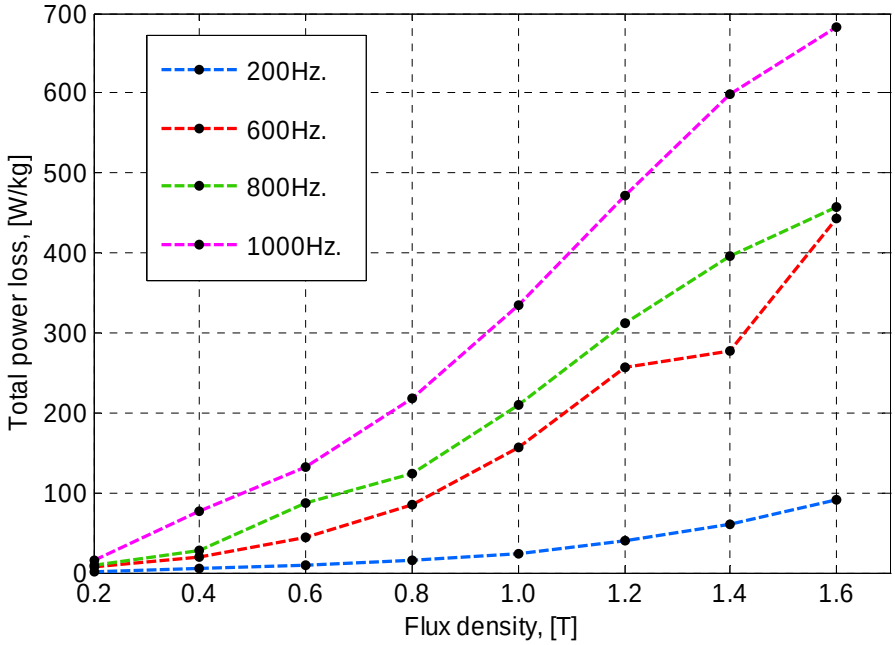

(b)

Figure 4.18: Rotational power losses in (W/kg) vs. increasing flux density (0.2 T - 1.6 T) for different rotational fundamental frequencies on cross-sample, (a) frequencies 10 Hz - 100 Hz, and (b) frequencies 200 Hz - 1000 Hz.

Chapter 5

Parameter Estimation of Dynamic Loss-Model with Nonlinear Least-Square Method

In this part of the work, an explanation of the method capable of optimizing parameters of a comprehensive dynamic loss-model (Belahcen 2008) of electrical steel will briefly be introduced. The method is based on the minimization of the deviation of the simulated trajectory of the model from a known behavior which is here the total power loss measured, P_{m}. The method allows the identification of parameters from measurements obtained from the field tester to improve the dynamic behavior of the loss-model.

5.1 Dynamic Loss-Model of Electrical Steel

For both alternating and rotational core loss modeling, and based on the empirical three-term formula used to separate the core losses, a dynamic loss-model has been proposed (Belahcen 2008). The goal of this work is to optimize the parameters of this model consisting of four terms, classical eddy-current, alternating and rotational hysteresis and excess losses. The model has been used to compute the iron losses in a 37 kW induction machine fed from a sinusoidal and frequency converter voltage supply (Belahcen 2008). The model is investigated under different magnetization frequencies of the fundamental flux density waveform ranging in the intervals $(10\ \mathrm{Hz} \le f \le 1000\ \mathrm{Hz})$. The four-term equations of the model are illustrated in the following subsections.

5.1.1 Classical Eddy-Current Losses

For an infinitesimal variation of the magnetic flux density vector $\partial \boldsymbol{B}$, the classical eddy-current energy dissipation is modeled as

$$\partial w_c = k_c \left| \frac{\partial \boldsymbol{B}}{\partial t} \right| |\partial \boldsymbol{B}| \qquad (5.1)$$

where k_c is the classical eddy-current loss coefficient that depends on the thickness and conductivity of the material.

5.1.2 Hysteresis, Excess and Rotational Losses

For an infinitesimal variation of the amplitude of the flux density vector $\partial|\boldsymbol{B}|$, the proposed models for the excess and hysteresis energy dissipation are shown in Equations (5.2) and (5.3), respectively

$$\partial w_e = k_e \left(\left| \frac{\partial |\boldsymbol{B}|}{\partial t} \right| \right)^{0.5} \partial |\boldsymbol{B}| \tag{5.2}$$

$$\partial w_h = k_h |\boldsymbol{B}| \partial |\boldsymbol{B}| + k_r \frac{1 - \frac{|\boldsymbol{B}|}{B_s}}{1 + b(1 - \frac{|\boldsymbol{B}|}{B_s})^2} |\boldsymbol{B}| |\partial \theta| \tag{5.3}$$

where θ is the phase angle of the flux density vector, $\partial\theta$ is an infinitesimal variation of this angle and k_e is the excess loss coefficient while k_h and k_r are respectively the hysteresis and rotational loss coefficients. B_s is the saturation flux density which is here fixed to be 2.0 T and b is a constant parameter related to the texture and grain size of the material.

By integrating the Equations (1.5), (2.5), and (3.5) over one cycle of the fundamental frequency, the losses P_c, P_e and P_h in watts per kilogram are respectively given as

$$P_c = \frac{k_c}{\rho T} \int_0^T \left(\left| \frac{\partial \boldsymbol{B}}{\partial t} \right| \right)^2 \mathrm{d}t \tag{5.4}$$

$$P_e = \frac{k_e}{\rho T} \int_0^T \left(\left| \frac{\partial |\boldsymbol{B}|}{\partial t} \right| \right)^{1.5} \mathrm{d}t \tag{5.5}$$

$$P_h = \frac{k_h}{\rho T} \int_0^T |\boldsymbol{B}| \frac{\partial |\boldsymbol{B}|}{\partial t} \, \mathrm{d}t + \frac{k_r}{\rho T} \int_0^T \frac{1 - \frac{|\boldsymbol{B}|}{B_s}}{1 + b(1 - \frac{|\boldsymbol{B}|}{B_s})^2} |\boldsymbol{B}| \frac{|\partial \theta|}{\partial t} \, \mathrm{d}t \tag{5.6}$$

The total loss, P_t in watt per kilogram dissipated in the electrical steel sheet can then be determined as the sum of the classical eddy-current, P_c excess, P_e, and hysteresis, P_h, losses

$$P_t = P_c + P_e + P_h \quad . \tag{5.7}$$

Based on a large amount of experimental results on the electrical steel sheet sample under alternating and rotating flux excitations with various flux density magnitudes and frequencies, the five parameters of the dynamic loss-model k_c, k_e, k_h, k_r and b can be optimized using the *curve-fitting* technique or so called *nonlinear least-squares* criterion. The curve fitting is executed based on the initial parameters of the loss-model and measured data.

5.2 The Method of Least-Squares

In order to optimize the parameters of the loss-model, the curve fitting process matches the curve obtained from the total power loss predicted by using the loss-model, P_t, to the curve obtained from the total power loss measured, P_m. Nevertheless, for a given set of data, the fitting curve of a given type is generally not unique. Thus, a curve with a minimal deviation from all data points is desired. This best-fitting curve can be obtained by the method of least squares.

The method of least squares assumes that the best-fit curve of a given type is the curve that has the minimal sum of the deviations squared (least square error).

Suppose that the data points are (P_{t1},P_{m1}), (P_{t2},P_{m2}), ..., (P_{tn},P_{mn}) where $P_{t1}, P_{t2}, ..., P_{tn}$ are predicted by using the loss-model and $P_{m1}, P_{m2}, ..., P_{mn}$ are the observed measurements. The fitting curve $f(P_t)$ has the deviation (error) d from each data point, i.e., $d_1 = P_{m1} - f(P_{t1})$, $d_2 = P_{m2} - f(P_{t2})$, ..., $d_1 = P_{mn} - f(P_{tn})$. The best fitting curve and the differences between the model predictions and the observed values are combined in the following least-squares function

$$\Pi = d_1^2 + d_2^2 + ... + d_n^2 = \sum_{i=1}^{n} d_i^2 = \sum_{i=1}^{n} \left[P_{mi} - f(P_{ti}) \right]^2 = \text{a minimum}. \qquad (5.8)$$

A routine for the loss-model identification has been written in MATLAB software and is given in Appendix A.

5.3 Results of Parameter Fitting

The parameters of the dynamic loss-model are determined by the nonlinear least-squares method. The block scheme of the parameter identification can be seen in Figure 5.1,

where the measured experimental data, (B_x, B_y, H_x, H_y) and initial parameters, $x_0 = [k_{c0}, k_{e0}, k_{h0}, k_{r0}, b_0]$ are given. The dynamic loss-model generates total power loss curves based on measured data and the initial parameters. The comparison between the experimental and modeled total losses provides an error *d*. Depending on this error, the nonlinear least-squares method modifies the input parameters of the loss-model. The cycle runs until the error gets small enough. The program of the identification has been written in MATLAB software and is given in Appendix A. The speed of convergence of this program was substantially dependent on the initial parameters given in Table 5.1. In general, the efficiency of the parameter identification program depends on the quality of the measured data and initial values.

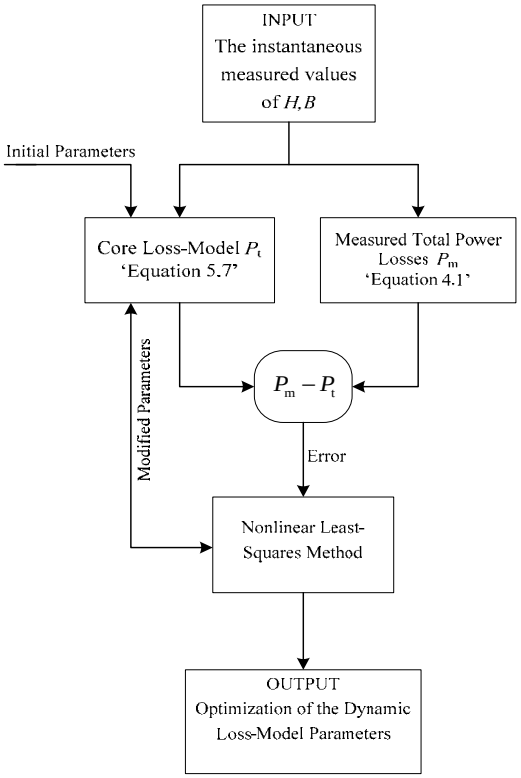

Figure 5.1: The block scheme of the loss-model identification.

Table 5.1 shows the physical properties of the loss-model parameters as the first column while the initial values can be seen in the second column of the table. The third column contains the result of the identification.

Table 5.1: Physical properties of loss-model parameters and initial test of the loss-model identification.

Parameter	Physical property	Initial parameters	Fitted parameters
k_c	Classical eddy-current loss coefficient	1.3112×10^{-5}	2.34×10^{-14}
k_e	Excess loss coefficient	2.9525×10^{-5}	3.56×10^{-4}
k_h	Hysteresis loss coefficient	0.0214	0.00974
k_r	Rotational loss coefficient	0.055	0.00337
b	Coefficient related to the texture and grain size of the material	16.0	16.36

Figure 5.2 show the results of the parameter fitting, where the measured curves are denoted by, 'o', and the fitted curves are denoted by, '□'. The figure illustrates the fitting results considering the complete set of data obtained from the measurements.

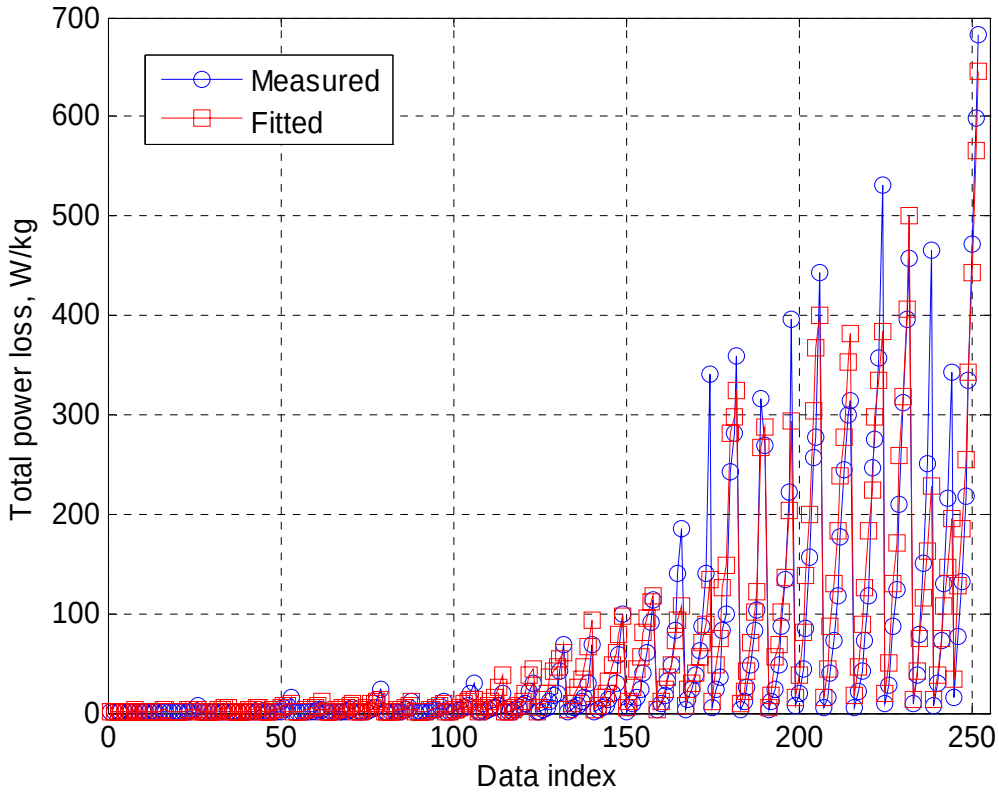

Figure 5.2: Results of parameter identification of loss-model at different magnetization frequencies of the fundamental flux density waveform ranging in the intervals $(10\ \text{Hz} \le f \le 1000\ \text{Hz})$.

The data obtained from the experimental work under alternating and rotating flux excitation was huge, and the parameter identification program was executed by taken into consideration the whole of these data sets as shown in Figure 5.2. However, the deviation between the model and the observed measurements cannot be clearly seen in a single figure.

In order to show greater details, a series of close ups of the sections of the figure are given in Figure 5.3 and Figure 5.4. These smaller figures clarify the results obtained from fitting the predicted losses to the measured losses.

The curves illustrated in Figure 5.3 and Figure 5.4 show that, the accuracy of the fitting at lower frequencies is worse than in the case of higher frequencies, and at 50 Hz it is much better.

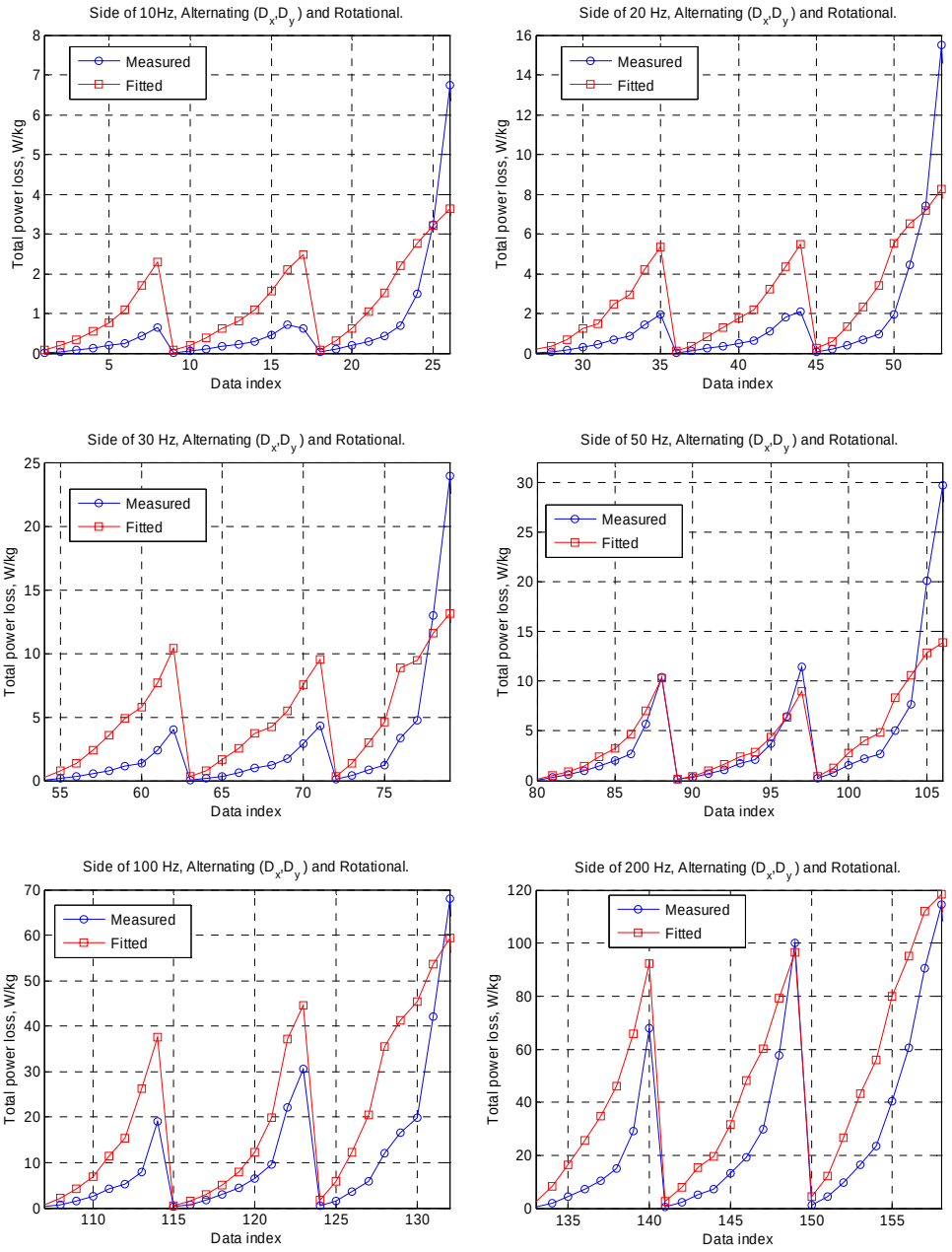

Figure 5.3: '*Zoom in*' of the curves illustrated in Figure 5.2 and fitting results at each side of the fundamental frequencies 10 Hz, 20 Hz, 30 Hz, 50 Hz, 100 Hz and 200 Hz.

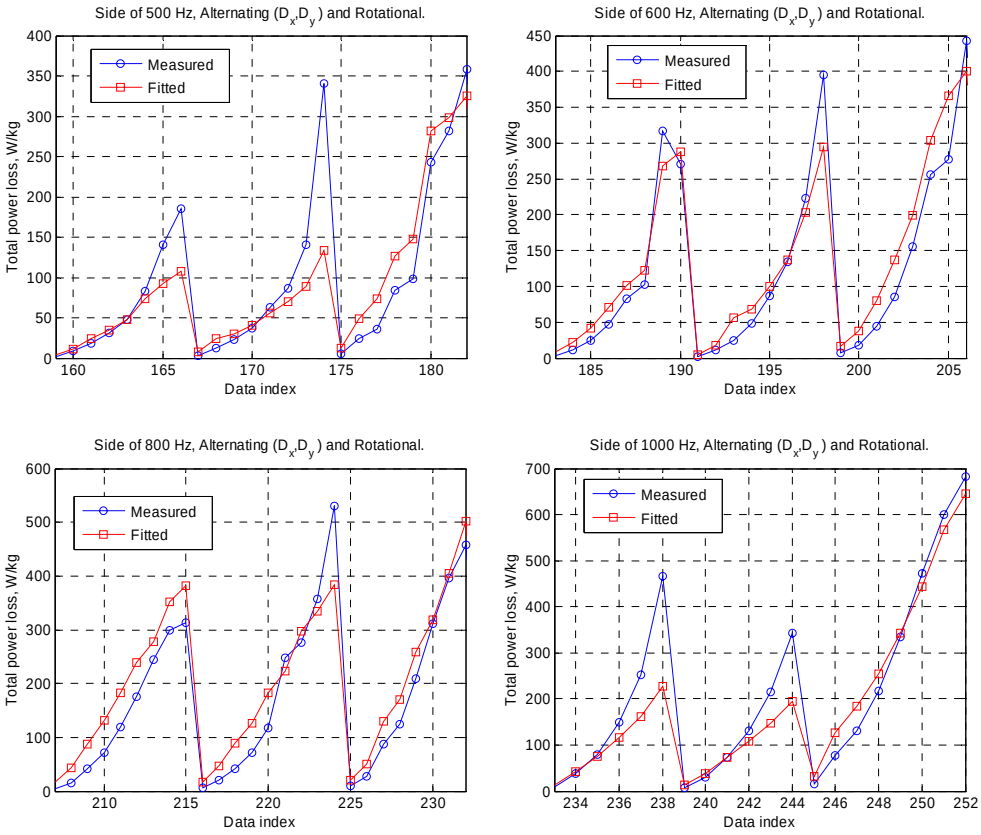

Figure 5.4: '*Zoom in'* of the curves illustrated in Figure 5.2 and fitting results at each side of the fundamental frequencies 500 Hz, 600 Hz, 800 Hz and 1 kHz.

Chapter 6

Conclusions

6.1 Summary

In this thesis, a method of measuring the magnetic properties of cross-shaped electrical steel sheet under both alternating and rotating flux conditions using vertical yoke and search coils was presented. The magnetic field strength components were measured by using two tangential field-strength sensing coils. The flux density was measured using a voltage induced in 2-turns search coils threaded through 1 mm diameter holes drilled through the sheet and the power losses were calculated and plotted in different conditions of excitation by using a program written in MATLAB software.

The results obtained from the measuring device showed that the effects of increasing magnetic flux density and frequency on the dynamic hysteresis loops will in turn affect the total power losses in the electrical steel sheet. Behavior of the *B*-*H* loops was investigated under a range of flux densities from 0.2 T to 1.8 T which is the maximum value of flux density that has been reached. This maximum value was easy to reach under the alternating and rotating fields for the fundamental frequencies 10 Hz to 600 Hz. However, this peak becomes difficult to reach at high frequencies.

The loci of the magnetic field strength, the loci of the magnetic flux density, and the *B*-*H* loops presented in the rolling direction of the sample were different from those obtained in the transverse direction of the sample when the field applied was rotational. The likely reason that could cause this variation is the anisotropy of the material.

The method used has the advantage that the sample can be very easily placed into and removed from the measuring device as well as the fact that the installation of the *B*-coils and *H*-coils in the sample was not difficult. Furthermore, a desired rotating flux within the

measurement region at the sample center was generated easily except for those at high frequencies. The results showed that the method presented in this thesis was useful in measuring the magnetic properties of an electrical steel sheet. However, some problems appeared concerning the accuracy of the measurements under a rotating flux. Still the possibility to solve these problems remains in optimizing the yoke constructions as well as the control system and sensing coils.

Losses in the sample due to the rotating flux and different conditions of excitation were measured and compared with the losses under the same conditions of excitation but due to an alternating flux. The results showed that rotational losses were larger than those caused by the alternating flux.

Finally, the data obtained from the experimental work was used to estimate the parameters of a comprehensive dynamic loss-model by using the least-squares criterion. Identification procedures which have been constructed in MATLAB software are given in Appendix A. The quality of the method was greatly dependent on the quality of the model proposed as well as the measurements obtained from the experimental work.

6.2 Recommendations for Further Work

In order to further understand the mechanism of rotational core losses, considerable work for measurement experiment and theoretical modeling needs to be developed and improved, in the following ways:

1. Improvement of rotational core loss measuring techniques, including improved design of the tester with optimum magnetic field sensors (*B*-*H* coils) for more accurate measurement of the *B*-*H* relationship.
2. Development of a control system for controlling the locus of the rotating flux density vector when the specimen becomes saturated.
3. Development of a new modeling and measurement method for rotational core losses, including the calculation of the hysteresis and eddy-current as well as anomalous core losses.
4. Further understanding of the mechanisms of rotational hysteresis loss, including vector hysteresis modeling and experimental verification of the theory.

References

Akbaba, M. and Fakhro, S. Q. (1992), 'Field distribution and iron loss computation in reluctance augmented shaded-pole motors using finite element method', *IEEE Trans. Energy Conv.*, **7**, 302-307.

Alkar, K. (2007) 'Measuring power losses of electrical steel sheets in one- and two-dimensional magnetic fields', Master's thesis, Helsinki University of Technology , Finland, available at: http://lib.tkk.fi/Dipl/2007/urn010204.pdf.

Amar, M. and Kaczmarek, R. (1995), 'A general formula for prediction of iron losses under nonsinusoidal voltage waveform', *IEEE Trans. Magn.*, **31**, 2504-2509.

Amar, M., Kaczmark, R., and Protat, F. (1994), 'Magnetic losses in PWM voltage excitation schemes', ICEM, Paris, France.

Arkkio, A. and Niemenmaa, A. (1992), 'Estimation of losses in cage induction motors using finite element techniques', ICEM, Manchester, UK, 317-321.

Atallah, K. and Howe, D. (1993), 'Calculation of the rotational power loss in electrical steel laminations from measured *H* and *B*', *IEEE Trans. Magn.*, **29**, 3547-3549.

Atallah, K., Zhu, Z. Q., and Howe, D., (1992), 'An improved method for predicting iron losses in brushless permanent magnet DC drives', *IEEE Trans. Magn.*, **28**, 2997-2999.

Belahcen, A. and Arkkio, A., (2008), 'Comprehensive Dynamic Loss-Model of Electrical Steel Applied to FE Simulation of Electrical Machines', *IEEE Trans. Mag.*, **44**, 886-889.

Bertotti, G. (1985), 'Physical interpretation of eddy current losses in ferromagnetic materials', *J. Appl. Phys.*, **57**, 2100-2126.

Bertotti, G. (1988), 'General properties of power losses in soft ferromagnetic materials', *IEEE Trans. Magn.*, **24**, 621-630.

Bertotti, G. (1998), *Hestersis in magnetism, Institute Electtrotecnico Nazionale Calileo Ferraris*. AP academic press, Torino Italy.

Bertotti, G., Boglietti, A., Chiampi, M., Chiarabaglio, D., Fiorillo, F., and Lazzari, M. (1991), 'An improved estimation of iron losses in rotating electrical machines', *IEEE Trans. Magn.*, **27**, 5007-5009.

Bertotti, G., Canova, A., Chiampi, M., Chiarabaglio, D., Fiorillo, F., and Rietto, A. M. (1994), 'Core loss prediction combining physical models with numerical field analysis', *J. Magn. Magn. Mater.*, **133**, 647-650.

Boglietti, A., Ferraris, P., Lazzari, M., and Profumo, F. (1991), 'Iron losses in magnetic materials with six-step and PWM inverter supply [induction motors]', *IEEE Trans. Magn.*, **27**, 5334-5336.

Boon, C. R. and Thompson, J. E. (1965), 'Alternating and rotational power loss at 50c/s in 3% silicon-iron sheet', *IEE Proc.*, **112**, 2147-2151.

Brix, W., Hempel, K. A. and Schult, F. J. (1984), 'Improved method for the investigation of the rotational magnetization process in electrical steel sheets', *IEEE Trans. Magn.*, **20**, 1708-1710.

Brix, W., Hempel, K. A., and Schrceder, W. (1982), 'method for the measurement of rotational power loss and related properties in electrical steel sheets', *IEEE Trans. Magn.*, **18**, 1496-1471.

Cecchetti, A., Ferrari, G., Masoli, F., and Soardo, G. (1978), 'Rotational power losses in 3% SiFe as a function of frequency', *IEEE Trans. Magn.*, **14**, 356-358.

Darwaz, K., Marthouret, F., and Masson, J. P. (1994), 'Iron losses prediction in various waveforms excitations', ICEM, Paris, France.

Dlala, E. (2008) 'Magnetodynamic vector hysteresis models for steel laminations of rotating electrical machines', Doctoral Dissertation, Helsinki University of Technology , Finland, available at: http://lib.tkk.fi/Diss/2008/isbn9789512292776/

Enokizono, M., and Tanabe, I. (1991), 'Studies on a new simplified rotational loss tester', *IEEE Trans. Magn.*, **33**, 4020-4022.

Enokizono, M., and Tanabe, I. (1997), 'Studies on a new simplified rotational loss tester', *IEEE Trans. Magn.*, **33**, 4020-4022.

Enokizono, M., Suzuki, T., Sievert, J., and Xu, J. (1990), 'Rotational power loss of silicon steel sheet', *IEEE Trans. on Magn.*, **26**, 2562-2564.

Enokizono, M., Suzuki, T., Sievert, J., and Xu, J. (1990), 'Rotational power loss of silicon steel sheet', *IEEE Trans. Magn.*, **26**, 2562-2564.

Findlay, R. D., Stranges, N., and MacKay, D. K. (1994), 'Losses due to rotational flux in three phase induction motors," *IEEE Trans. Energy Conv.*, **9**, 543-549.

Fiorillo, F. and Rietto, A. M. (1990), 'Rotational and alternating energy loss vs. magnetizing frequency in SiFe laminations', *J. Magn. Magn. Mater.*, **83**, 402-404.

Fiorillo, F., and Novikov, A. (1990), 'An improved approach to power losses in magnetic laminations under nonsinusoidal induction waveform', *IEEE Trans. Magn.*, **26**, 2904-2910.

Fiorillo, F., and Novikov, A. (1990), 'Power losses under sinusoidal, trapezoidal and distorted induction waveform', *IEEE Trans Magn.*, **26**, 2559-2561.

Goodenough, J. B. (2002), 'Summary of losses in magnetic materials', *IEEE Trans. Magn.*, **38**, 3389-3408.

Guo, Y., Zhu, J. G., Zhong, J., Lu, H., and Jin, J. X. (2008) 'Measurement and modeling of rotational core losses of soft magnetic materials used in electrical machines: A review', *IEEE Trans. Magn.*, **44**, 279-291.

Guo, Y. G., Zhu, J. G., and Zhong, J. J. (2005), 'Measurement and modelling of magnetic properties of soft magnetic composite material under 2D vector magnetizations,' J. Magn. Magn. Mater., **302**, 14-19.

Ivanyi, A., Fuzi, J., and Pfiitzner, H. (1998), '2D/3D models for a three phase fed single sheet tester', *IEEE Trans. Magn.*, **34**, 3004-3007.

Jamil, M.K., and Demerdash, N.A. (1990), 'Harmonics and core losses of permanent magnet DC motors controlled by chopper circuits', *IEEE Trans. Energy Conv.*, **5**, 408-414.

Kaczmarek, R., Amar, M., and Protat, F. (1996), 'Iron loss under PWM voltage supply on Epstein frame and in induction motor core', *IEEE Trans. Magn.*, **32**, 189-194.

Katarzyna, F., Paavo, R., and Anouar, B. (2008), 'measurement of magnetic properties under alternating field with a vertical rotational single sheet tester', 10th International workshop on 1&2 dimensional magnetic measurement and testing, Przeglad Elektrotechniczny, January 2009.

Kaplan, A. (1961), 'Magnetic core losses resulting from a rotating flux', *J. Appl. Phys.*, **32**, 370-371.

Li, J. and Jufer, M. (1994), 'Modeling and dynamical simulation of witched reluctance motors, including iron losses', ICEM, Paris, France.

Loises, G., and Moses, A. J. (2001), 'Critical evaluation and limitation of localized flux density measurements in electrical steels', *IEEE Trans. Magn.*, **37**, 2755-2757.

Mori, K., Yanase, S., Okazaki, Y., and Hashi, S. (2005), '2D magnetic rotational loss of electrical steel at high magnetic flux density', *IEEE Trans. Magn.*, **41**, 3004-3007.

Moses, A. J. (1990), 'Electrical steel: past, present and future developments' *IEE Proc.-A*, **137**, 233-245.

Moses, A. J., Thomas, B., and Thompson, J. E. (1972), 'Power loss and flux density distributions in the T-joint of a three phase transformer core', *IEEE Trans. Magn.*, **8**, 3310-3312.

Nakata, T., Takahashi, N., Fujiwara, K., and Nakano, M. (1993), 'Measurement of magnetic characteristics along arbitrary directions of grain-oriented silicon steel up to high flux densities', *IEEE Trans. Magn.*, **29**, 3544-3546.

Nee, H. P. and Nipp, E. (1994), 'A contribution to the calculation of harmonic iron losses of inverter-fed induction motors', ICEM, Paris, France, 698-703.

Péter, K., and Amália, I. (2004), 'Parameter identification of Jiles-Atherton model with nonlinear least-square method', Physica B, **343**, 59-64.

Philips, D. A., Dupre, L. R., and Melkebeek, J. A. (1995), 'Comparison of Jiles and Preisach hysteresis models in magnetodynamics', *IEEE Trans. Magn.*, **31**, 3551-3553.

Saitz, J. (1997), 'Calculation of iron losses in electrical machines', Helsinki University of Technology, Laboratory of Electromechanics, Report 51, Espoo, Finland, 57p.

Sievert, J. (1990), 'Recent Advances in the one- and two-dimensional magnetic measurement technique for electrical sheet steel', *IEEE Trans. Magn.*, **26**, 2553-2558.

Slemon, G. R., and Liu, X. (1990), 'Core losses in permanent magnet motors', *IEEE Trans. Magn.*, **26**, 1653-1655.

Strange, N., and Findlay, R. D. (2000), 'Measurement of rotational iron losses in electrical sheet', *IEEE Trans. Magn.*, **36**, 3457-3459.

Stranges, N., and Findlay, R. D. (*2000*), 'Measurement of rotational iron losses in electrical sheet', *IEEE Trans. Magn.*, 3**6**, 3457-3459.

Young, F. J., and Schenk, H. L. (1996), 'Iron losses in elliptically polarized magnetic fields', *J. Appl. Phys.*, **37**, 1210-1211.

Zhu, J. G., and Ramsden, V. S. (1993), 'Two dimensional measurement of magnetic field and core loss using a square specimen tester', *IEEE Trans. Magn.*, **29**, 2995-2997.

Zurek, S., and Meydan, T. (2004), 'Rotational power losses and vector loci under controlled high flux density and magnetic field in electrical steel sheets', *IEEE Trans. Magn.*, **42**, No. 10, 2815-2817.

Appendix A

The M-Files which have been constructed in MATLAB for parameter identification of the loss-models with Nonlinear Least-Square Method

M-File 1: The main fitting program for obtaining the parameters of the core loss model.

```
close all
clear all
ptype=1;  %W/kg.
%ptype=2; %W/m3.
sample=1; %which material sample to be fitted!
psort=0;  %for sorting the measured loss in advance.
[BxBy,Ptm,dt,T,ro,kk]=dataindex(sample,ptype,psort); %total power loss
measured(conventional equation).
input=[dt; T ; BxBy']; %the flux density waveforms Bx,By.
f=1./T;
[initialpar, lb,ub]=initialConditions(ptype,ro);
[newParameters,error] =
lsqcurvefit(@MyIronPowerLoss,initialpar,input,Ptm,lb,ub);
Kc_o=newParameters(1);
Ke_o=newParameters(2);
Kh_o=newParameters(3);
Kr_o=newParameters(4);
Kb_o=newParameters(5); %Kb=b.
%using the new parameters to get new output values.
Pt=MyIronPowerLoss(newParameters,input); % prediction of the model which
will fitt to Ptm.
%sortbym=1; %sorting the powers according the measured loss after
fitting.
sortbym=0;  %sorting the powers according the calculated loss after
fitting.
if(sortbym==1)
Ptm_s=sort(Ptm);
for i=1:length(Ptm)
inds(i)=find(Ptm==Ptm_s(i));
Pt_s(i)=Pt(inds(i));
f_s(i)=f(inds(i));
end
else
Pt_s=sort(Pt);
for i=1:length(Pt)
inds(i)=find(Pt==Pt_s(i));
Ptm_s(i)=Ptm(inds(i));
f_s(i)=f(inds(i));
end
end
index=kk:length(Ptm)+kk-1;
plotfit(index,ptype,psort,Ptm,Ptm_s,Pt,Pt_s);
```

M-File 2: The initial parameters of the core loss-model.

```
function [initialpar, lb,ub]=initialConditions(ptype,ro)
switch ptype
case 1    %W/kg.
Kc=1.3112e-5;
Ke=2.9525e-5;
Kh=0.0214;
Kr=0.055;
b=16.0;
initialpar=[Kc Ke Kh Kr b];
lb = [0 0 0 0];    %define the lower bound.
ub =[20 20 20 30]; %define the upper bound.
case 2   %W/m3.
Kc=1.3112e-5;
Ke=2.9525e-5;
Kh=0.0214;
Kr=0.055;
b=16.0;
initialpar=ro*[Kc Ke Kh Kr b];
lb = ro*[0 0 0 0];     %define the lower bound.
ub = ro*[20 20 20 30]; %define the upper bound.
end
```

M-File 3: Routines of the core loss-model.

```
function pt= MyIronPowerLoss (param,input) % corelossmodel
Kc = param(1);
Ke = param(2);
Kh = param(3);
Kr = param(4);
b  = param(5); %b=Kb
ww=size(input);
[f1 f2]=find(input);
m=ww(2);
m1=max(f1)/2-(ww(1)-max(f1))/2+1;
for j=1:m
dt=input(1,j);
T=input(2,j);
f=1./T;
NTPER=T/dt;
Bx=input(3:m1,j)';
By=input(ww(1)/2+2:max(f1),j)';

%Eddy Current Model.
dBx=numder(Bx);
dBy=numder(By);
dBxdt=dBx/dt;
dBydt=dBy/dt;
dB=dBx+dBy;
IdBI=sqrt(dBx.^2+dBy.^2);
IdBIdt=IdBI/dt;
dBdt=dBxdt+dBydt;
IdBdtI=sqrt(dBxdt.^2+dBydt.^2);
dpc=Kc.*IdBdtI.^2;
pc=numint(dpc)/NTPER;

%Excess Loss Model
IBI=sqrt(Bx.^2+By.^2);
```

```
dIBI=numder(IBI);
dIBIdt=dIBI/dt;
IdIBIdtI=abs(dIBIdt);
dpe=Ke.*IdBdtI.^1.5;
pe=numint(dpe)/NTPER;

%Hysteresis Loss Model
Bs=2.0;
Theta=atan2(By,Bx);
for i=1:length(Theta)
    if Theta(i)<0
        Theta(i)=Theta(i)+2*pi;
    end
end

dTheta=numder(Theta);
IdThetaI=abs(dTheta);
IdThetaIdt=IdThetaI./dt;
dph=Kh.*IBI.*IdBdtI+Kr.*((1-IBI./Bs)./(1+b.*(1-
IBI./Bs).^2)).*IBI.*IdThetaIdt;
ph=numint(dph)/NTPER;
pt(j)=ph+pe+pc;    %w/kg
end
return
```

M-File 4: Numerical derivative.

```
function dy= numder(y)
nn=length(y);
 dy(1)=y(2)-y(1);
 dy(nn)=y(nn)-y(nn-1);
for i=2:nn-1
    dy(i)=((y(i)-y(i-1))+(y(i+1)-y(i)))/2;
end

return
```

M-File 5: Numerical integration.

```
function p=numint(dp)
p=0;
for i=2:length(dp)
    p=p+0.5*(dp(i)+dp(i-1));
end
return
```

M-File 6: loading the data obtained from the experimental work.

```
function [BxBy,Ptm,dt1,T1,ro,k]=dataindex(sample,ptype,psort)
BHG=zeros(500,5000,5);
switch (sample)

 case 1
    ro=7600;

%10Hz.

%Measurements due to alternating flux in x direction.
x=load('data/sampleG/F10Bx0.21By0.017.txt');BHG(1,1:length(x),1:5)=x;
x=load('data/sampleG/F10Bx0.42By0.016.txt');BHG(2,1:length(x),1:5)=x;
x=load('data/sampleG/F10Bx0.61By0.033.txt');BHG(3,1:length(x),1:5)=x;
x=load('data/sampleG/F10Bx0.81By0.042.txt');BHG(4,1:length(x),1:5)=x;
x=load('data/sampleG/F10Bx0.99By0.051.txt');BHG(5,1:length(x),1:5)=x;
x=load('data/sampleG/F10Bx1.2By0.12.txt');  BHG(6,1:length(x),1:5)=x;
x=load('data/sampleG/F10Bx1.5By0.31.txt');  BHG(7,1:length(x),1:5)=x;
x=load('data/sampleG/F10Bx1.6By0.57.txt');  BHG(8,1:length(x),1:5)=x;

%Measurements due to alternating flux in y direction.
x=load('data/sampleG/F10Bx0.017By0.22.txt'); BHG(9,1:length(x),1:5)=x;
x=load('data/sampleG/F10Bx0.0026By0.44.txt');BHG(10,1:length(x),1:5)=x;
x=load('data/sampleG/F10Bx0.024By0.66.txt'); BHG(11,1:length(x),1:5)=x;
x=load('data/sampleG/F10Bx0.026By0.88.txt'); BHG(12,1:length(x),1:5)=x;
x=load('data/sampleG/F10Bx0.025By1.txt');    BHG(13,1:length(x),1:5)=x;
x=load('data/sampleG/F10Bx0.039By1.2.txt');  BHG(14,1:length(x),1:5)=x;
x=load('data/sampleG/F10Bx0.1By1.4.txt');    BHG(15,1:length(x),1:5)=x;
x=load('data/sampleG/F10Bx0.23By1.6.txt');   BHG(16,1:length(x),1:5)=x;
x=load('data/sampleG/F10Bx0.4By1.7.txt');    BHG(17,1:length(x),1:5)=x;

%Measurements due to rotating flux.
x=load('data/sampleG/F10Bx0.2By0.19.txt'); BHG(18,1:length(x),1:5)=x;
x=load('data/sampleG/F10Bx0.42By0.4.txt'); BHG(19,1:length(x),1:5)=x;
x=load('data/sampleG/F10Bx0.63By0.63.txt');BHG(20,1:length(x),1:5)=x;
x=load('data/sampleG/F10Bx0.81By0.89.txt');BHG(21,1:length(x),1:5)=x;
x=load('data/sampleG/F10Bx0.95By1.1.txt'); BHG(22,1:length(x),1:5)=x;
x=load('data/sampleG/F10Bx1.2By1.3.txt');  BHG(23,1:length(x),1:5)=x;
x=load('data/sampleG/F10Bx1.5By1.5.txt');  BHG(24,1:length(x),1:5)=x;
x=load('data/sampleG/F10Bx1.6By1.6.txt');  BHG(25,1:length(x),1:5)=x;
x=load('data/sampleG/F10Bx1.8By1.8.txt');  BHG(26,1:length(x),1:5)=x;
.
.
.
%1000 Hz.


%for another sample.
case 2
    ro=7600;

  end
m =max(find(BHG(:,1,1)));
k =min(find(BHG(:,1,1)));
jj=0;
for j=k:m
    jj=jj+1;
   jd=max(find(BHG(j,:,1)));
```

```
t(jj,:)=BHG(j,:,1);
Bx(jj,:)=BHG(j,:,2);
By(jj,:)=BHG(j,:,3);
Hx(jj,:)=BHG(j,:,4);
Hy(jj,:)=BHG(j,:,5);
BxBy(jj,:)=[Bx(jj,:) By(jj,:)];
[k1 k2]=find(t(jj,:));
T(jj)=t(jj,max(k2))-t(jj,1);
f(jj)=1/T(jj);
dt(jj)=t(jj,5)-t(jj,4);


tloss(jj)=0;

for i=2:length(Bx(jj,1:jd))
    tloss(jj)=tloss(jj)+0.5*(Hx(jj,i)+Hx(jj,i-1))*(Bx(jj,i)-Bx(jj,i-
1))+...
    0.5*(Hy(jj,i)+Hy(jj,i-1))*(By(jj,i)-By(jj,i-1));
end


switch ptype
 case 1
        Ptm(jj)= abs(tloss(jj)/(ro*T(jj))); %total losses in W/kg

 case 2
        Ptm(jj)= abs(tloss(jj)/T(jj));  %total losses in W/m3
end


end

if(psort==1)
Ptm_s=sort(Ptm);
for i=1:length(Ptm)
inds(i)=find(Ptm==Ptm_s(i));
Bx1(i,:)=Bx(inds(i),:);
By1(i,:)=By(inds(i),:);

BxBy(i,:)=[Bx1(i,:) By1(i,:)];
T1(i)=T(inds(i));
f1(i)=f(inds(i));
dt1(i)=dt(inds(i));
end
for i=1:length(Ptm)
Ptm(i)=Ptm_s(i);
end
else
T1=T;
f1=f;
dt1=dt;

end

end
```

M-File 7: Plotting of the fitting results.

```
function plotfit(index,ptype,psort,Ptm,Ptm_s,Pt,Pt_s);

figure(1),
a1=plot(index,Ptm,'-o');
xlabel('Data index','FontSize',12,'FontName','Times')
if(ptype==1)
ylabel('Total power loss, W/kg','FontSize',12,'FontName','Times')
else
ylabel('Total power loss, W/m^3','FontSize',12,'FontName','Times')
end
legend('Experimental')
hold on
a2=plot(index,Pt,'-sr');
legend([a1,a2],'Measured','Fitted')
if(psort==0)
figure(2),
a1=plot(index,Ptm_s,'-o');
xlabel('Data index','FontSize',12,'FontName','Times')
if(ptype==1)
ylabel('Total power loss, W/kg','FontSize',12,'FontName','Times')
else
ylabel('Total power loss, W/m^3','FontSize',12,'FontName','Times')
end
legend('Experimental')
hold on
a2=plot(index,Pt_s,'-sr');
legend([a1,a2],'Measured','Fitted')
end
```